

# **Integrated Ocean Drilling Program Expedition 324 Preliminary Report**

**Testing plume and plate models of ocean plateau  
formation at Shatsky Rise, northwest Pacific Ocean**

4 September–3 November 2009

Expedition 324 Scientists



Published by  
Integrated Ocean Drilling Program Management International, Inc.,  
for the Integrated Ocean Drilling Program

## **Publisher's notes**

Material in this publication may be copied without restraint for library, abstract service, educational, or personal research purposes; however, this source should be appropriately acknowledged. Core samples and the wider set of data from the science program covered in this report are under moratorium and accessible only to Science Party members until 3 November 2010.

### Citation:

Expedition 324 Scientists, 2009. Testing plume and plate models of ocean plateau formation at Shatsky Rise, northwest Pacific Ocean. *IODP Prel. Rept.*, 324. doi:10.2204/iodp.pr.324.2009

### Distribution:

Electronic copies of this series may be obtained from the Integrated Ocean Drilling Program (IODP) Scientific Publications homepage on the World Wide Web at [www.iodp.org/scientific-publications/](http://www.iodp.org/scientific-publications/).

This publication was prepared by the Integrated Ocean Drilling Program U.S. Implementing Organization (IODP-USIO); Consortium for Ocean Leadership, Lamont Doherty Earth Observatory of Columbia University, and Texas A&M University, as an account of work performed under the international Integrated Ocean Drilling Program, which is managed by IODP Management International (IODP-MI), Inc. Funding for the program is provided by the following agencies:

National Science Foundation (NSF), United States

Ministry of Education, Culture, Sports, Science and Technology (MEXT), Japan

European Consortium for Ocean Research Drilling (ECORD)

Ministry of Science and Technology (MOST), People's Republic of China

Korea Institute of Geoscience and Mineral Resources (KIGAM)

Australian Research Council (ARC) and New Zealand Institute for Geological and Nuclear Sciences (GNS), Australian/New Zealand Consortium

Ministry of Earth Sciences (MoES), India

## **Disclaimer**

Any opinions, findings, and conclusions or recommendations expressed in this publication are those of the author(s) and do not necessarily reflect the views of the participating agencies, IODP Management International, Inc., Consortium for Ocean Leadership, Lamont-Doherty Earth Observatory of Columbia University, Texas A&M University, or Texas A&M Research Foundation.

## Expedition 324 participants

### Expedition 324 scientists

**William W. Sager**  
**Co-Chief Scientist**  
Department of Oceanography  
Texas A&M University  
College Station TX 77843-3146  
USA  
[sager@ocean.tamu.edu](mailto:sager@ocean.tamu.edu)

**Takashi Sano**  
**Co-Chief Scientist**  
Department of Geology and Paleontology  
National Museum of Nature and Science  
3-23-1 Hyakunin-cho, Shinjyuku-ku  
Tokyo 169-0073  
Japan  
[sano@kahaku.go.jp](mailto:sano@kahaku.go.jp)

**Jörg Geldmacher**  
**Expedition Project Manager/Staff Scientist**  
United States Implementing Organization  
Integrated Ocean Drilling Program  
Texas A&M University  
College Station TX 77843-3146  
USA  
[geldmacher@iodp.tamu.edu](mailto:geldmacher@iodp.tamu.edu)

**Gerardo (Gerry) Iturrino**  
**Logging Staff Scientist**  
Borehole Research Group  
Lamont-Doherty Earth Observatory  
of Columbia University  
PO Box 1000, 61 Route 9W  
Palisades NY 10964  
USA  
[iturrino@ldeo.columbia.edu](mailto:iturrino@ldeo.columbia.edu)

**Helen Evans**  
**Logging Staff Scientist**  
Borehole Research Group  
Lamont-Doherty Earth Observatory  
of Columbia University  
PO Box 1000, 61 Route 9W  
Palisades NY 10964  
USA  
[helen@ldeo.columbia.edu](mailto:helen@ldeo.columbia.edu)

**Renat Almeev**  
**Igneous Petrologist**  
Institute of Mineralogy  
University of Hannover  
Callinstrasse 3  
D-30167 Hannover  
Germany  
[r.almeev@mineralogie.uni-hannover.de](mailto:r.almeev@mineralogie.uni-hannover.de)

**Atsushi Ando**  
**Micropaleontologist (foraminifers)**  
BK21 Coastal Environmental System School  
Division of Earth Environmental System  
Pusan National University  
San30 Jangjeon-dong, Geumjeong-gu  
Busan 609-735  
Korea  
[ando@pusan.ac.kr](mailto:ando@pusan.ac.kr)

**Claire Carvallo**  
**Paleomagnetist**  
Institut de Minéralogie et de Physique  
des Milieux Condensés (IMPMC)  
Université Pierre et Marie Curie  
Campus Boucicaut  
140 rue de Lourmel  
75015 Paris  
France  
[Claire.Carvallo@impmc.jussieu.fr](mailto:Claire.Carvallo@impmc.jussieu.fr)

**Adélie Delacour**  
**Igneous Petrologist (alteration)**  
Laboratoire de Dynamique Terrestre  
et Planétaire  
Observatoire Midi-Pyrénées, Université Paul  
Sabatier  
14 Avenue Edouard Belin  
31400 Toulouse  
France  
[delacour@ntp.obs-mip.fr](mailto:delacour@ntp.obs-mip.fr)

**Andrew R. Greene**  
**Igneous Petrologist**  
Department of Geology and Geophysics  
University of Hawaii  
1680 East-West Road  
Honolulu HI 96822  
USA  
[agreene@soest.hawaii.edu](mailto:agreene@soest.hawaii.edu)

**Amber C. Harris**  
**Physical Properties Specialist**  
Graduate School of Oceanography  
University of Rhode Island  
Box 200, South Ferry Road  
Narragansett RI 02882  
USA  
[aharris@gso.uri.edu](mailto:aharris@gso.uri.edu)

**Sandra Herrmann**  
**Micropaleontologist (nannoplankton)**  
ETH Zurich  
Geological Institute  
Department of Earth Sciences  
Sonneggstrasse 5, NO G46  
CH-8092 Zurich  
Switzerland  
[sandra.herrmann@erdw.ethz.ch](mailto:sandra.herrmann@erdw.ethz.ch)

**Ken Heydolph**  
**Inorganic Geochemist**  
Leibniz-Institute of Marine Sciences  
IFM-GEOMAR  
Wischhofstrasse 1-3  
D-24148 Kiel  
Germany  
[kheydolph@ifm-geomar.de](mailto:kheydolph@ifm-geomar.de)

**Naoto Hirano**  
**Structural Geologist**  
Center for Northeast Asian Studies  
Tohoku University  
41 Kawauchi, Aoba-ku  
Sendai 980-8576  
Japan  
[nhiro@cneas.tohoku.ac.jp](mailto:nhiro@cneas.tohoku.ac.jp)

**Akira Ishikawa**  
**Inorganic Geochemist**  
Institute for Research on Earth Evolution  
(IFREE)  
Japan Agency of Marine-Earth Science and  
Technology (JAMSTEC)  
2-15 Natsushima-Cho, Yokosuka  
Kanagawa 237-0061  
Japan  
[akr@jamstec.go.jp](mailto:akr@jamstec.go.jp)

**Moo-Hee Kang**  
**Geophysics**  
Petroleum and Marine Division  
Korea Institute of Geosciences and Mineral  
Resources (KIGAM)  
92 Gwahang-no, Yuseong-gu  
Daejeon 305-350  
Korea  
[karl@kigam.re.kr](mailto:karl@kigam.re.kr)

**Anthony A.P. Koppers**  
**Igneous Petrologist**  
(<sup>40</sup>Ar/<sup>39</sup>Ar geochronology)  
College of Oceanic and Atmospheric Sciences  
Oregon State University  
104 COAS Administration Building  
Corvallis OR 97331-5503  
USA  
[akoppers@coas.oregonstate.edu](mailto:akoppers@coas.oregonstate.edu)

**Sanzhong Li**  
**Structural Geologist**  
College of Marine Geosciences  
Ocean University of China  
Number 238, Songling Road  
Qingdao, Shandong  
People's Republic of China  
[sanzhong@ouc.edu.cn](mailto:sanzhong@ouc.edu.cn)

**Kate Littler**  
**Sedimentologist**  
Department of Earth Sciences  
University College London  
Gower Street  
London WC1E 6BT  
United Kingdom  
[kate.littler@googlemail.com](mailto:kate.littler@googlemail.com)

**John Mahoney**  
**Inorganic Geochemist**  
Department of Geology and Geophysics  
School of Ocean and Earth Science and  
Technology  
University of Hawaii  
1680 East-West Road  
Honolulu HI 96822  
USA  
[jmahoney@hawaii.edu](mailto:jmahoney@hawaii.edu)

**Noritaka Matsubara**  
**Sedimentologist/Volcanologist**  
Graduate School of Science and Technology  
Ibaraki University  
2-1-1 Bunkyo, Mito  
Ibaraki 310-8512  
Japan  
[nd5408y@mcs.ibaraki.ac.jp](mailto:nd5408y@mcs.ibaraki.ac.jp)

**Masaya Miyoshi**  
**Igneous Petrologist**  
Beppu Geothermal Research Laboratory  
Institute for Geothermal Sciences  
Kyoto University  
Noguchibaru, Beppu  
Oita 874-0903  
Japan  
[miyoshi@bep.vgs.kyoto-u.ac.jp](mailto:miyoshi@bep.vgs.kyoto-u.ac.jp)

**David T. Murphy**  
**Igneous Petrologist (alteration)**  
School of Natural Resource Sciences  
Queensland University of Technology  
Level 3R Block, Gardens Point  
Brisbane State QLD 4001  
Australia  
[david.murphy@qut.edu.au](mailto:david.murphy@qut.edu.au)

**James H. Natland**  
**Igneous Petrologist**  
Rosenstiel School of Marine and Atmospheric  
Science  
University of Miami  
4600 Rieckenbacker Causeway  
Miami FL 33149  
[jnatland@rsmas.miami.edu](mailto:jnatland@rsmas.miami.edu)

**Masahiro Ooga**  
**Paleomagnetist**  
Department of Environmental System Science  
Doshisha University  
1-3 Tatara Miyakodani,  
Kyo-Tanabe City  
Kyoto 610-0321  
Japan  
[ooga\\_masahiro@yahoo.co.jp](mailto:ooga_masahiro@yahoo.co.jp)

**Julie Prytulak**  
**Physical Properties Specialist**  
Department of Earth Sciences  
University of Oxford  
Parks Road  
Oxford OX1 3PR  
United Kingdom  
[Julie.Prytulak@earth.ox.ac.uk](mailto:Julie.Prytulak@earth.ox.ac.uk)

**Kenji Shimizu**  
**Igneous Petrologist**  
Institute for Research on Earth Evolution  
(IFREE)  
Japan Agency for Marine-Earth Science and  
Technology (JAMSTEC)  
2-15 Natsushima-cho, Yokusuka  
Kanagawa 237-0061  
Japan  
[shimmy@jamstec.go.jp](mailto:shimmy@jamstec.go.jp)

**Masako Tominaga**  
**Paleomagnetist**  
Department of Geology and Geophysics  
Woods Hole Oceanographic Institution  
Clark 241B MS22  
Woods Hole MA 02543  
USA  
[mtominaga@whoi.edu](mailto:mtominaga@whoi.edu)

**Mike Widdowson**  
**Volcanologist**  
Department of Earth and Environmental  
Sciences  
The Open University  
Walton Hall  
Milton Keynes MK7 6AA  
United Kingdom  
[M.Widdowson@open.ac.uk](mailto:M.Widdowson@open.ac.uk)

**Stella C. Woodard**  
**Sedimentologist**  
Department of Oceanography  
Texas A&M University  
College Station TX 77843  
USA  
[swoodard@ocean.tamu.edu](mailto:swoodard@ocean.tamu.edu)

## Education and outreach

**Nasseer Idrisi**  
**HBCU Educator**  
Center for Marine and Environmental Studies  
University of the Virgin Islands  
2 John Brewers Bay  
St. Thomas VI 00802  
USA  
[nidrissi@uvi.edu](mailto:nidrissi@uvi.edu)

**Yuko Uchio**  
**Educator and Communications Officer**  
Department of Public Relations  
Museum of Nature and Science  
7-20, Ueno Park, Taito-ku  
Tokyo 110-8718  
Japan  
[yuchio@kahaku.go.jp](mailto:yuchio@kahaku.go.jp)

## Technical support

**Heather Barnes**  
**X-Ray/Microbiology Laboratory**

**John Beck**  
**Imaging Specialist**

**Lisa Brandt**  
**Chemistry Laboratory**

**Chad Broyles**  
**Curator**

**Etienne Claassen**  
**Marine Instrumentation Specialist**

**Roy Davis**  
**Laboratory Officer**

**David Fackler**  
**Applications Developer**

**Kazuho Fujine**  
**Chemistry Laboratory**

**Ron Grout**  
**Operations Superintendent**

**Gus Gustafson**  
**Downhole Tools/Thin Section Laboratory**

**Margaret Hastedt**  
**Paleomagnetism Laboratory**

**Dwight Hornbacher**  
**Applications Developer**

**Jurie Kotze**  
**Marine Instrumentation Specialist**

**Zenon Mateo**  
**Core Laboratory**

**Erik Moortgat**  
**Underway Geophysics Laboratory**

**Matthew Nobles**  
**Marine Computer Specialist**

**Chieh Peng**  
**Assistant Laboratory Officer**

**Steve Prinz**  
**Assistant Laboratory Officer**

**Kerry Swain**  
**Logging Engineer**

**Andrew Trefethen**  
**Marine Computer Specialist**

**Maxim Vasilyev**  
**Physical Properties Laboratory**

**Kelly VonDrehle**  
**Publications Specialist**

## Abstract

Oceanic plateaus are giant volcanic features whose existence implies an extraordinary flux of magma from mantle to lithosphere. By understanding their formation, these large igneous provinces can be important indicators of fundamental processes of mantle convection and geodynamics. Although it is widely thought that oceanic plateaus arise from massive eruptions resulting from the arrival of a deep mantle plume head at the lithosphere, an alternative explanation is that plateau eruptions are related to decompression melting of unusually fusible mantle beneath fast-spreading ridges. Shatsky Rise was cored during Expedition 324 because it is a unique oceanic plateau, formed during the Late Jurassic and Early Cretaceous at a rapidly spreading triple junction, with characteristics that could be attributed to either model of formation. Shatsky Rise is also a monster volcanic construct whose formation style is poorly understood. The goal of Expedition 324 was to core the igneous rocks of Shatsky Rise and the sediments above to examine the age, physical volcanology, geochemistry, and tectonic evolution of the rise as well as the sedimentation history.

Five sites were cored and four were logged, with one site (U1346) on the summit of Shirshov Massif and two sites each on Ori (Sites U1349 and U1350) and Tamu (Sites U1347 and U1348) Massifs. Basaltic lava flows were recovered at four of these sites and complement previous Ocean Drilling Program Site 1213 (south flank of Tamu Massif) in providing a record of lava flow emplacement on Shatsky Rise. Instead of lava flows, cores from Site U1348 recovered a thick sequence (~120 m) of volcanoclastic sediments topped with shallow-water carbonaceous sandstones. Lavas recovered at Sites U1347 and U1350 are fresh enough to be suitable for high-quality radiometric age dating and planned geochemical/isotopic studies. Although lavas from Site U1346 and U1349 were moderately to highly altered, it is expected that they will provide important age information with suitable treatment and will be useful for most geochemical studies. Even though the volcanoclastic rocks of Site U1348 are highly altered, a single interval containing relatively fresh glass shards will provide valuable constraints on magma source characteristics.

Shatsky Rise lava flows occur primarily as packages of pillow basalt and massive inflation units, frequently interbedded with volcanoclastic sediment. The richest massive inflation flows, up to ~23 m thick, occur on Tamu Massif at Sites 1213 and U1347. They are similar to massive flows cored on Ontong Java Plateau and found in continental flood basalt provinces. At Site U1347, the relationship of pillows and massive flows suggests magmatic cycles that began with the emplacement of massive sheet

flows and waned with pillow lavas. Moreover, paleomagnetic inclination trends at both Sites 1213 and U1347 imply that little time passed between the emplacement of individual flows. The implication is that Tamu Massif concluded with massive, high-effusion rate eruptions. Massive flows are also found at Sites U1349 and U1350, on Ori Massif's summit and flank, respectively, but the entire 53 m succession of igneous rocks cored at Site U1346, on the Shirshov Massif summit, consists of pillow lavas. The massive flow units are thinner at Ori Massif than most flows penetrated on Tamu Massif. Moreover, Site U1350 geochemical and paleomagnetic inclination trends imply greater time and more eruptive variability. The simplest conclusion from the observed trends in lava flow style across the three main edifices of Shatsky Rise is that the average eruptions become smaller and less effusive from Tamu to Ori to Shirshov massifs.

Recovered basement rocks from the two summit sites (U1346 and U1349) on Shirshov and Ori massifs show the most severe alteration, apparently from both low and moderately higher temperature fluid-rock interaction, the latter especially for Site U1349. In contrast, lavas cored on the deeper flanks of the massifs show evidence of only light to moderate low-temperature alteration. Although these highly altered sites represent only two individual cases, this dichotomy suggests that alteration and fluid-rock interaction was more intense on plateau summits. Apparently, the summits were a focus of heat and water circulation. Rocks at the flank sites (1213, U1347, and U1350) were apparently affected by lesser fluid flow and temperatures. Lavas at these sites seem to have been rapidly paved over by subsequent flows and thereby sealed from extensive seawater contact/circulation.

Several sites attest that volcanic debris is more important on Shatsky Rise than anticipated. A significant portion (~40 m) of the Site U1349 section, located on a summit ridge on Ori Massif, consists of volcanoclastic breccia. Site U1348, which is situated on a buried volcanic high on Tamu Massif, yielded a succession consisting entirely of volcanoclastic material, mainly hyaloclastic sediment. In addition, volcanoclastic sediments were found at Sites U1346 and U1347. These observations indicate that volcanoclastic eruptions made an important contribution to the formation of Shatsky Rise, especially on the higher, shallower parts of the volcanoes.

Shipboard geochemical data show that the lava flows consist of variably evolved tholeiitic basalt. Site U1347 and U1350 lavas, least affected by alteration, have broad similarities with Site 1213 basalts and display compositional ranges overlapping those of Ontong Java Plateau basalts and mid-ocean-ridge basalt (MORB), although more with

the latter. Samples from Site U1347 and many samples from Site U1350 resemble enriched-type ocean ridge basalts. A broad generalization is that Shatsky Rise basalts are slightly enriched in incompatible elements compared to normal MORB (N-MORB). This suggests a mantle source slightly richer in the more incompatible elements than N-MORB source mantle and/or that Shatsky Rise magmas formed by slightly lower degrees of partial melting and possibly in the presence of residual garnet. Alteration-resistant element ratios indicate that basalts from Sites U1346, U1348, and U1349 are also tholeiites. Site U1349 basaltic flows appear to represent significantly less differentiated magmas than those recovered from other sites and have similarities to picritic Ontong Java Plateau basalts (i.e., the high-Mg Kroenke type).

Multiple lines of evidence indicate that Shatsky Rise volcanoes had summits at or above sea level. Benthic foraminifers and/or sediment facies at all sites except Site U1350 (a lower flank site) show evidence of shallow-water deposition. Lavas at Site U1349 have alteration and flow structures consistent with subaerial eruption and weathering as well as intercalations of shallow-water sediments (e.g., oolites). Most of the volcanoclastic deposition at Site U1348 occurred below sea level, but the succession was topped with shallow-water sediment. Two of the sites showing evidence of shallow-water deposition (Sites U1347 and U1348) are significantly downslope from today's highest points of basement level on Tamu Massif, implying that the summit was a large, emergent island. All together, evidence from Expedition 324 strongly implies that during Jurassic and Cretaceous times, Shatsky Rise was an archipelago of large volcanic islands.

## Introduction and background

Knowledge about large igneous provinces (LIPs) has played a fundamental role in shaping the prevailing view of mantle geodynamics, that of largely plate-driven flow in the upper mantle punctuated by rising, thermally driven plumes from the lower mantle (e.g., Davies, 1992). The largest LIPs, which include the oceanic plateaus, continental flood basalts, and volcanic passive margins, reach volumes of several  $10^6$  to several  $10^7$  km<sup>3</sup> and are apparently the product of relatively short lived, massive magmatic episodes that represent the largest nonridge volcanic process on Earth (e.g., Coffin and Eldholm, 1994). In terms of magma flux, volume, and extent, such LIPs dwarf even the most prodigious present-day hotspots, such as Iceland and Hawaii. Magma production rate for the largest LIPs rivaled or even surpassed that of the global mid-ocean ridge system for short periods of time (e.g., Tarduno et al., 1991; Duncan

and Richards, 1991; Mahoney et al., 1993; Coffin and Eldholm, 1994). Moreover, because many of the largest LIPs formed during the Mesozoic, they may represent a mantle convection regime different from that of the ridge volcanism–dominated Cenozoic (e.g., Stein and Hoffman, 1994; Machel and Humler, 2003).

A widely accepted explanation for plateaus and continental flood basalts is the plume head hypothesis, which posits large (several hundred to ~2000 km in diameter), bulbous, primarily thermal diapirs that are created at depth in the mantle, probably within the core/mantle boundary zone, and which rise toward the surface, causing cataclysmic volcanism when they impact the lithosphere (e.g., Richards et al., 1989; Griffiths and Campbell, 1990). Similar to the related plume hypothesis for volcanism at hotspots (Morgan, 1972, 1981; Sleep, 2007), the plume head hypothesis has been accepted by many scientists because it provides a simple framework that seems to tie together many observations. Moreover, the plume head phenomenon occurs naturally in numerical and laboratory experiments, given appropriate rheologic conditions (e.g., Whitehead and Luther, 1975; Griffiths and Campbell, 1990, 1991). The trouble is that there is currently no unequivocal geological evidence proving that the plume head mechanism has operated within Earth. Many existing data are indirect indicators of eruptive rate and magmatic volume and could be explained by alternative hypotheses. Ongoing debate about the number, characteristics, and even existence of mantle plumes (e.g., Smith and Lewis, 1999; Anderson, 2001, 2005; Foulger, 2002; Courtillot et al., 2003; Sleep, 2003; Foulger and Natland, 2003; DePaolo and Manga, 2003; Foulger, 2007) makes it desirable to consider alternative explanations for plateaus. Because ocean plateaus are arguably the most direct expression of mantle plume heads (in contrast to continental LIPs, whose magmas must have passed through continental lithosphere), understanding oceanic plateau formation is thus critical to understanding mantle geodynamics.

In order to address the plume head versus alternative hypotheses, it is necessary to study a plateau for which the relation of the plateau to contemporaneous mid-ocean ridges is known. Unfortunately, this condition is not met for plateaus formed during the Cretaceous Normal Superchron (a.k.a., Cretaceous Quiet Period)—like the Ontong Java, Manihiki, and Kerguelen plateaus—because of the lack of magnetic reversals and thus linear seafloor magnetic anomalies to mark the locations of spreading ridges. Shatsky Rise, located in the northwest Pacific (Figs. **F1**, **F2**), is the only large intraoceanic plateau formed at a time of magnetic reversals. Contemporaneous magnetic lineations exist around and within the plateau, providing a framework that allows the development of a tectonic model (Nakanishi et al., 1999; Sager et al., 1999).

This model is currently based on geophysical inferences with little geological evidence from sampling.

Shatsky Rise is also unique because it has characteristics that suggest both plume head and ridge-controlled origins (Sager, 2005). The plateau's size, morphology, apparent eruption rate, and age progression are consistent with a plume head origin (Sager and Han, 1993; Nakanishi et al., 1999; Sager et al., 1999; Sager, 2005). In contrast, the plateau formed at a triple junction during a time of ridge reorganization, which suggests a link to ridge tectonics (Sager et al., 1999; Sager, 2005). Furthermore, Nd-Pb-Sr isotopic data for the few basalts cored and dredged from Shatsky Rise prior to Expedition 324 show a similarity to Pacific mid-ocean-ridge basalt (MORB), not the expected ocean island-type signature of a plume head eruption (Mahoney et al., 2005). Whether or not this MORB affinity is representative of all of Shatsky Rise or whether it characterizes only a few minor, late-stage magmas is a major unanswered question. However, the fact that existing data can be interpreted both ways suggests that this plateau is uniquely suited for testing plume head versus ridge tectonics models. Moreover, because several, perhaps many, oceanic plateaus formed at triple junctions (e.g., Winterer et al., 1976; Larson et al., 2002; Sager, 2005; Ishikawa et al., 2005; Smith, 2007), Shatsky Rise probably represents a significant class of ocean plateau, if indeed it is not representative of all.

## **Plateau formation hypotheses**

Ocean plateaus are remote and difficult to sample. The resulting geological ignorance has led investigators to propose several plateau-formation mechanisms. One class of explanation calls upon anomalous behavior of tectonic plates, such as leaky transform faults (Hilde et al., 1976) or spreading ridge reorganizations (e.g., Anderson et al., 1992; Foulger, 2007). Another class invokes a mantle plume, usually as a plume head (Richards et al., 1989; Mahoney and Spencer, 1991; Duncan and Richards, 1991; Coffin and Eldholm, 1994). A third type of mechanism explains plateau formation as a result of a large meteorite impact (Rogers, 1982; Roddy et al., 1987).

The mantle plume hypothesis has been widely accepted, in part because of known shortcomings or lack of development of other hypotheses. The meteorite impact hypothesis was first proposed before discovery of the Chicxulub impact crater (e.g., Hildebrand and Boynton, 1990) and several other large impact sites that were subsequently documented on the continents. Combined with a lack of evidence linking plateaus and impacts, the idea lay fallow for many years. However, this hypothesis

has been revisited for the Ontong Java Plateau (Ingle and Coffin, 2004; Tejada et al., 2004) because evidence from the plateau does not neatly fit other hypotheses. Plate boundary mechanisms have gained only limited support, partly because they require the assumption of extensive regions of shallow, near-solidus asthenosphere that differ geochemically from the shallow asthenosphere that forms mid-ocean ridges, and partly because they may not be able to produce the volumes of magma required for the largest plateaus, such as the Ontong Java. Creating LIPs by cracks, even in a thick part of an oceanic plate, requires that a seemingly small perturbation unleash a massive volcanic event. Consequently, large volumes of anomalously warm asthenosphere or unusually chemically “fertile” (fusible) mantle, primed to undergo massive decompression melting, must be assumed (Anderson et al., 1992; Foulger, 2007).

Plume-based explanations for plateaus have been bolstered by a wide acceptance of the mantle plume hypothesis for oceanic islands. The idea that thermal (and perhaps chemical) instabilities from the lower mantle rise to the base of the plate and cause hotspot volcanism initially became popular because it provided a neat explanation for age-progressive volcanic chains (Wilson, 1963; Morgan, 1971, 1972; Glen, 2005; Anderson and Natland, 2005). As more age-progressive seamount chains have been found, this explanation has been used repeatedly, with one result being an unlikely large number of proposed plumes. In part, this problem stems from loose application of the plume definition. Recent reexamination of hotspots led Courtillot et al. (2003) and Anderson (2005) to conclude that only a small number fit the original plume concept, that of a thermal diapir originating at or near the core/mantle boundary. Instead, many hotspots, especially smaller ones, likely have shallower sources that may or may not be related to significant thermal upwelling.

The plume head hypothesis arose as an offshoot of the traditional plume hypothesis. It was observed experimentally that if viscosity conditions are appropriate, then perturbations in a gravitationally unstable fluid layer form large, bulbous heads that rise through the overlying fluid and that the heads are followed by tails of rising, lower-layer material (Whitehead and Luther, 1975; Richards et al., 1989; Griffiths and Campbell, 1990). Such models led to the idea that mantle plumes form near the core/mantle boundary, begin with massive diapirs (plume heads) that rise through the mantle and are fed and followed by a narrow conduit of the same lower-layer material (plume tail). Other versions of the plume-head model start plumes from a shallower level, which serves either as the primary source region (e.g., Allègre and Turcotte, 1985; White and McKenzie, 1989; Kellogg et al., 1999) or as a barrier to a lower-mantle plume head, which then creates an upper-mantle plume head by heating from be-

low (Tackley et al., 1993). All of these hypotheses are similar in that they require large thermal (and/or chemical) anomalies that arise at depth and carry deep mantle material to the base of the plate.

Impingement of a plume head on the lithosphere is thought to lead to voluminous production of basaltic magma, forming an oceanic plateau or continental flood basalt, depending on the type of lithosphere (e.g., Richards et al., 1989; Campbell, 1998). Wide acceptance of this hypothesis rests on radiometric ages indicating that several flood basalts and plateaus were formed rapidly, on the ocean island-like Nd-Pb-Sr-Hf isotopic signatures of many flood basalt sources, and on several long-lived seamount chains that can be traced back to a flood basalt province (e.g., Campbell, 1998). Recently, however, dating results from Ocean Drilling Program (ODP) Leg 183 on the Kerguelen Plateau and the Caribbean LIP indicate a longer, more complex emplacement history than previously thought (Duncan, 2002; Coffin et al., 2002; Hornle et al., 2004). Also, although Ontong Java basalts have an ocean island-type isotopic signature and most of the plateau appears to have formed rapidly (at ~120 Ma), an associated postplateau seamount chain is lacking; plus, the initial depth of much of the plateau was well below that predicted by the plume head model and the amount of post-eruptive subsidence has been less than predicted (e.g., Mahoney et al., 2001; Fitton et al., 2004). The effect of such complications for the plume head model is still being sorted out.

One possible explanation for complex geologic histories for plumes comes from the thermochemical plume hypothesis, in which plume buoyancy is fueled not only by a difference in temperature between the plume and surrounding mantle, but also by density differences resulting from chemical composition (Davaille et al., 2003, 2005; Farnetani and Samuel, 2005; Lin and van Keken, 2006a, 2006b). The primary implications of this type of plume is that it may not behave as a simple thermal plume would, potentially having an extended residence in the lower mantle, perhaps stalling at intermediate mantle depths and not resulting in the magnitude of uplift expected from a thermal plume, and having more than one pulse of flood basalt volcanism.

## **Why study Shatsky Rise?**

During the middle 1990s, scientific ocean drilling studies focused on Kerguelen and Ontong Java plateaus because they are by far the largest, most outstanding examples of LIPs. A serious limitation to understanding the origin of these two plateaus is that

they formed mainly during the Cretaceous Long Normal Superchron, so their relationship to contemporaneous spreading ridges cannot be determined. Shatsky Rise is important because it is the only large intraoceanic plateau that formed during a time of magnetic reversals and the magnetic lineations that run through the plateau (Fig. F3) imply that it formed at a triple junction. Knowledge of oceanic plateaus is still so rudimentary that we cannot be certain whether Shatsky Rise and Ontong Java Plateau, for example, formed by the same mechanism. Many other plateaus have formed at triple junctions (Sager, 2005), so Shatsky Rise probably represents a class of ridge-related plateaus, if not all ocean plateaus.

Although there are a dozen or so large oceanic plateaus, Shatsky Rise is unique in its setting and holds critical clues to understanding plateau formation. It is a high priority for study for a number of reasons.

- With an area of  $\sim 4.8 \times 10^5 \text{ km}^2$  (about the same as Japan or California) and a total volume of  $\sim 4.3 \times 10^6 \text{ km}^3$ , Shatsky Rise is one of the largest ocean plateaus (Sager et al., 1999). Moreover, bathymetric ridges and lava geochemistry suggest Shatsky Rise and Hess Rise (Fig. F1) may have arisen from the same source (Bercovici and Mahoney, 1994), which would nearly double the magmatic output. Magmatism of this scale requires something significantly unusual about the physical and/or chemical state of the source mantle.
- The fact that Shatsky Rise formed during a time of magnetic reversals makes it easier to understand than any other large ocean plateau. Magnetic anomalies can be used not only to date the plateau and surrounding lithosphere, but also to understand how plateau morphology is related to ridge tectonics (e.g., Sager et al., 1999; Nakanishi et al., 1999).
- Morphology, apparent age progression, and magnetic lineations together indicate that the rise volcanism was spread out laterally, perhaps owing to rapid movement of the Pacific plate over the source mantle (Nakanishi et al., 1999; Sager et al., 1999). In contrast, the volcanic record of larger plateaus formed on a slowly moving plate (e.g., Ontong Java Plateau) may mainly consist of a vertically stacked pile. Therefore, the tectonic and geochemical evolution of Shatsky Rise is easier to address through drilling (i.e., shallow holes distributed laterally).
- Shatsky Rise formed at a ridge-ridge-ridge triple junction of rapidly spreading ridges; consequently, the lithosphere was young and thin, so lithospheric contamination of magmas should be minimal.
- Because of its location exactly along the track of a migrating triple junction and the fact that it appears to share both ridge and plume characteristics, Shatsky Rise is

uniquely suited to testing plume head versus ridge-controlled hypotheses of plateau genesis.

Why was drilling required on Shatsky Rise? Although the main edifices of Shatsky Rise have some basaltic outcrops, dredged samples of igneous basement suitable for geochemical and geochronological work have proven difficult to get and harder to study. Because of the Late Jurassic to Early Cretaceous age of the oldest part of the plateau, outcrops on these edifices have probably been exposed for long periods. All outcrops dredged to date are coated with thick ferromanganese oxide deposits that make basement rock recovery difficult. Likewise, all existing dredge samples are highly altered. Although dredged basalts were recovered during the 1994 site survey cruise, the recovered samples are highly altered and did not produce reliable radiometric dates, even with modern techniques (M. Pringle, unpubl. data). Likewise, all but a very few samples were unsuitable for chemical or isotopic studies (Tejada, 1998; Tatsumi et al., 1998). In addition, the dredge sites were all promontories, ridges, and other high points that may not be representative of the main plateau-building lavas. In sum, the only way to obtain samples that can address the origin of Shatsky Rise is by drilling a series of holes across the plateau and recovering hundreds of meters of basement igneous rock.

## **Prior research on Shatsky Rise**

By the late 1960s, it was known that Shatsky Rise is ancient because Early Cretaceous sediments were cored from its summit (Ewing et al., 1966). Although seismic refraction experiments have not yet imaged the Moho beneath the high parts of the plateau, they have revealed anomalously thick crust with a similar velocity structure to normal oceanic crust but several times thicker (Den et al., 1969; Gettrust et al., 1980). Seismic profiling showed that the tops of the rise edifices hold thick piles of pelagic sediments (up to 1.2 km), whereas sediments on the rise flanks are thin or absent in places (Ewing et al., 1966; Ludwig and Houtz, 1979; Neprochnov et al., 1984; Sliter and Brown, 1993).

Several Deep Sea Drilling Project (DSDP) and ODP cruises have cored Shatsky Rise over a span of 32 years. In succession, DSDP Legs 6 (Sites 47–50), 32 (Sites 305 and 306), and 86 (Site 577) as well as ODP Legs 132 (Site 810) and 198 (Sites 1209–1214) cored atop the highest, southern massif of the rise (Tamu Massif) (Fig. F2). Many of the holes had only shallow penetration. Drilling during Leg 32 probed deep into the sedimentary cap, recovering Berriasian (earliest Cretaceous) sediments ~50 m above

the expected level of basement at Site 306 (Fig. F2). This finding was significant because it implied that Tamu Massif formed during latest Jurassic or earliest Cretaceous time. Coring during ODP Leg 198 recovered sediments from all three of the Shatsky Rise massifs (Shipboard Scientific Party, 2002a), including Ori Massif (Site 1208) and Shirshov Massif (Site 1207). At both sites, only the upper part of the sedimentary section was cored, reaching Late Cretaceous sediments. Igneous basement has been reached only twice. During Leg 6, drilling stopped at the top of supposed basement at Site 50, recovering only a few pebbles of basalt, perhaps from a basal conglomerate (Fischer, Heezen, et al., 1971). At Site 1213 on the southwest flank of Tamu Massif (Fig. F2), a 46 m section of slightly altered basaltic flows or sills intruding earliest Berriasian sediments (Shipboard Scientific Party, 2002b) was cored. These basalts produced the first reliable radiometric date for Shatsky Rise, as well as valuable chemical and Nd-Pb-Sr isotopic data (Mahoney et al., 2005).

Magnetic lineations mapped in the northwest Pacific revealed that Shatsky Rise sits at the confluence of two lineation sets, the northeast-trending Japanese lineations and the northwest-trending Hawaiian lineations (Fig. F3) (Larson and Chase, 1972; Hilde et al., 1976). This circumstance indicates that the plateau formed at a triple junction separating the Pacific, Farallon, and Izanagi plates (Larson and Chase, 1972). Subsequent studies revealed that the triple junction jumped repeatedly during the time it occupied the location of the rise and that it must have been geometrically unstable to follow the path of the rise (Sager et al., 1988, 1999; Nakanishi et al., 1999). Furthermore, age constraints (Cretaceous sediments and the Site 1213 radiometric date), seismic stratigraphy, and isostatic compensation all indicate that the age of the rise is near that of the adjacent seafloor (Sager et al., 1999), implying that the triple junction and rise formation are linked. Current thought is that a plume head is the link—a source of heat, uplift, and volcanism that both created the rise and captured the triple junction (Sager et al., 1988, 1999).

Magnetic data were also instrumental in supporting the idea that Shatsky Rise formed from a plume head. Sager and Han (1993) postulated that the rise formed rapidly, based on modeling of the magnetic anomaly over Tamu Massif. They noted that the magnetic anomaly implies a mainly reversed polarity, in turn implying that most of the edifice may have formed during a single interval of reversed polarity. With simple calculations using the massif volume and an estimate of the length of the single polarity period, the authors inferred that the massif formed with an eruption rate similar to those of several large flood basalts ( $\sim 1.8 \text{ km}^3/\text{y}$ ).

More recent analyses have refined and expanded these conclusions. Paleomagnetic analysis of Site 1213 basalt samples gives inclination values that are most consistent with a reversed magnetic polarity (Tominaga et al., 2005). Furthermore, the mean  $^{40}\text{Ar}/^{39}\text{Ar}$  age from two basalt samples is  $144.6 \pm 0.8$  Ma ( $2\sigma$ ) (Mahoney et al., 2005), a value indistinguishable from the age of the Jurassic/Cretaceous boundary (145.5 Ma) and which correlates with magnetic Anomaly M19 in the Gradstein et al. (2004) timescale. This result limits the formation of much of the Tamu Massif to between Anomalies M21 and M19, a period of 1.5 m.y. If Tamu Massif formed during a single polarity interval, it is likely either M20 or M19, with durations of 0.4 and 0.75 m.y., respectively. Assuming the volume of the massif between Anomalies M21 and M19 formed in 1.5 to 0.4 m.y. (and making the conservative assumption that it formed on existing [very young] 7 km thick crust) implies volcanic emplacement at rates of 1.2 to 4.6  $\text{km}^3/\text{y}$  (Sager, 2005). Again, such values are in the range of estimates for several large continental flood basalts (e.g., Richards et al., 1989; Johnston and Thorkelson, 2000). Although these estimates are intriguing, they were made by very indirect means and require confirmation from radiometric ages of igneous basement samples, particularly from other locations on the rise.

## Formation and tectonic history of Shatsky Rise

Much of what is known about the tectonics of Shatsky Rise is based on the magnetic lineations that surround the plateau and in some places transect it (Fig. F3) (Sager et al., 1988; Nakanishi et al., 1989, 1999). The lineations range from M21 (148–149 Ma; polarity ages from Gradstein et al., 2004), bordering the southwest edge of the plateau, to M1 (125–128 Ma) at the northern tip of Papanin Ridge (Figs. F2, F3). Magnetic lineations have been mapped on the southeast flank of Tamu Massif, on flanks all around Ori and Shirshov massifs, in the basins between massifs, and all through Papanin Ridge (Fig. F3). Indeed, little of Shatsky Rise is without magnetic lineations. This observation led to the conclusion that the rise consists of three large edifices (Tamu, Ori, and Shirshov massifs) surrounded by lithosphere that is not greatly modified by plateau-building igneous activity (Sager et al., 1999; Nakanishi et al., 1999).

Shatsky Rise volcanism displays a progression in both age and volume along the trace of the triple junction. Rise volume decreases markedly with distance from Tamu Massif. This edifice has an estimated total crustal volume of  $2.5 \times 10^6$   $\text{km}^3$ , whereas Ori and Shirshov massifs each have volumes of  $0.7 \times 10^6$   $\text{km}^3$ . Papanin Ridge, at the north end of the plateau, has a volume of  $0.4 \times 10^6$   $\text{km}^3$ , and the low ridge implies a low volcanic flux over a long period (Sager et al., 1999). Age also apparently decreases with

distance from Tamu Massif with the ages of the volcanic edifices close to that of the underlying lithosphere, as suggested by isostasy (Sandwell and MacKenzie, 1989). The 144.6 Ma date for the Site 1213 sills is close to Anomaly M19, implying the bulk of the massif is Anomaly M19 age or older. Ori and Shirshov massifs must be younger than Tamu Massif because they reside on lithosphere younger than Anomaly M19. The youngest magnetic lineation beneath both Ori and Shirshov massifs is Anomaly M14 (140 Ma) and Papanin Ridge is underlain by Anomalies M10 to M1 (134–125 Ma). These observations are consistent with a northeastward-younging trend and volcanism following the triple junction path.

Magnetic lineations also show that a geometrically stable triple junction was moving northwest (in a Pacific plate reference frame) prior to Anomaly M22 time (Fig. F4). At Anomaly M21 time, the triple junction began to reorganize, with the Pacific-Izanagi isochrons showing a 30° rotation, leading to microplate formation and an 800 km eastward jump of the junction to the location of Tamu Massif (Sager et al., 1988, 1999; Nakanishi et al., 1999). Afterward, until Anomaly M3 time (126 Ma) Shatsky Rise formed along the trace of the triple junction. During this time the triple junction jumped repeatedly—at least nine times (fig. 4 in Nakanishi et al., 1999). In addition, the main volcanic massifs have sides parallel to spreading ridges and transform faults. Together, these observations imply that rise volcanism was episodic and tied to ridge jumps (Sager et al., 1999).

## Prior geochemical data

Chemical and isotopic data from igneous rocks are important for understanding the formation of ocean plateaus because such data provide key information on mantle sources and the conditions of magma genesis. For Shatsky Rise, such data are few. Only a small number of dredges have recovered basalt and all of the samples are highly altered, making the interpretation of geochemical data difficult. Tatsumi et al. (1998) concluded from Nb-Zr-Y data that a seamount within the rise has an ocean island–like composition similar to volcanoes of the South Pacific Superswell region, a finding that was interpreted as evidence for a plume head, lower mantle source. Whether or not superswell mantle sources come from the lower mantle is a subject of debate (e.g., Janney and Castillo, 1999; Lassiter et al., 2003; Natland and Winterer, 2005), but in any case the seamount is located in a basin between Tamu and Ori massifs (dredge D11; Fig. F2) and may have been formed after the rise itself.

In contrast, the Site 1213 basalts and two of the least altered dredge samples from the Tamu and Ori massifs (dredges D9 and D14; Fig. F2) display distinctly MORB-type isotopic characteristics (Mahoney et al., 2005). Age-corrected Nd and Pb isotope ratios of these rocks (e.g.,  $\epsilon\text{Nd}_{(t)} = +9.8$  to  $+8.6$ ) are within the range for Pacific MORB and, despite seawater alteration effects, Sr isotope values (0.70269–0.70302) are also MORB-like (Fig. F5). Furthermore, the Site 1213 basalts have broadly MORB-like incompatible element patterns (Fig. F5). The plume head model predicts ocean island-like, not MORB-like, isotopic compositions (e.g., Campbell, 1998). Thus, at face value the few existing data do not support a plume head origin. However, Site 1213 basalts were interspersed with sediments and the D9 and D14 dredge hauls sampled summit ridges; such late-stage volcanic products may not be representative of the main plateau-building lava pile beneath.

## Sea level indicators

A plume head should produce both dynamic and constructional uplift, implying that much of the area atop a plateau will initially be subaerial, particularly if formed on young lithosphere as with Shatsky Rise (e.g., Griffiths and Campbell, 1990, 1991). For most of Shatsky Rise, evidence on basement paleodepth is lacking; however, a dredge from the upper flank (dredge D12; Fig. F2) of Tamu Massif recovered shallow-water fossils (rudist casts and corals) (Sager et al., 1999). Because the summit of Tamu Massif is higher, it must have been at or above sea level. Furthermore, a flat summit on Shirshov Massif (beneath the sediment cap) is seen in seismic profiles (Sager et al., 1999) and may indicate erosion by wave action. Thus, it appears likely that conditions during emplacement were sufficient to raise some areas of the rise above sea level. The anticipated recovery during Expedition 324 of sediments (including benthic fossils) resting immediately above the igneous basement may help to constrain paleodepths of the rise summits.

## What formed Shatsky Rise—a plume head or ridge tectonics?

Shatsky Rise initially was attributed to plume volcanism because it is a very large, somewhat linear igneous construct (Sager et al., 1988; Nakanishi et al., 1989). Indirect evidence of a rapid eruption rate led to the proposal that the plateau formed from a plume head (Sager and Han, 1993; Nakanishi et al., 1989; Sager et al., 1999). At first blush, this explanation seems a good one. It predicts a trail of age-progressive volcanism tracking the motion of the plate over a nearly fixed source (Morgan, 1971, 1972). Shatsky Rise seems to fit this criterion because existing age constraints imply

that the rise becomes younger northeastward. Aseismic ridges and seamount chains connect Shatsky Rise with Hess Rise, apparently continuing the eastward-younging trend. Moreover, a similarity of ages and trends between Shatsky and Hess rise and the Mid-Pacific Mountains even suggests that the volcanic tracks record the motion of the Pacific plate over nearly fixed mantle sources (Sager, 2005).

Arrival of a plume head should cause voluminous flood basalt-type magmatism, with peak volcanism occurring over a brief period (<2 m.y. in several continental flood basalts), and significant amounts of initial uplift (e.g., Richards et al., 1989; White and McKenzie, 1989; Campbell and Griffiths, 1990; Duncan and Richards, 1991). As summarized above, existing evidence indeed suggests that at least the highest portions of Tamu Massif were initially shallow. Although emplacement rates are not known for most of Shatsky Rise, the radiometric age of the Site 1213 basalts combined with the nearby seafloor magnetic lineations suggests that Tamu Massif was constructed at a very high average rate between 1.2 and 4.6 km<sup>3</sup>/y. The upper value is more than a quarter of the 16.8 km<sup>3</sup>/y of new ocean crust (e.g., Larson, 1991) estimated to be formed worldwide today at ocean ridges. Moreover, the estimated  $1.8 \times 10^6$  km<sup>3</sup> volume of the initial Tamu Massif eruption implies a source volume equivalent to a sphere 224–408 km in diameter, assuming a mean melt fraction between 5% and 30% (cf., Coffin and Eldholm, 1994), a volume consistent with supply by an actively upwelling plume head.

The geometry of Shatsky Rise also appears to support the plume head hypothesis. Apparently, the emplacement rate of igneous rock waned with time, as shown by the northeastward decrease in size coupled with the ages inferred from magnetic lineations; this decrease is consistent with a transition from plume head to plume tail (Sager et al., 1999). A plume-type hypothesis is likewise an attractive explanation for the odd behavior of the Pacific-Farallon-Izanagi triple junction during the ~20 m.y. that the plateau was forming. The arrival of a plume head, a major source of heat and tensional stress on the lithosphere, is a potential reason for the initial 800 km jump of the triple junction. Heat and flux of upwelling mantle from a plume might have “pinned” the triple junction near the plume head (and later, tail), explaining the repeated triple junction jumps and the observation that the triple junction did not migrate away from the rise as it should have given the velocities of surrounding plates (Sager et al., 1988). In short, a plume head is a plausible explanation for many Shatsky Rise characteristics.

However, some important observations are not explained easily by the plume head model. The MORB-type isotopic signature of the existing Shatsky basalts already has been noted. Another nagging point is the ridge reorganization that occurred near the time that Shatsky Rise formed. Just after Anomaly M21 time, synchronous with the beginning of Shatsky Rise eruptions, the Pacific-Izanagi Ridge rotated  $\sim 30^\circ$  (Sager et al., 1988). It is generally accepted that plate motion is driven primarily by subduction (e.g., Lithgow-Bertelloni and Richards, 1998), so it is unclear how a plume head could cause plate velocity to change by acting on the trailing boundary at the ridge. Although a plume may tend to “capture” nearby ridges because it is a major source of heat and actively upwelling mantle (e.g., Kleinrock and Phipps Morgan, 1988), the ridge reorientation occurred  $>800$  km from the alleged plume center. If plume activity and plate motions are independent or only loosely coupled, as is widely believed (e.g., Eldholm and Coffin, 2000), the temporal proximity of these two events would have to be a coincidence.

Another apparent coincidence is the proximity of plume head and triple junction. Although a ridge or triple junction may jump or reorganize to stay near a plume (e.g., Kleinrock and Phipps Morgan, 1988), this assumes that the ridges are already near the plume. How likely is a plume head to rise within 800 km of a triple junction? Assuming plumes form randomly, the probability of one striking within 800 km of a triple junction is only  $\sim 0.4\%$ . Having a plume head randomly “find” a triple junction would seem to be a low probability event.

Curiously, western Pacific bathymetry and magnetic lineations seem to imply that other similar plume-ridge coincidences occurred. Some other plateaus formed along or near the paths of the Pacific-Farallon-Izanagi triple junction as well as the Pacific-Farallon-Phoenix triple junction, located on the east end of the Pacific plate. Moreover, many of these plateaus are located near proposed ridge reorganizations. After Shatsky Rise, Hess Rise may have formed near the track of the Pacific-Farallon-Izanagi triple junction as it jumped eastward. Similarly, Magellan Plateau, the oldest part of the Mid-Pacific Mountains, and probably the Manihiki Plateau were all formed near the track of the Pacific-Farallon-Phoenix triple junction (Sager, 2005). Explaining all of these plateaus by plume heads independent of ridge dynamics requires many recurrences of a low-probability event. To remain plausible, the plume head hypothesis must assume that plumes and triple junctions are somehow attracted to each other.

How could ridge tectonics lead to plateau formation? Triple junctions could be the key. Ridges that meet at a triple junction are a focal point for strong upwelling (e.g.,

Georgen and Lin, 2002), but present-day triple junctions are clearly not sites of plateau formation. The discrepancy between the excess volcanism associated with Late Jurassic and Early Cretaceous Pacific triple junctions and the paucity of such activity during the Late Cretaceous through Cenozoic may be explained by the “fertile” mantle hypothesis (a.k.a., the “perisphere” hypothesis; e.g., Anderson et al., 1992; Anderson, 1995; Smith and Lewis, 1999; Smith, 2003; Foulger, 2007). This hypothesis states that extensive regions of the shallow asthenosphere have a lower melting point (because of higher volatile content, a more mafic composition, and/or higher potential temperature) than the asthenosphere beneath the present-day ridge system. Although the fertile mantle hypothesis is rejected as a general explanation by some, the Late Jurassic–Early Cretaceous Pacific may be a very special case. During this period, much of the Pacific plate (which was then far smaller than at present) may have been located over an anomalously hot region of asthenosphere that now lies beneath the South Pacific Superswell and which has long been an area of oceanic island and seamount production (e.g., McNutt and Fischer, 1987; Staudigel et al., 1991). Today, this area is far from a spreading center and is characterized by several short-lived, poorly understood hotspots that may represent shallow-sourced plumes or entirely non-plume processes (e.g., Janney and Castillo, 1999; Lassiter et al., 2003; Courtillot et al., 2003; Koppers et al., 2003). Triple junction formation in such an area may have promoted excess melting of anomalously fusible mantle and thus plateau formation. The MORB-type isotopic ratios of the few existing Shatsky samples, all of which are from the last stages of volcanism at their sites, are explicable in this context because isotopically normal MORB-source mantle is predicted to underlie the shallow asthenosphere and to well up and gradually replace it as it melts out and advects away from the melting region (e.g., Anderson, 1995).

Finally, could the rise have been formed by meteorite impact, as Rogers (1982) suggested? This hypothesis readily accounts for the MORB-type isotopic ratios of the Shatsky Rise basalts, as removal of the lithosphere by the impacting object would cause massive melting of the underlying mantle, which normally should be MORB-type mantle. However, this hypothesis requires the coincidence of a large impact (itself a rare event) within 800 km of a preexisting triple junction, and it fails to explain the 30° Pacific-Izanagi Ridge reorientation at Anomaly M21 time and the lack of any evidence for the predicted massive destruction and disruption of seafloor over a very large area surrounding the impact site (Mahoney et al., 2005).

In summary, Shatsky Rise clearly formed in association with plate-velocity changes and ridge and triple junction reorganizations during a period when several plateaus

appear likely to have formed near ridges in general and triple junctions in particular. Although the plume head hypothesis can explain many features of Shatsky Rise, it requires significant ad hoc coincidences or modifications. Alternatively, the rise may be explained by anomalous volcanism induced by changes in plate boundaries and lithospheric stress over a region of anomalously fusible mantle. Such a hypothesis requires no coincidence of triple junction location and site of plume impingement and can explain the MORB-type signature of late-stage basalts from Shatsky Rise. However, it also relies on unusual circumstances. Indeed, no matter what the hypothesis, unusual circumstances of some sort appear to be required. At present, data for and against each hypothesis are incomplete and largely circumstantial, and new data are required to move debate forward. This was a primary reason for drilling Shatsky Rise.

## Site survey data and stratigraphic interpretation

### Data acquisition

The primary data used for selection of sites are low-fold seismic reflection profiles collected during Cruise TN037 of the R/V *Thomas G. Thompson* in 1994. This data set was also used for Leg 198 and is described in some detail in the Leg 198 *Initial Reports* (Klaus and Sager, 2002), including plots of most ship tracks and seismic lines. Cruise TN037 also collected swath bathymetry, gravity, and magnetic data. Bathymetry and magnetic anomaly analyses are described in Sager et al. (1999) and Nakanishi et al. (1999), respectively.

Seismic data were collected with a six-channel Teledyne streamer with 25 m active sections. On any given seismic line, one of two alternate seismic sources was used: (1) a single generator-injector air gun (45/105 in<sup>3</sup>) or (2) a four-air gun array (80, 108, 150, and 200 in<sup>3</sup>). The generator-injector air gun was mainly used for seismic lines shot between the main bathymetric edifices. It was towed at ~7 nmi/h and achieved two-fold coverage. The air gun array was used primarily on the mountain tops to penetrate the thicker sediment cover in those locations. The array was typically towed at ~5 nmi/h and it provided three-fold coverage. Data were digitized at a 1 ms rate and recorded in Society of Exploration Geophysicists (file format "Y") format. Final shot spacing was 25–37 m. The data were processed through to migration using Sioseis and ProMax software (Klaus and Sager, 2002). Included in the processing train were band-pass filtering (30–150 Hz to 0.25 s two-way travelttime [TWT] below seafloor, 20–150

Hz from 0.25–1.0 s TWT, and 6–70 Hz below 1.0 s TWT), deconvolution, normal moveout correction, stacking, and finite difference migration.

## Seismic stratigraphy

Interpretation of the seismic layering is relatively straightforward because of the drilling previously done on Shatsky Rise. A review of the stratigraphy cored during Leg 198 as well as previous cruises is contained in the Leg 198 *Initial Reports* (Shipboard Scientific Party, 2002a). In general the summits of the high edifices of Shatsky Rise contain thick sections (up to ~1.2 km thickness) of pelagic sediments. Over the flanks, this sedimentary section is usually much thinner or absent.

The sediment pile is mainly Cretaceous chalk and limestone covered by Cenozoic ooze. Sliter and Brown (1993) divided the section into five units and this was found to be consistent with Leg 198 drilling results (Shipboard Scientific Party, 2002a). Units I and II consist of foraminifer nannofossil ooze with minor clay. Unit I is Neogene in age (often Miocene to Holocene), whereas Unit II is of Paleogene age. Both have similar seismic character, with parallel-continuous layers, and are often separated by a seismic horizon of modest strength. Units III–V consist of Cretaceous chalk and occasional limestone layers with minor clay and abundant layers and nodules of chert and porcellanite. Indeed, the soft chalk layers interspersed with hard chert and porcellanite have frustrated efforts to recover cores from the top of Shatsky Rise since the beginning of scientific ocean drilling. The three Cretaceous units are often divided by two prominent seismic horizons, dubbed R1 and R2 by Sliter and Brown (1993). In addition, the Leg 198 scientific party used R0 for the horizon nearest the top of the Cretaceous section. The uppermost and lowermost Cretaceous layers show depositional character that is most uniform; however, the middle unit is more sculpted and often shows evidence of erosion and onlap with instances of slumping. The uppermost Cretaceous layer (Unit III) is Turonian to Maastrichtian in age and lies between R1 and R0. The mid-Cretaceous layer (Unit IV) is Aptian to Cenomanian in age and is bounded by R2 and R1. At the bottom of the pile is Unit V, which is Berriasian to Barremian in age and resides between igneous basement and R2 on seismic profiles.

The Cruise TN037 seismic data occasionally show some character in the portion of the record interpreted as igneous basement. Usually, seismic basement is a strong, irregular reflector below which few coherent reflections are seen. In some places on the Ori Massif, dipping reflectors were noted in acoustic basement. These are likely to be dipping lava flows. On the southwest flank of Tamu Massif, igneous basement was

a surprise. All along the seismic line over that flank of Tamu Massif, seismic basement has an odd, layered appearance for about 0.1 s TWT below the interpreted top of the igneous section. Drilling at Site 1213 during Leg 198 cored 46 m into acoustic basement with this signature, recovering three flow units interpreted as sills (Shipboard Scientific Party, 2002b). At most proposed sites on Shatsky Rise, acoustic basement is strong, has no consistent internal reflectors, and is interpreted as the top of the lava pile.

## Scientific objectives

### Testing plume and plate models

The primary objective of drilling on Shatsky Rise was to sample relatively fresh igneous basement rocks at multiple sites on the plateau. Such samples would allow several important problems to be addressed.

*1. Determine the basement age to constrain the time evolution of the plateau.*

Along with the preexisting radiometric dates from Site 1213, geochronologic data will show whether Tamu Massif erupted in a short period, as is currently postulated. A short time span suggests a plume head-like eruption, whereas a longer time span may indicate lower rates of effusion inconsistent with a plume head. The age distribution will place constraints on the type of mechanisms that can explain the initial Shatsky Rise eruptions. In addition, dates from the other Shatsky Rise edifices, Ori and Shirshov massifs, will show whether these edifices were constructed at or near the time of crustal formation and whether the northern part of Shatsky Rise shows an age progression.

*2. Determine geochemical and isotopic compositions of igneous rocks cored from Shatsky Rise.*

Although the signature of a lower mantle source is still debated, it is widely expected that mantle plumes erupt igneous rocks with ocean island basalt (OIB) chemical composition and isotopic characteristics postulated to represent the lower mantle or portions of it, such as high ratios of  $^3\text{He}/^4\text{He}$  (e.g., Courtillot et al., 2003). Patterns of geochemical variation across Shatsky Rise will also help establish the plateau formation mechanism. For example, variability could be consistent with evolution or zoning of the mantle source or, alternatively, geochemical characteristics could be homogeneous, as is the case for sampled portions of the Ontong Java Plateau.

3. *Determine the source temperatures and degrees of partial melting that produced Shatsky Rise lavas.*

Estimation of source temperatures and the degree of partial melting could be critical to distinguish between an upper or lower mantle source or to test models of abnormal mantle fertility for Shatsky Rise lavas. In general, high degrees of partial melting would be expected for a plume head eruption that is associated with high mantle temperature, especially in locations where the lithosphere is thin (e.g., near a ridge-ridge-ridge triple junction). For example, partial melting of as much as 30% is interpreted for Ontong Java Plateau basalts from phase petrology and the pattern of incompatible element abundances from igneous rock samples (Fitton et al., 2004). On the other hand, regions of abnormally high mantle fertility tapped by the triple junction could result in similarly large melt fractions and high melt extraction rates (e.g., Foulger and Anderson, 2005). Evidence for source temperatures above the ambient mantle temperature, however, may be an important indicator for the existence of thermal (deep-sourced) mantle plumes. Recently, Putirka (2008) proposed an improved method of olivine thermometry to estimate mantle source temperature. Herzberg et al. (2007) also proposed a method to estimate the mantle temperature by using major element composition and phase equilibria. Such approaches may be particularly powerful if combined with results from other studies such as combined He and Os isotope studies (e.g., Brandon et al., 2007).

## **Large igneous province geology**

1. *Determine the physical volcanology of Shatsky Rise eruptions.*

Shatsky Rise is a monster volcanic construct. Although they share many characteristics with the thousands of seamounts scattered across the Pacific plate, the Shatsky Rise volcanic edifices exhibit some important differences. One of the more notable is the slope of the rise volcano flanks, which is much lower ( $\sim 1^\circ$ ) than those of typical seamounts ( $\sim 5^\circ$ ) (Sager et al., 1999). Another is the apparent mantling of Tamu Massif's southwest flank by sills or sheet flows, as interpreted from Site 1213 data and the seismic character of acoustic basement. Both observations may be indicative of high-effusion rate eruptions. Thus the volcanic stratigraphy may provide important clues about the eruptions of Shatsky Rise igneous rocks. This stratigraphy will be developed from description of igneous rock cores and comparison with logging data.

*2. Determine the magnetic polarity of TAMU Massif and paleolatitudes of Shatsky Rise.*

From a study of the magnetic anomaly of Tamu Massif, Sager and Han (1993) concluded that the edifice is largely of reversed magnetic polarity and was therefore erupted in a short period of time during a period of reversed magnetic polarity. Although inconclusive owing to the small number of independent samples of the magnetic field and the low paleolatitude, the paleomagnetism of igneous samples from Site 1213 is consistent with reversed polarity (Tominaga et al., 2005). Paleomagnetic studies of Tamu Massif sites will establish whether other sites are also of reversed polarity, which would support the hypothesis that this massif formed in a short period of time. In addition, the Jurassic and Early Cretaceous paleolatitude of the Pacific plate is uncertain, so paleomagnetic samples from Shatsky Rise have the potential to help establish the paleolatitude of the rise and the Pacific plate.

*3. Determine paleodepths of Shatsky Rise.*

Evidence of subaerial or shallow water paleodepths for the summits of Shatsky Rise massifs will be useful for constraining models of plateau formation. Plume head models predict significant uplift associated with introduction of a large starting-plume head beneath oceanic lithosphere (e.g., Olson and Nam, 1986). Indeed, there is evidence that the Kerguelen Plateau formed subaerial landmasses that later subsided below sea level as they moved away from the plume head source (Wallace, 2002). In contrast, Ontong Java Plateau basalts were emplaced well below sea level (Fitton et al., 2004). Seismic profiles of Shatsky Rise also imply that summits of Tamu Massif and Shirshov Massif were above sea level at eruption and subsided to the present depth, but the prediction has yet to be confirmed by sampling. Samples collected during coring of the rise summits during Expedition 324 will establish whether they were originally shallow or subaerial or were emplaced in a deepwater environment. Paleodepths will be established from a number of different indicators, such as microfossils, the types and structures of sediments, conditions of alteration, and measurement of volatile abundances in basaltic glass (e.g., Roberge et al., 2005).

*4. Determine magma evolution and magma chamber process of Shatsky Rise.*

Geochemical studies of oceanic plateaus suggest that many compositional variations in extrusive lavas are controlled by magma evolution processes (fractional crystallization, magma mixing, assimilation, and reaction with cumulates) in large-scale magma chambers. Understanding magma evolution processes in large magma chambers will also help to understand the formation of the cumulative part of the lower

oceanic crust. For example, a primary picritic magma must have lost 20%–80% minerals by fractionation in shallow magma chambers to produce Ontong Java Plateau basalts (Fitton et al., 2004). Current geochemical data from Shatsky Rise, although sparse, also suggest basement rocks experienced significant fractionation before their eruption (Mahoney et al., 2005). However, the magma chamber scale and evolution mechanism of oceanic plateaus are not clear compared to well-studied MORB. Systematic basement sampling during this expedition could provide information about the magma evolution process from chemical variations of whole rocks. Examination of chemical zoning profiles of phenocryst phases (olivine, plagioclase, and clinopyroxene), recording physiochemical properties (temperature, pressure, and magma compositions) during their growth, can further contribute to reconstruct the history of magma evolution.

## **Coring and drilling strategy**

The goal of Expedition 324 was to core as much igneous rock as possible in the time available to the project. Science objectives dictated that this coring be distributed over a large area of Shatsky Rise, sampling all three major edifices (Tamu, Ori, and Shirshov massifs) to study geochemical, geologic, and age trends. Furthermore, because Tamu Massif is postulated as a possible plume head eruption, it was considered important to sample several sites across that edifice to examine trends within. The original proposal contained six drill sites as targets. Because of time limitations imposed by a long transit assigned to Expedition 324, this plan was cut to five sites, with three located on Tamu Massif and one each on Ori and Shirshov massifs. Proposed Site SRSR-8 (not drilled) was planned on the southwest flank of Tamu Massif, proposed Site SRSR-3B (Site U1347) at the summit of that edifice, and proposed Site SRSR-6 (Site U1348) was planned to sample the lower north flank. The other two sites, proposed Sites SRCH-5 (Site U1349) and SRNH-2 (Site U1346) were planned at the summits of Ori and Shirshov massifs, respectively.

Of these five sites, four were moved from the originally proposed locations to places where sediment cover was thinner for more rapid penetration of the sedimentary cover. In addition, the drilling plan, which only included rotary core barrel (RCB) drilling, was modified to drill through the uppermost sedimentary cover without coring to ~50 m above the presumed igneous basement. Although the primary purpose of this move was to speed up drilling through the sediment cover, it was deemed acceptable because the sediments have been cored on many drilling cruises and recov-

ery is usually very low because of hard cherts interfingering with soft chalk in the Cretaceous part of the sediment cap.

Because of time limitations, coring deeper than possible with a single bit was proposed only in one location, proposed Site SRSB-3B, on the summit of Tamu Massif. At three of the other sites, the strategy was to core only to ~100 m. For proposed Site SRCH-5, only a single bit was envisioned, but we would drill to bit destruction or ~200 m, whichever came first. Proposed Site SRSB-3B was the only multiple-bit hole planned. At this site, two bits would be used, with a free-fall funnel (FFF) for reentry, allowing penetration of ~200–300 m into igneous basement.

Although three of the proposed holes were to be short, downhole logging was planned at all sites. In each hole, two logging strings would be run, the triple combination (triple combo) and Formation MicroScanner (FMS). The triple combo would provide density, resistivity, and radiogenic isotope logs as well as caliper measurements that would assess the diameter and condition of the hole. Following the triple combo, the FMS log would be run to provide a resistivity-based image of the borehole wall. Often this log is run in tandem with the sonic log to acquire acoustic velocity data from the formation; however, because of the short length of planned Expedition 324 holes, the sonic log was not to be regularly paired with the FMS. At the planned deep-penetration site, proposed Site SRSB-3B, an additional log, the Ultrasonic Borehole Imager (UBI), an acoustic imaging device, was planned to provide an additional image of the borehole wall.

The final transit for Expedition 324 was to the south and this dictated that the drilling proceed from the northernmost site, proposed Site SRNH-2, to the southernmost, proposed Site SRSB-8, so that transit time would be minimized. This was not the ideal arrangement because Tamu Massif sites were given highest priority, but the lost time incurred by sailing back over Shastsky Rise on the final transit was unacceptable. This merely dictated that the science party keep close track of progress during the expedition so that operations did not get far behind the plan.

Although much of Expedition 324 went as planned, actual operations differed slightly from the plan because of weather and science-related changes (see [“Operations”](#)). After visiting Site U1346 as planned, passing typhoon Choi-Wan forced the ship to sail southward, away from Ori Massif. As a result, Site U1347 was the second site cored. Sites U1348 and U1349 were subsequently drilled in reverse order because the ship approached them from the south, rather than the north as planned. Finally,

proposed Site SRS8-8 was not cored at all. As the expedition waned, the science party decided that cores from this site would likely give samples of sheet flows similar to those at nearby Site 1213 (~50 km away). Instead, the science party decided to drill Site U1350, an proposed alternate site (SRCH-4) on the lower east flank of Ori Massif, as the last site during Expedition 324.

## Results

### Site U1346

Site U1346 is situated at the north edge of the Shirshov Massif summit in northern Shatsky Rise where acoustic basement is nearly flat, implying a subaerially eroded summit platform (Sager et al., 1999) (Figs. F6, F7). A single hole was drilled (Hole U1346A), penetrating 191.8 m below the seafloor, with 139.2 m of sedimentary cover and 52.6 m of igneous rock (Table T1).

Because the primary goal of drilling Hole U1346A was to recover the igneous basement, sediment coring began only ~70 m above the suspected basement/sediment interface. Despite difficult drilling conditions, ~4 m of sediments were recovered in the first six cores prior to entering into basaltic basement. The recovered sedimentary material represents various lithologies and depositional environments, with an average recovery of 10.2% between 100.5 and 141.7 m core depth below seafloor, method A (CSF-A). The uppermost sedimentary interval, stratigraphic Unit I (Cores 324-U1346A-1W through 3R) yielded only small isolated pieces of dark-colored chert fragments (Fig. F8). Recovery in Cores 324-U1346A-4R through 6R improved because of a reduction in the amount of chert in the formation. This short sequence of lithified sediments included an intriguing sequence of intermingled basalt and limestone in Section 324-U1346A-4R-1, interpreted as a debris flow (stratigraphic Unit II). In this unit, soft-sediment deformation occurs around the larger volcanic clasts indicating that the clasts impacted the sediment, either rolling downslope from the eruption source or as a mass flow deposit generated through post-eruptive erosion of the volcanic edifice. Section 324-U1346A-4R-2 contained a series of laminated volcanoclastic sequences, with grading from very coarse sand to clay, which are interpreted as turbiditic in origin (Unit III). The remaining sediments (stratigraphic Unit IV), from the base of Section 324-U1346A-4R-2 to the top of 6R-1, are composed of clay-bearing limestones and calcareous mudstones containing abundant shell fragments and other biogenic components, along with glauconite and altered volcanoclastics. Taken to-

gether, these components are suggestive of a relatively shallow marine depositional environment in close proximity to a volcanic material source.

Calcareous nannofossils in the recovered sediments are rare to abundant and moderately to poorly preserved. The age of four samples from Cores 324-U1346A-4R and 5R is assignable to the Berriasian to Hauterivian. Within the foraminifer assemblage obtained from Section 324-U1346A-4R-CC, the planktonic group is completely absent. Benthic foraminifers are well-preserved, diverse, and representative of the neritic-upper bathyal assemblage (estimated paleodepth  $\leq 500$  m). Various other biogenic sedimentary components were observed in the samples examined for foraminifer analyses; these were dominantly radiolarians with lesser amounts of ostracodes, inoceramid prisms, echinoid plates, sponge spicules, bryozoan, and carbonaceous fragments.

Basement coring at Site U1346 on Shirshov Massif documented a ~53 m thick stack of highly vesicular basaltic pillow lavas or lava “inflation units” (stratigraphic Unit V) beneath the succession of pelagic nannofossil-bearing chalks and cherts, volcanogenic silts and sands, and volcanoclastic debris (Fig. F9). Within the lava stack, individual pillow (or inflation) units were readily identified by the presence of chilled glassy margins, upper and lower chill zones (Fig. F10), characteristic pillow vesicle patterns, and crystal grain-size variations. In total, 40 individual “lava cooling units” were recognized in the cores from Unit V, but the entire unit was interpreted to represent a single eruptive event.

The pillow basalts are generally vesicular in nature and have zones that are moderately vesicular (30%–50% vesicles). Although they appear macroscopically aphyric, a closer inspection reveals that microphenocrysts of olivine and pyroxene were originally present but are now totally replaced by calcite. All samples contain large proportions of less altered, very fine grained plagioclase laths set in a variolitic matrix.

Extensive low-temperature water-rock alteration has left a marked impression on all igneous rocks recovered at this site, resulting in near complete replacement of pyroxene, olivine, and glassy pillow rinds and complete replacement of glassy mesostasis. In contrast, plagioclase shows only slight to moderate alteration. Based on rock color and mineralogy, three types of alteration were determined in Hole U1346A: (1) a green alteration, recovered only in volcanoclastic debris interspersed with sediment at the top of the hole (Unit II; interval 324-U1346A-4R-1, 0–39 cm); (2) a dark gray alteration; and (3) a brown alteration. In the basement pillow lavas, the dark gray alter-

ation is most abundant and is interspersed with the brown alteration throughout the hole. The most abundant secondary minerals observed in the basaltic rocks are clay minerals, and the nature of clay minerals changes with respect to alteration type, from predominantly green clays, including nontronite, in the green alteration, to green and brown clays in the gray alteration, including saponite, to mainly brown clays in the brown alteration. Calcite is also abundant in all alteration types, replacing pyroxene and olivine, rarely the groundmass, and filling vesicles and veins. Sulfide minerals are present only in stratigraphic Unit II and the upper portions of basement pillow lavas in Sections 324-U1346A-7R-1 and 8R-1. These mineral assemblages suggest that the basaltic rocks from Hole U1346A have extensively interacted with seawater-derived and CO<sub>2</sub>-rich fluids at low temperature and more locally with S-rich hydrothermal fluids.

Despite the moderate to complete alteration, shipboard analysis of major and several trace elements by inductively coupled plasma-atomic emission spectroscopy (ICP-AES) of lava samples recovered from stratigraphic Unit V reveals that the rocks are tholeiitic basalt (Fig. F11). The concentrations of many elements, including K, Si, Ca, P, Sr, Ba, and Ni, were modified significantly by the alteration. However, several elements, including Ti, Zr, Y, Cr, V, and Sc, appear to have been affected relatively little. Relationships among these elements indicate a strong similarity with the older basalts recovered from Site 1213, which lies ~870 km southwest of Site U1346.

Both syn- and postmagmatic structures can be recognized within the Hole U1346A igneous complex. The main synmagmatic structural features are amygdules, pillow structures, irregular vein networks or curved veins, and breccias. Postmagmatic structures include conjugate veins and joints. Dip angles of the veins in the hole from top to bottom become gradually steeper; however, joint dips are generally low. The structures observed throughout Unit V are consistent with the interpretation as a pile of stacked pillows whose sizes differ from ~20 to 200 cm.

Gamma ray attenuation (GRA) measurements of the basement sections reveal that there is low variability in bulk density despite changes in the style and degree of alteration. Magnetic susceptibility appeared to be a more sensitive tracer of alteration, and several regions were identified where magnetic susceptibility covaried with changes in alteration style. Thermal conductivity measurements averaged 1.52 W/(m·K), with no significant relationship with depth.

*P*-wave velocity measurements of 24 discrete samples showed no appreciable anisotropy or depth relationship and averaged 4.5 km/s throughout the core with a maximum of ~5.6 km/s and a minimum of ~3.5 km/s. Moisture and density measurements of bulk, dry, and grain density of the discrete samples confirmed indications from the GRA density (measured on whole cores) that there was little systematic change in the density of the basaltic sequence with depth. Porosity was high and ranged from 8% to 33%, with the highest values closer to the top of the hole.

In total, 20 discrete samples obtained from Hole U1346A were measured to investigate paleomagnetic remanence of the upper part of the Shirshov Massif basement. Most of samples show a stable component between 300°–475°C steps and have low unblocking temperatures (400°–450°C), which is characteristic of titanomagnetite (-magnetite). Alternating-field demagnetizations show that the magnetization is stable after 10–15 mT demagnetization. The samples from Hole U1346A are characterized by shallow negative inclinations with an arithmetic mean of  $-20.3^\circ \pm 5.3^\circ$  ( $1\sigma$ ).

Downhole logging data obtained from Hole U1346A included natural and spectral gamma ray, density, photoelectric factor (PEF), and electrical resistivity measurements from three depths of investigation. Interpretations of gamma ray and electrical resistivity downhole logs were used to identify 14 logging units in Hole U1346A with three in the section covered by the bottom-hole assembly (BHA), four in the sedimentary sequences in the open hole interval, and seven in the basaltic basement. The sedimentary sequence shows several prominent gamma ray anomalies associated with U enrichment. The most prominent anomaly is found at the sediment/basement interface and may be indicative of focused hydrothermal fluid flow. Shallower anomalies recorded through the BHA may represent oceanic anoxic events previously interpreted in this area. Electrical resistivity measurements in the basaltic basement show four distinctive massive zones characterized by higher resistivity values, which may represent individual thick lava flows. Relatively high K content in the basement section also indicates a high degree of hydrothermal alteration.

## Site U1347

Site U1347 is situated on the upper flank, east of the summit of Tamu Massif in southern Shatsky Rise (Fig. F12). The site location was chosen at a spot where sediments are thin and the “layered basement” signature seen elsewhere on southern Tamu Massif was also thin (Fig. F13). Drilling in a single hole (U1347A) penetrated 317.5 m below

the seafloor, including a 157.6 m sedimentary section and a 159.9 m igneous section (Table T1).

Coring recovered 17.7 m of sediment (stratigraphic Units I–III) in Cores 324-U1347A-1W through 11R over a stratigraphic interval of ~158 m before entering basaltic basement. The recovered sediments are dominated by radiolarian-rich volcanoclastic siltstones, with varying proportions of glauconite (Fig. F8). There are also minor intervals of chert and claystone. Bioturbation is often pervasive in the silty facies, with rip-up clasts and erosional contacts as common features, suggestive of turbulent and transient depositional events. Sediments were also present as relatively thin interbeds between the massive basaltic flows and pillow basalt units within the igneous complex. These sediments are similar in character and composition (e.g., predominantly radiolarian-bearing siltstones) to the sediments above basement, although some show features consistent with thermal alteration as a result of subsequent basalt emplacement.

Calcareous nannofossils and foraminifers from the sediments of Site U1347 are generally moderate to poor in preservation and low in abundance and diversity. Intercalated sediments in the underlying basement section are almost barren of both microfossil taxa. Fortunately, the age of four samples from Cores 324-U1347A-2R and 10R is assignable to the Berriasian to Valanginian based on calcareous nannofossils. The foraminifer assemblage is marked by the absence of planktonic forms. Benthic foraminifers, though the total number of specimens is limited, are characterized by a neritic assemblage in the lower part of the sediment section (Cores 324-U1347A-6R through 8R) and bathyal assemblage upsection (Cores 324-U1347A-1R through 2R). Therefore, an overall deepening trend from <200 m to 200–2500 m is inferred. Samples processed for foraminifer analyses are to a large extent dominated by volcanogenic lithic fragments and minerals; the major biogenic component is radiolarians with peaks in size, abundance, and diversity in Cores 324-U1347A-6R through 8R.

After penetrating the sediment section (stratigraphic Units I–III), a 159.9 m thick volcanic basement succession (Units IV–XVI) (Fig. F9) was encountered, consisting of “packages” of massive basalt flows and pillow inflation units intercalated by five sedimentary successions of up to ~5 m thick. Based on the dominant type of eruptive unit, the volcanic basement can be described in three main packages or groups. From top to bottom, these are: Group 1, an upper “layered” series of four massive lava flows (~8–19 m thick) (Fig. F14) intercalated with two ~5 m thick sediment packages and totaling ~60 m in thickness (Units IV, V, VII, and IX); Group 2, a ~75 m lava stack con-

sisting for the most part of pillow basalts (each ~0.2–1.0 m thick) (Fig. F15) and medium-sized inflation units (1–2 m thick), interspersed by relatively thin sedimentary intercalations and three larger (~3–6 m thick) basalt flows (Units X, XII, and XIV); and Group 3, a lower set of two particularly massive basaltic lava flows consisting of a very thick upper (~23 m) homogeneous lava flow that overlies a unit of similar character at the bottom of the hole (Units XV and XVI). In many instances, the high recovery (average = 64.2%) for Hole U1347A igneous basement yielded well-preserved lower- and upper-contact zones with chilled margins, baked sediment contacts, and folded pahoehoe-type upper crusts. The frequent recovery of thick (often fresh) glassy rinds within the pillow-unit stack indicates that alteration was essentially buffered in these rocks.

In Group 1 the three uppermost massive flows are aphyric (stratigraphic Units IV, V, and VII) and petrographically different from the sparsely to moderately pyroxene-plagioclase phyric basalt in the fourth flow (Unit IX) and the lavas lower in the succession. Examination of unit thicknesses within Group 2 reveals a pattern of repetition, beginning with massive inflation units, passing upward into predominantly medium-sized units, and then into a sequence of closely packed pillow lavas, before the cycle is repeated. These repetitions may represent repeated eruptive pulses during which the lava effusion rate diminishes. Group 3 includes the lowest two lava flows recovered (Units XV and XVI) with well-developed chilled margin zones at their tops (glassy to microcrystalline in the topmost ~2 m) and thinner ones (~0.5 m) at their bases. Thick glassy rinds were not recovered in these flows and vesiculation is confined to the upper 2–3 m, below which the flows become very homogeneous and massive and largely nonvesicular. It may be deduced from their large thickness that these are likely to be laterally extensive “tabular flow” units, possibly similar in dimension to those described in flood basalt provinces.

The majority of the volcanic units are plagioclase-pyroxene phyric basalts. Toward the cores of the lava flows and pillows, crystallinity increases to 50% and in some cases to 95%. Most notable are the appearance of plagioclase phenocrysts in the fourth massive flow in the upper volcanic series (stratigraphic Unit IX), the rarity or absence of clinopyroxene phenocrysts in the lower pillow stack (Units XII and XIV), and their absence in the lowermost massive flows (Units XV and XVI). In all cases the basalts were saturated in both clinopyroxene and plagioclase, whereby these minerals always seem to occur together as clusters, glomerocrysts, and intergrown in the matrix between the larger micro- and phenocrysts. The rocks appear, therefore, to have been in a condition of low-pressure plagioclase-clinopyroxene cotectic crystallization

during all stages of their cooling and differentiation. Olivine phenocrysts occur rarely as early coprecipitating liquidus minerals and now are completely replaced by clays and calcite. Remnants of fresh olivine with melt inclusions or spinel were discovered only in a few thin sections. Titanomagnetite is highly variable throughout the lava succession, which is also reflected in highly variable magnetic susceptibility measurements. For instance, glass in the chilled margins has no discernable titanomagnetite and consequently low magnetic susceptibilities. However, spherulitic overgrowths on plagioclases and larger (sometimes elongate skeletal) titanomagnetite grains increase significantly toward the cores of the (thicker) lava flows, well correlatable to increased magnetic susceptibility readings.

Overall, basalts of Hole U1347A appear to have more differentiated compositions compared with basalts from basement at several other sites cored on Shatsky Rise (Sites 1213, U1346, and U1349). This is evident from the predominance of plagioclase and clinopyroxene intergrowths at all stages of crystallization in these basalts, the scarcity of olivine, and the almost complete absence of Cr spinel. This phenocryst assemblage and character of intergrowths compare well to those of rather evolved low-temperature gabbros that formed in “shallow” crustal magma chambers beneath fast- and superfast-spreading ridges.

Alteration within the volcanic section varies from slight to moderate (estimated to range from 5% to 50%). Generally, both the primary mineralogy (with the exception of extensive olivine replacement) and even the finer spherulitic textures in the interstices between phenocrysts and microcrysts are well preserved, especially close to pillow margins. Sometimes fresh glass is still present in the groundmass. In contrast, away from the pillow margins, the glassy mesostasis in the general groundmass is almost completely replaced. Plagioclase and clinopyroxene are generally well preserved throughout the hole, either in the groundmass or as phenocrysts. Clay minerals, together with calcite, are the most abundant secondary minerals in Hole U1347A, replacing primary phases and glassy mesostasis and filling vesicles and veins. Pyrite is widespread throughout the hole, being present in the groundmass, vesicles, and veins. Three main types of veins were observed in Hole U1347A: (1) calcite veins, which predominate; (2) green clay veins, and (3) composite veins of calcite + green clays ± pyrite. There is an average of ~3 veins/m in the basement lavas and average vein thickness is ~1 mm. No significant variation in alteration mineralogy was observed in Hole U1347A and alteration of the basaltic rocks is interpreted to result from interaction with seawater-derived fluids at relatively low temperature (<100°C).

There are two kinds of structures distinguished within the igneous complex, pillow structures and sheet flow structures. The typical sheet flow structure is normally characterized by three parts: (1) the upper lava crust, (2) the middle lava core, and (3) the basal zone. Dip angles of both veins and joints in the hole become gradually steeper downhole. The entire structure of the Hole U1347A igneous complex is consistent with interpretation as stacked layers of pillows and massive basalt sheet flows. Taking the horizontal sedimentary bedding into account, structural observations indicate that the site has undergone no tilting or horizontal-axis block rotation.

Onboard measurements of major and several trace elements by ICP-AES reveal that the Site U1347 lavas are tholeiitic basalts (Fig. F11). The chemical effects of post-eruptive alteration are smaller than for samples of other Expedition 324 sites, especially the highly altered rocks cored at Sites U1346 and U1349. In general, both the major and trace element compositions of the Site U1347 basalts are consistent with them being variably more evolved relatives of the basalts at Site 1213 on the southern flank of Tamu Massif. Compared to normal ocean-ridge basalts, the Site U1347 lavas exhibit modest relative enrichment in the more highly incompatible elements, qualitatively similar to that seen in the Site 1213 basalts. This result suggests a mantle source slightly richer in the more incompatible elements than normal ocean-ridge source mantle and/or that the Site U1347 magmas formed by slightly smaller amounts of partial melting and possibly in the presence of residual garnet.

Magnetic susceptibility in the igneous material is typically  $\sim 2000 \times 10^{-5}$  SI and GRA density is from 2.4 to 2.6 g/cm<sup>3</sup>. The massive flow (stratigraphic Unit XV) below  $\sim 290$  m CSF-A notably reached magnetic susceptibilities as high as  $3800 \times 10^{-5}$  SI and also has the highest measured densities. Total counts of natural radiation measured in igneous material was between 2 and 4 cps throughout the hole, which is an order of magnitude less than observed at Site U1346. Fifty-eight thermal conductivity measurements of igneous material were performed, yielding an average of  $1.59 \pm 0.200$  W/(m·K) ( $2\sigma$ ). One sedimentary measurement of  $1.007 \pm 0.017$  W/(m·K) ( $2\sigma$ ) was also obtained. In general, the massive igneous units have slightly higher thermal conductivity than pillow units. This is seen particularly well in the final massive flow unit below  $\sim 290$  m CSF-A, which has a thermal conductivity of  $1.733 \pm 0.092$  W/(m·K) ( $2\sigma$ ;  $n = 11$ ).

*P*-wave velocity measured on discrete samples showed no appreciable anisotropy but appeared to vary with stratigraphic units. The massive flow (stratigraphic Unit XV) and upper pillow basalts (Unit X) have high compressional wave velocities (up to 7.04

km/s). The high velocities were coincident with low porosity (<5%) and high bulk densities (>2.75 g/cm<sup>3</sup>) measured by discrete sampling.

A total of 61 discrete samples were measured to investigate paleomagnetic remanence of the upper part of the Tamu Massif basement. Only about half of the samples demagnetized by thermal demagnetization show a stable component, whereas most samples demagnetized by alternating-field demagnetization show a fairly stable component between 15 and 80 mT. Most samples have low unblocking temperatures of ~300°–400°C, which is characteristic of titanomagnetite (-magnetite). We suggest four magnetic zones downhole: (1) the top igneous core section (Section 324-U1347A-12R-1) with shallow negative inclination ( $-6^\circ \pm 7^\circ$ ;  $1\sigma$ ); (2) Sections 324-U1347A-17R-2 through 26R-1 (stratigraphic Units IV–VII), with an average inclination of  $28^\circ \pm 13^\circ$ ; (3) Sections 324-U1347A-26R-2 through 29R-4 (Units IX–XIV), with an average inclination of  $20^\circ \pm 14^\circ$ ; and (4) Sections 324-U1347A-26R-2 through 29R-4 (Unit XV), with an average inclination of  $54^\circ \pm 27^\circ$ . Whereas results in upper three zones appear reasonably reliable, detailed rock magnetic analyses are necessary to interpret the erratic magnetic behavior of the lowermost zone.

Downhole logging data obtained from Hole U1347A included natural and spectral gamma ray, density, neutron porosity, PEF, and electrical resistivity measurements from three depths of investigation. Interpretations of gamma ray and electrical resistivity downhole logs were used to identify 15 logging units in Hole U1347A with 3 in the sediment sequences and 12 in the basaltic basement. These units correlate well with those defined by core material logging. Electrical resistivity measurements in the basaltic basement show distinctive high-resistivity zones that likely represent massive flows and pillow flow units interspersed with low-resistivity zones that mark sediment interbeds. Natural gamma ray measurements show five intervals of higher readings that indicate interbedded sediments within the basaltic basement. These sedimentary intervals also display higher K values. FMS images show zones of distinctive pillow lavas, zones with high fracture density, and intervals that seem to represent massive lava flows.

## Site U1348

Site U1348 is located on the north flank of Tamu Massif (Fig. F12). The target for drilling was the upper part of a basement high where sediments are thin (Fig. F16). A single hole (U1348A) was drilled at the site, with 324.1 m of penetration below the seafloor (Table T1).

A thick sequence (~120 m stratigraphically) of volcanoclastic sediments, topped with shallow water calcareous sandstones, greenish clays, nannofossil ooze, and chert, was recovered from Hole U1348A (Fig. F8). The uppermost cores (stratigraphic Unit I) contained red chert interbedded with a remarkably well preserved, section of Cenozoic–Late Cretaceous nannofossil ooze over a meter long (Core 324-U1348A-2R). Yellow brecciated cherts were also recovered stratigraphically below the red cherts and above highly silicified, altered sandstones. Below this, a sequence of shallow-water bioclastic sandstones (Unit II) with volcanic clasts was found (Cores 324-U1348A-10R through 13R). This sequence includes an interval of bright green zeolitic clays. Although basaltic basement was not reached at this site, Cores 324-U1348A-14R through 26R recovered a unique sequence of highly altered marine volcanoclastic rocks (Units III–VI). Based on the marine fossil content and bedding structures, these have been interpreted to represent a mixture of in situ and re-deposited material that was erupted in a submarine environment.

Micropaleontological investigations revealed that the sediments from the upper cores of stratigraphic Unit I (Cores 324-U1348A-1W through 10R) are pelagic in origin and, although recovery was dominated by chert-rich lithologies, are generally suited for calcareous microfossil studies. A few centimeters of gray ooze in the wash barrel's core catcher (Core 324-U1348-1W) and in the uppermost centimeters of the undisturbed nannofossil ooze are rich in the Cenozoic (Miocene) calcareous and siliceous microfossils (Core 324-U1348-2R). Microfossils of mid- to Late Cretaceous age occur in Cores 324-U1348A-2R through 10R. Calcareous nannofossils are subject to progressive reduction in the abundance, diversity, and preservation state with increasing burial depth. Planktonic foraminifers contained in this interval are generally well preserved and abundant. A series of primary/secondary zonal marker species that correlate well to the standard biochronology are recorded by planktonic foraminifers, ranging from the early Aptian to early Campanian (120–80 Ma), and they are used for construction of the age model for this site. Therefore, the underlying units are considered to be >120 Ma in age. Benthic foraminifers show remarkable changes in abundance and diversity throughout the hole, and the subsidence history of Tamu Massif from the upper to lower bathyal depth can be discerned.

The ~120 m thick volcanoclastic succession of stratigraphic Units III–VI (Cores 324-U1348A-14R and below) consists predominantly of hyaloclastite (Figs. F9, F17). The lithology ranges from matrix-supported clay- or sand-sized hyaloclastite to dominantly heavily compacted granule- or pebble-sized clast-supported hyaloclastite in the bottom of the hole. Petrography reveals that the volcanic glass shards and larger

vitric clasts are thoroughly altered, with minor admixtures of bioclastic materials, fossil debris, and well-preserved calcitic fossils at some horizons. In contrast to other Expedition 324 drill sites, no massive or pillow lava flow successions were encountered.

The hyaloclastite succession proved difficult to interpret because of pervasive, and often complete, alteration of the volcanogenic constituents, which masks both original composition and structure. A minority of sparsely vesicular hyalobasalt fragments occur, especially in the upper horizons (stratigraphic Units III–IV), yet high proportions of altered volcanic glass shards and clasts occur throughout, increasing to almost completely form the hyaloclastitic rocks in the clast-supported packages of Unit VI. Under the microscope these fragments originally consisted of only sparsely vesicular vitric clasts, broken down into a high abundance of glass shards, which were subsequently exposed to intense alteration processes and compaction. The predominance of altered glass shards throughout Units III–VI is indicative of substantial submarine volcanism. Sedimentary reworking of these primary hyaloclastite constituents is evident in some units.

With only one exception, the original hyaloclastite composition has been entirely transformed to secondary palagonite, zeolite, and calcite. This replacement commences with the alteration of the volcanic glass shards to palagonite, which is mainly composed of montmorillonite and nontronite. This process starts along the rims and continues with the development of alteration spherules within the glass shards (spherulitization). Further progression of this process resulted in complete replacement of the edges of these shards, followed by replacement of the glass cores by a combination of zeolite and calcite. Some rare lithic fragments show similar texture and alteration degree to basaltic rocks recovered at the top of Hole U1347A. However, even these clasts show almost complete replacement of primary phases and transformation to brown clays. Clay minerals, together with calcite and zeolites, are the predominant secondary minerals in Hole U1348A. Vitric and lithic clasts are cemented by calcite and/or zeolites, with variations in their occurrences and proportions downhole. Fibrous and tabular zeolites (i.e., phillipsite) commonly form a corona alteration around the palagonite particle rims and cement, with or without calcite, the volcanic clasts.

In one unique horizon, cusped sparsely vesicular fragments of volcanic glass, consisting of numerous unaltered contiguous glass shards, were recognized in one continuous ~26 cm interval (324-U1348A-23R-1, 110–126 cm, and 23R-2, 1–8 cm). In the rest of the core these hyaloclastite fragments are identifiable only from their pseudomor-

phed glass shard outlines. However, toward the bottom of the hole (in stratigraphic Unit VI) even these pseudomorphed forms have been mostly obliterated through alteration and by a large amount of compaction of this hyaloclastite material by the overburden of this succession. The rare preservation of the few glass fragments in Sections 324-U1348A-23R-1 and 23R-2 seems to result from an early “armoring” of these vitric clasts by impermeable calcite. In these samples, the glass clasts contain no phenocrysts and preserve only a sparsely microcrystic primary mineralogy of fresh olivine and intergrown plagioclase and pyroxene. These clasts are only sparsely vesicular and typically show the incipient and/or partial transformation to palagonite, seen so pervasively throughout this succession.

Two kinds of structures, primary structure and postdepositional structure, are observed in the volcanoclastic stratigraphic Units III–VI. Bedding as primary structure is often displayed by layered fine and granular hyaloclastite sequences that are interbedded in coarser hyaloclastitic breccia. Sedimentary stratification, including graded bedding and cross bedding, is observed particularly in the fine-grained hyaloclastics. Most strata, however, are parallel and show only shallow dips ( $<30^\circ$ ). Postdepositional structures cut through the bedding, including microfaults and veins. Veins are typically 0.1 to 1.5 cm thick. Both microfaults and veins show steep dip angles  $>50^\circ$ .

Two samples from clay-rich layers in sedimentary stratigraphic Unit II have relatively high concentrations of  $\text{SiO}_2$ ,  $\text{K}_2\text{O}$ , and Zr and very low concentrations of CaO,  $\text{P}_2\text{O}_5$ , and  $\text{TiO}_2$ , as determined by ICP-AES. The clay-rich layers may contain a large proportion of material derived through wind or water transport from continental crust and/or one or more magmatic arcs. However, some of the  $\text{SiO}_2$  in these two layers may have come from circulating solutions that originated in overlying or underlying beds.

Clasts and bulk samples of volcanoclastic material from stratigraphic Units III, V, and VI show the chemical effects of complete alteration, greater even than that at Site U1346, on average. However, the Zr-Ti relationship among the samples is similar to that seen for the tholeiitic basalts of Site U1347 (Fig. F11) and suggests that the Site U1348 volcanoclastic rocks were derived from magmas broadly similar in composition to those that fed the Site U1347 lavas.

Physical properties (magnetic susceptibility and bulk density) of clastic stratigraphic Units III–VI correlated well with varying concentrations of volcanoclastic material (versus more calcite rich intervals). Average magnetic susceptibility generally decreased downhole from  $\sim 40\text{--}45 \times 10^{-5}$  SI near the top of Core 324-U1348A-15R to less

than  $20 \times 10^{-5}$  SI near the bottom of the hole (Core 324-U1348A-26R). A few excursions to  $100 \times 10^{-5}$  SI occurred in intervals 324-U1348A-17R-1, 0–10 cm, and 58–60 cm; 19R-1, 106–108 cm; 20R-1, 18–118 cm; and 20R-4, 73–92 cm. GRA bulk density and bulk density of discrete samples are between 1.8 and 2.4 g/cm<sup>3</sup>. Natural gamma radiation averaged between 10 and 30 cps, with highest spectral peaks corresponding to <sup>40</sup>K. Porosity of discrete samples was high (27%–55%). *P*-wave velocity of discrete samples, from 2.0 to 3.3 km/s, varied inversely with porosity and directly with bulk density.

Because no basaltic basement was recovered and hyaloclastites typically have weak magnetism, paleomagnetic measurements were only made on eight discrete samples from the recovered volcanoclastic sediment. These samples likely carry a depositional remanent magnetization instead of a thermoremanent magnetization. Therefore, any directional result will be more complicated to interpret. The 2G cryomagnetometer was used for these measurements because the natural remanent magnetization of these samples was too weak to be measured on the Molspin Minispin magnetometer (a few tens of mA/m). Only alternating-field (AF) demagnetizations were carried out, using the DTech degausser. The low magnetic susceptibilities (between  $4 \times 10^{-4}$  SI and  $8 \times 10^{-4}$  SI) indicate that magnetic minerals are not abundant in these samples. Compared to the basalt samples from other Expedition 324 holes, the samples have a higher median destructive field (between 10 and 25 mT), which suggests that the magnetization carriers are single-domain grains. In five cases, once the low-coercivity overprint is removed, it is possible to isolate a stable component pointing towards the origin. Inclinations are mostly shallow and positive, between 4° and 23°, although, one sample gives a negative inclination (–9°).

Downhole logging data obtained from Hole U1348A included natural and spectral gamma ray, density, PEF, and electrical resistivity measurements from three depths of investigation. Interpretations of gamma ray and electrical resistivity downhole logs were used to identify 15 logging units in Hole U1348A with 1 in the section covered by the BHA, 5 in the sedimentary sequences in the open hole interval, and 9 in the volcanoclastic section. Electrical resistivity measurements show distinctive higher resistivity zones that likely represent less altered intervals interspersed with low-resistivity zones that mark sediment interbeds and more altered sequences. Natural gamma ray measurements show several intervals of higher readings that indicate interbedded sediments and higher alteration. These intervals also display higher K, U, and Th values. FMS images show zones with distinct horizontal layering, dipping beds, and vesicular or brecciated intervals. Preliminary structural analyses of dipping

beds show features striking northeast–southwest and dipping mostly 20°–30° to the southeast.

## Site U1349

Site U1349 is located at the summit of Ori Massif (Fig. F18) on a flat-topped basement ridge (Fig. F19) thought to have been possibly planed flat by sea level erosion. Hole U1349A was the only hole drilled at the site. It penetrated 250.4 m beneath the seafloor, through 165.1 m of sediment and 85.3 m of igneous basement (Table T1).

In total, 10.1 m of sediment was obtained from Cores 324-U1347A-1W through 7R over a stratigraphic interval of 49 m (average recovery = ~20%) (Fig. F8). Cores 324-U1349A-1W through 4R recovered predominately red chert with occasional ooze and porcellanite intervals (stratigraphic Unit I). Below this, a friable sand-silt-claystone sequence was found that also contains granules of highly weathered volcanic material (Units II and III). This interval, however, is so disturbed by drilling that further interpretation of the rock is difficult. Most of Cores 324-U1349A-5R and 6R contain greenish gray volcanoclastic sandstones and lapillstones, likely deposited by turbiditic flows. A thin, yellowish red clay-rich horizon in Section 324-U1349A-6R-CC is interpreted as a paleosol within the deepest purely sedimentary section recovered. In the underlying basement, several other thin sedimentary beds are found between basaltic lava flows. The most significant of these is a piece of oolitic limestone in Section 324-U1349A-9R-1 at 173.7 m CSF-A, which logging data suggest is ~6 m thick.

Calcareous microfossils occur in chalk that encrusts reddish cherts and in pinkish nannofossil ooze recovered in Cores 324-U1349A-1W through 4R, whereas the underlying siliciclastic and volcanoclastic sediments of Cores 324-U1349A-4R through 7R are barren. The nannofossils are rare to common in abundance but poorly preserved throughout. Planktonic foraminifers are represented in exceptionally high abundance and diversity with good preservation in the nannofossil ooze recovered in Core 324-U1349A-2R. Zonal marker and other age-diagnostic species strongly indicate a narrowly constrained age at the middle–late Albian transition. Although available foraminifer material is scarce, other examined levels above and below are also marked by the occurrences of some age-diagnostic species, allowing the entire age range of Cores 324-U1349A-1W through 4R to be estimated as Albian–Cenomanian. Core 324-U1349A-2R also yields a diverse benthic foraminifer assemblage, and the estimated bathymetric range is middle bathyal.

Volcanic basement was encountered in Core 324-U1349-7R at 165.1 m CSF-A (Fig. F9). The cored basaltic succession of stratigraphic Unit IV is ~55 m thick (Sections 324-U1349A-7R-2 through 13R-4) and consists of 25 lava units characterized by high (40%–75%) vesicularity, the presence of magma mixing features (Fig. F20), and, in all but the interiors of the thickest inflation units, a pervasive reddish brown Fe oxyhydroxide hematite alteration. This succession also contains 10 recovered weathered flow tops readily identified by a reddening over ~5–10 cm intervals, tentatively interpreted as subaerial alteration occurring between the emplacements of successive eruptive units. In the top ~10 m of this lava succession, the flow inflation units are relatively thin (~0.3–1.1 m) and, whereas many have highly vesicular reddened flow tops, a number of examples preserve interflow carbonate sediment. The most significant of these is an oolitic limestone that is preserved at the top of a highly vesicular flow. Other instances of this interflow carbonate sedimentation are preserved only as carbonate infilling of vesicular voids within flow tops. In addition to the subaerial exposure inferred elsewhere in Unit IV, these filled-vesicle flow tops record contrasting periods of shallow marine inundation of the evolving lava field. The lowermost part of Unit IV contains a series of much thicker (1–6 m) massive flows. Preliminary comparisons to degassing models for basalt in Hawaii, and assuming 0.05–0.5 wt% H<sub>2</sub>O concentrations in the source, imply pressures below 15–20 bar in order to produce the high 40–70 vol% vesicularity in the lavas of Unit IV, corresponding to <100 m water depth.

Beneath the lava succession of stratigraphic Unit IV is a transition to flow breccia at 221.7 m CFS (Fig. F9). This section consists of ~29 m of an alternating assemblage of massive lava pods and fragmental basalt. The lava pods are vesicular, though to a lesser degree than the flow tops in Unit IV, on average ~1 m thick, but range in thickness between 0.5 and 2 m. These cored assemblages are interpreted as a series of autobrecciated inflation units (Unit V).

Petrographic examination reveals that the basalts of both stratigraphic Units IV and V are all Cr spinel-bearing and olivine-phyric. Based on ICP-AES analyses these basalts have >8%–15% MgO and thus may be termed picritic. Olivine phenocrysts are sparsely to moderately abundant (up to 4%) but are usually entirely altered to iddingsite, clays, and Fe oxyhydroxides. The groundmass of some rocks contains abundant “ophimottle” crystal aggregates up to ~5 mm in size and consisting of well-preserved clinopyroxene optically intergrown with plagioclase. Fe oxyhydroxides and secondary hematite are present in the groundmass and responsible for the brownish red color of the rocks in the lower part of Units IV.

Extensive water-rock interactions under variable temperature conditions resulted in complete replacement of glassy mesostasis and olivine phenocrysts in both stratigraphic Unit IV and V. Both plagioclase and clinopyroxene are generally well preserved in Unit IV, whereas below ~218 m CSF-A (bottom of Unit IV and Unit V, from Section 324-U1349A-13R-5 to 16R-7), alteration is more pronounced with near complete replacement of clinopyroxene and almost complete replacement of plagioclase microliths. The overall alteration of the basaltic rocks ranges from high to complete. Three types of alteration were determined in Hole U1349A (from top to the bottom): (1) a red-brown alteration (upper and middle of Unit IV), (2) a transition alteration (bottom of Unit IV), and (3) a green alteration (Unit V). In addition, subaerially weathered flow tops have been identified within Unit IV. Clay minerals (saponite, nontronite, and montmorillonite) are the predominant secondary minerals in Hole U1349A samples, replacing glassy mesostasis and primary phases (olivine, plagioclase, and pyroxene) and filling vesicles and veins. Calcite and hematite are also abundant secondary minerals, especially in Unit IV. Secondary mineral assemblages change with depth from clay minerals + hematite + calcite in the red-brown alteration to clay minerals + chlorite + zeolite ± hematite in the transition zone to saponite ± serpentine in the green alteration. This suggests variations in alteration conditions starting with subaerial oxidative tropical weathering within Unit IV. Upon submergence of the lavas, relatively low temperature oxidizing seawater alteration occurred at the top of the hole (in the red-brown alteration) and transitioned to more reducing and higher temperature alteration toward the bottom of the hole (in the green alteration).

The severe alteration has affected and modified the bulk-rock chemical compositions of the basement rocks significantly. In addition, chemical evidence is present for accumulation of olivine, and possibly clinopyroxene, crystals in the melt. The combined effects of crystal accumulation and alteration hinder interpretation of magmatic liquid compositions. However, shipboard measurements indicate that the Site U1349 samples are the least differentiated of any Shatsky Rise basement rocks analyzed. Both the lava section of Unit IV and the autobreccia of Unit V appear to be low-TiO<sub>2</sub>, low-Zr tholeiitic basalts with similarities to primitive ocean-ridge and Ontong Java Plateau basalts (Fig. F11).

Aspects of the mineralogy, especially the compositions of clinopyroxenes and intergrown plagioclase in the ophimottled rock, and of Cr spinel throughout, might further help in constraining the primary composition of the Hole U1349A lavas prior to alteration. Perhaps the most pressing question concerning the pervasive alteration of

stratigraphic Units IV and V has to do with the inferred high temperature assumed for some of it. Oxy-exsolution is observed in all titanomagnetite crystals and may indicate that alteration approached temperatures up to 600°C. However, no secondary minerals indicative of such high temperatures (epidote, actinolite, etc.) were observed.

Structural data are consistent with the interpretation that Hole U1349A penetrated several stacked sheet flow units that are sometimes intercalated by limestone. Evidence for apparently subaerial features (including pahoehoe structures) and submarine structures (including pillow lava and brecciated pillow lava) is obvious. The typical sheet flows at this site can be described with the typical three parts: (1) the upper lava crust with horizontal zones of hollow vesicles, (2) the middle lava core with quite regular well-developed veins in fine-grained groundmass and low vesicularity, and (3) the basal zone with less vesicles and few veins. In this hole, there are no joints to be observed, but veins are well developed. Vein dips become steeper downhole in the upper part of the igneous succession, become shallower again, and then steepen downhole again.

Physical property measurements of the recovered igneous and sedimentary material can be used to distinguish four of the five units (II–V) of Hole U1349A. No discrete samples were taken from the chert fragments of Unit I, nor was the material continuous enough for whole-round track measurements. Volcaniclastic sandstones and claystones of Unit II and volcaniclastic sandstones and lapillistones of Subunit IIIa yielded magnetic susceptibilities  $<1000 \times 10^{-5}$  SI, GRA densities  $<2.0$  g/cm<sup>3</sup> and natural gamma radiation (NGR) counts between 10 and 40 cps. Three discrete measurements of Unit II and Subunit IIIa revealed high porosities (20%–40%) accompanied by *P*-wave velocities  $<4.0$  km/s. Thermal conductivity measurements yielded low values between 1.01 and 1.57 W/(m·K), typical of sedimentary material.

Beneath the sandstones of Unit II and Subunit IIIa, a volcaniclastic conglomerate (Subunit IIIb) can be clearly distinguished by excursions to extremely elevated magnetic susceptibility. A distinct spike reaching almost  $4000 \times 10^{-5}$  SI, the highest value measured during Expedition 324, is derived from an individual volcanic clast in Section 324-U1349-7R-1 containing abundant groundmass magnetite. The upper oxidized portion of the vesicular basalts of Unit IV, lying below the conglomerate, have low magnetic susceptibility ( $<1000 \times 10^{-5}$  SI) and low total NGR counts ( $<20$  cps) similar to sedimentary Unit II and Subunit IIIb, but are distinguishable by higher GRA density ( $>2.0$  g/cm<sup>3</sup>). Discrete sample measurements confirm higher bulk density

(>2.5 g/cm<sup>3</sup>) and yield lower porosity (<10%) and higher *P*-wave velocities (4.0–6.0 km/s) compared to the sedimentary units. Core 324-U1349-11R in Unit IV marks the end of the oxidized material and shows an increase in magnetic susceptibility, averaging  $\sim 1000 \times 10^{-5}$  SI, with excursions to values  $>2000 \times 10^{-5}$  SI. The increase in magnetic susceptibility is not accompanied by any significant difference in GRA density, porosity, or *P*-wave velocity compared to the oxidized material above. Thermal conductivity measurements throughout Unit IV, irrespective of relative oxidation, yielded some of the highest values recorded during Expedition 324 and averaged  $1.799 \text{ W/(m}\cdot\text{K)} \pm 0.357$  ( $2\sigma$ ;  $n = 22$ ).

The autobrecciated basalt Unit V is clearly distinguishable from the vesicular basalts above by a decrease in magnetic susceptibility (average =  $100 \times 10^{-5}$  SI). Total counts from the NGR show a muted decrease to 5–10 cps, whereas GRA density remains similar to the basalts above. Discrete sampling reflects the heterogeneous distribution of clasts within Unit V, showing large variations in porosity, *P*-wave velocity, and, to a lesser extent, bulk density. Thermal conductivity measurements reflect the higher porosities measured in the unit, yielding values lower than the basalts, with an average of  $1.364 \text{ W/(m}\cdot\text{K)} \pm 0.305$  ( $2\sigma$ ;  $n = 10$ ).

A total of 32 basement samples were demagnetized for paleomagnetic studies (18 AF and 14 thermal demagnetizations). As expected, samples from volcanoclastic units show demagnetization results in which a characteristic remanent magnetization is difficult to isolate. These samples likely carry a depositional remanent magnetization, which makes the interpretation more complicated. Samples from olivine phyric amygdaloidal basalt flows were characterized by a high-coercivity, high-unblocking temperature magnetization carrier. It is still unclear whether this magnetization is carried by titanomagnetite, in which case it is a true thermoremanent magnetization, or by hematite, in which case it is a chemical remanent magnetization. Both minerals have been identified in thin section observations. In any case, additional rock magnetic measurements and interpretations are necessary in order to interpret these results. The average inclination in Hole U1349A is  $-4.3^\circ \pm 5.9^\circ$  ( $1\sigma$ ), suggesting that the lavas in Hole U1349A were formed near the magnetic equator.

Downhole logging data obtained from Hole U1349A included natural and spectral gamma ray, density, and electrical resistivity measurements from three depths of investigation. Interpretations of gamma ray and electrical resistivity downhole logs were used to identify 19 logging units in Hole U1349A with 1 in the section covered by the BHA, 5 in the sedimentary sequences in the open hole interval, and 13 in the

basaltic basement section. Electrical resistivity measurements show distinctive higher resistivity zones that likely represent less altered intervals interspersed with low-resistivity zones that mark more altered sequences. NGR measurements show a large peak just below the sediment/basement interface that may indicate a zone of concentrated hydrothermal alteration. This interval also displays very high U values and a smaller peak in K values. FMS images show zones with highly fractured intervals, potential veins, and vesicular or brecciated intervals.

## Site U1350

Site U1350 is located on the lower east flank of Ori Massif (Fig. F18) where sediments are thin and the underlying acoustic basement appears to be relatively strong and smooth (Fig. F21). The site was chosen because it has a setting similar to Site U1347, which yielded relatively fresh basalts, and because it would provide a valuable comparison with the summit of Ori Massif (Site U1349). A single hole (U1350A) was drilled at the site, penetrating 143.1 m of sediment and 172.7 m of igneous basement to a total depth of 315.8 m (Table T1).

Because recovery of the soft sediments overlying the igneous basement was poor, only one purely sedimentary unit was defined at Site U1350 (Unit I), which spans Cores 324-U1350A-1W through 6R (Fig. F8). Although it is likely Unit I is composed of both chert and soft calcareous ooze or chalk, only chert (predominantly black and less commonly reddish) with minor amounts of occluded porcellanite, was recovered. Well-preserved radiolarians, concentrated around relict burrow features, are common in the cherts of Unit I. Igneous basement was reached in Core 324-U1350A-6R at 143.1 m CSF-A (Table T1), but additional sediments were encountered interbedded with the basaltic strata in Units II and IV. These sediments were predominantly fine-grained carbonates with a persistent radiolarian component and volcaniclastics. Varying quantities of assorted bivalve and brachiopod fossils were also present. Sedimentary interbeds were especially prevalent in Unit IV (Cores 324-U1350A-25R and 26R), where carbonate-rich oozes have been intruded by small pillow basalts prior to lithification (Fig. F22).

Calcareous nannofossils sampled from chert-rich lithologies of Unit I and Subunit Ila (Cores 324-U1350A-1W through 9R) are frequent to high in abundance and moderately to poorly preserved. The assemblage is indicative of Early Cretaceous age. However, both planktonic and benthic foraminifers are almost barren in these two units, with only a few silica-replaced specimens. The intercalated limestone sediments of

Unit IV are severely recrystallized and do not yield any calcareous microfossils. A low-diversity, poorly preserved assemblage of radiolarians is present throughout the examined Site U1350 sediments. No contact between the overlying sediment of Unit I and the volcanic basement succession was recovered.

The upper part of the igneous basement (Unit II) (Fig. F9) contains both massive basalt flows and pillows, with the percentage of massive flows decreasing with depth. Below this a ~6 m thick layer of hyaloclastite and brecciated basalt (Unit III), followed by a lowermost succession of well-preserved plagioclase-phyric pillow lavas set in a matrix of intercalated micritic limestone (Unit IV), as described above. Unit II may be divided into an upper ~77 m thick succession (Cores 324-U1350A-6R through 16R) predominantly consisting of a series of larger inflation units, yielding recovered thicknesses of 1–2 m, with two larger 3–5 m thick flows that are sparsely intercalated with thin layers of volcanogenic limestone (Subunit IIa) (Fig. F23). Below this is a middle ~23 m thick transitional succession (Sections 324-U1350A-17R-1 through 19R-1) in which larger inflation units of 1–2 m are intercalated with smaller pillow lava units (Subunit IIb). The pillows display chilled margins, glassy contacts, and vesicle distribution patterns similar to those of pillow units observed in Holes U1346A and U1347A. At its base, Unit II concludes with a ~50 m stack of 0.2–0.9 m thick pillow lava units (Sections 324-U1350A-19R-2 through 24R-2) with well-preserved glassy contacts and chilled margins (Subunit IIc) (Fig. F24). Within Subunit IIc, the lowermost ~23 m consists of a well-preserved stack of units displaying pillow/pillow contacts, relatively thin glass rims, and chilled margins but lacking intercalated sediment layers. In this lowermost part the pillow units become sparsely plagioclase phyric (up to 2%), and magnetic susceptibility abruptly diminishes to lower values characteristic of Units III and IV below.

The pillows of Unit II lie atop ~6 m of hyaloclastite (Unit III) (Figs. F9, F25) consisting of gravel- to sand-sized glassy material, larger hyaloclastite fragments, and/or small pods (~5–15 cm) of aphyric basalt (Sections 324-U1350A-24R-3 through 24R-4). The rocks in the aphyric basalt pods appear to be petrographically similar to those of Unit II above, but on the whole the material is a sufficiently different facies of hyaloclastite to merit its own division and represents a thin series of autobrecciated inflation units. The lowermost ~1 m of core material of Unit III in Section 324-U1350A-24R-4 consists of gravel and pebble-sized fragments only, preventing identification of the contact between Unit III and the underlying volcanic succession.

The lowermost ~19 m thick sequence (Unit IV) (Fig. F9) consists of Cores 324-U1350A-25R and 26R with extremely high recovery (>90%). These cores preserve a stack of ~0.1–0.5 m thick plagioclase (~6%) phyric pillow lavas, including the sedimentary material that occurs between individual pillow lavas (Fig. F22). Glassy rinds and thick, chilled margins can be readily examined, and pillow/pillow and pillow/sediment contacts are abundant throughout. Thermal alteration effects can be observed at most basalt/sediment contacts, especially in examples where the pillow lava actively injected into soft sediment. The encasement of some pillow units within sediment indicates that the substrate onto and into which the pillow lavas were extruded was unconsolidated and/or fluidized by the entry of hot lava.

Thin section examination shows that crystallites in well-preserved glass rims are mainly plagioclase and clinopyroxene but that spinel is not present in the basalts of Hole U1350A. Groundmass textures consist of networks of interlocking acicular plagioclase around which both clinopyroxene and titanomagnetite have crystallized to varying proportions, depending on grain size and rate of cooling. Only in the transition succession of Subunit IIIb do some well-developed networks of interlocking clinopyroxene and plagioclase occur as clumps or aggregates at all grain sizes.

The entire basement section (massive lava flows, pillow lavas, and hyaloclastites) has been affected by slight to high degrees of low-temperature water-rock interactions, resulting in complete replacement of glassy mesostasis and olivine phenocrysts and slight to almost complete replacement of groundmass minerals (plagioclase and clinopyroxene). In contrast, plagioclase phenocrysts are generally well preserved throughout the hole, except in Unit IV. Fresh glass is commonly preserved on the margins of flows and pillows in Subunits IIa and IIb, rarely preserved in Subunit IIc, and not preserved in Units III and IV. One type of gray alteration was identified, with significant variation in alteration degree, from slight to moderate in the upper flow succession and hyaloclastites (Units II and III) to moderate to high in the plagioclase-phyric pillow succession (Unit IV). Clay minerals, together with calcite, are the predominant secondary minerals in Hole U1350A, replacing primary phases, glassy mesostasis, and filling vesicles and veins. Other alteration minerals observed in the basaltic cores are pyrite and zeolites, present as filling vesicles and veins, and possible sanidine replacing plagioclase phenocrysts in Unit IV. Four main vein types were identified in basaltic rocks of Units II to IV: (1) calcite veins ( $\pm$  pyrite), (2) saponite veins, (3) calcite and saponite veins ( $\pm$  pyrite), and (4) pyrite veins. A total of 461 veins and vein networks were recorded in the recovered 75 m, which corresponds to an average of 6.1 veins/m. Most of the veins in Hole U1350A are calcite veins, consisting

of either crystalline blocky calcite or crossfiber calcite. Alteration of Hole U1350A samples is comparable to alteration mineralogy encountered in Hole U1347A on Tamu Massif.

The chemical effects of the alteration are comparatively modest at Site U1350. The shipboard chemical data reveal that the basement section is composed of variably evolved tholeiitic basalts (Fig. F11). Broad similarities with the Site U1347 and Site 1213 basalts are present, but the Site U1350 lavas also differ in important respects: for example, they show systematic downhole variation in several key chemical parameters, exhibit a wider range of  $\text{TiO}_2$ , Zr, and Mg numbers, extend to higher Mg number values (as high as 68.5), and have higher Sr concentrations. They also show a wider spread of Zr/Ti ratios, implying that variations in amount of partial melting and/or source composition were important.

The overall structure of the basement can be divided by the hyaloclastite of Core 324-U1350A-24R (Unit III) into two kinds of extrusive structures: (1) sheet flow lavas with intercalated pillows in the upper part and (2) piled-up pillows in the lower part. Both parts are characterized by synmagmatic structures, including inter- and intrapillow structures. Interpillow structures are structures observed in the surrounding rocks. In the upper part of the hole, the surrounding rocks are characterized by hyaloclastite breccias or calcite fillings. In the lower part of the hole, interpillow structures are characterized by limestone, which shows only weak bedding. Intrapillow structures are similar in texture through out the hole, but differ in size from ~5 to ~30 cm depending on the size of the pillows. They are characterized by thin glassy margins, radially aligned vesicles, concentric vesicular zones, and spheroidal shapes. In addition, structural features can be divided by syn- and postmagmatic structures. Synmagmatic structural features are represented by amygdaloidal structure, irregular vein networks or curved veins, and breccias. Postmagmatic structures are conjugate veins and joints. Dip angles of both veins and joints recorded in the rocks from Hole U1350A vary irregularly with depth. A larger population of veins and/or joints is found in the lower part of the hole (Unit IV).

The physical property data obtained from the basement units can be separated into three distinct units or divisions based on magnetic susceptibility: (1) Cores 324-U1350A-7R through 11R (~150–190 m CSF-A), (2) Cores 12R through 21R (~190–270 m CSF-A), and (3) Cores 22R through 26R (~270–316 m CSF-A) and three distinct units based on NGR: (1) Cores 324-U1350A-7R through 10R (~150–175 m CSF-A), (2) Cores 11R through 24R (~175–295 m CSF-A), and (3) Cores 24R through 26R (~295–

316 m CSF-A). Interestingly, neither set of divisions corresponds with any of the stratigraphic units except for the lowermost NGR division. Magnetic susceptibility shows a decreasing downhole trend from  $>2000 \times 10^{-5}$  SI in the upper portion of Subunit IIa to  $<1000 \times 10^{-5}$  SI in the lowermost Unit IV. A sharp decrease in magnetic susceptibility is found between Cores 324-U1350A-21R and 22R within the pillow basalts of Subunit IIc. This decrease corresponds to the disappearance of sediment interbeds and the onset of a continuous stack of pillows.

Data from the NGR logger yields generally low counts ( $<5$  cps) with two notable exceptions. These exceptions occur in the upper portion of Subunit IIa and in the lower Unit IV. Examination of spectra from both of these intervals shows that counts are dominated by products of the  $^{40}\text{K}$  decay chain. This is in agreement with the increased K-rich alteration clays seen in the lowermost Unit IV. The GRA bulk density is consistently around  $2.5 \text{ g/cm}^3$  throughout Units II–IV. Measurements of discrete bulk density samples agree fairly well with the maximum values of the whole-round data, having uniform values with an average of  $2.61 \pm 0.17 \text{ g/cm}^3$  ( $2\sigma$ ). Porosity measurements on discrete samples are from 3.43% to 28.45% and display a good negative correlation with *P*-wave velocity, as expected. *P*-wave velocity shows no appreciable anisotropy and averages  $4.793 \pm 1.249 \text{ km/s}$ , which is typical for basaltic material and of a similar range to measured velocities from recovered igneous material in all sites. Overall, discrete physical property measurements do not change significantly with different stratigraphic units.

A total of 42 samples were analyzed for paleomagnetism (18 AF and 24 thermal demagnetizations). AF demagnetizations were characteristic of low-coercivity magnetic minerals, except for the samples from Sections 324-U1350A-25R-2 to 26R-1. All the AF-demagnetized samples have a stable direction pointing toward the origin, but the inclinations derived from principal component analysis (PCA) show a large spread, between  $-12^\circ$  and  $27^\circ$ . Thermal demagnetizations indicate a large distribution of Ti content in the samples. PCA carried out on the thermal demagnetization specimens defined stable magnetization components but also lead to a scatter of inclination values. Overall, inclinations are shallow, both positive and negative, but with large variations even within the same stratigraphic unit.

Because the logging tools were unable to leave the drill pipe and enter open hole, only gamma ray measurements could be recorded from inside the BHA. The gamma ray data in the shallow sediments show an anomaly from seafloor to  $\sim 25$  m wireline log

matched depth below seafloor. The contributions to this anomaly are mainly an increase in Th and a smaller contribution from U.

## Synthesis

### Sediments

Despite the fact that the recovery of igneous basement was the main objective of Expedition 324, >100 m of sedimentary material was recovered from the five sites on Shatsky Rise. The variety of different sediments ranging in age from Early Cretaceous to middle Cenozoic represents a range of different depositional environments. As anticipated, the dominant stratigraphic facies in the uppermost cores at all sites is chert interbedded with chalk and calcareous oozes. At every site, these sediments make up “Unit I” (Fig. F8). The combination of indurated chert and soft chinks undoubtedly contributed to the consistently poor recovery of this unit, which was often limited to one or two chert fragments per core. The sediments comprising Unit I are indicative of pelagic carbonate and silica-rich deposition at each of the massifs, initiated once that portion of the volcanic platform had subsided out of the photic zone. Age constraints within this facies are somewhat difficult to determine, but generally range from Berriasian through to middle Cenozoic, suggesting that open-marine sedimentation was the dominant mode of deposition for the majority of Shatsky Rise’s post-eruptive history. The persistently high radiolarian component present in many of the stratigraphic units is testimony to high rates of productivity, probably associated with the position of Shatsky Rise near the paleoequator during much of the Early to mid-Cretaceous.

Other (nonpelagic) sedimentary material was also recovered from many of the sites, including bioclastic limestones, radiolarian-rich siliciclastics, and thick volcanoclastic sequences (Fig. F8). This unexpected diversity of basal material may help to illuminate the complex history of sedimentation and subsidence at Shatsky Rise, after the main volcanic-edifice building phase had ceased but before fully pelagic sedimentation was initiated. Interestingly, sediments were found interbedded with igneous material comprising the basaltic basement at several of the sites. These sediments, largely undated thus far, may yet yield invaluable information about the relative duration of eruptive events and the environment into which these igneous units were emplaced.

The discovery of shallow-water sediments, and even subaerial basal sediments at many of the sites, suggests Shatsky Rise may have been a semiemergent archipelago

rather than a purely submarine edifice during the Early to mid-Cretaceous. Lithologic and biologic indicators for shallow marine depositional environments include carbonate-rich sediments, shallow-water fossil assemblages, and the occurrence of possible wood fragments, glauconite, and sedimentary structures suggestive of shallow water deposition.

Tamu Massif at the southern end of Shatsky Rise is thought to represent the oldest part of the Shatsky Rise chain. At the southernmost site drilled during Expedition 324, Hole U1347A on the eastern flank of the massif, Early Cretaceous sediments (Berriasian to late Valanginian) were found overlying basement, confirming age estimates from previous paleomagnetic studies. These sediments include a ~60 m sequence of graded and laminated radiolarian-rich sand-silt-claystones (Fig. F8), which contained diverse trace fossils and occasional body fossils, such as the ammonite fragments found in Core 324-U1347A-8R. The sedimentary material is fine grained, probably of volcanic origin, and contains bedding structures indicative of deposition by turbiditic currents. Glauconitic radiolarites and silicified limestones overlie these laminated siltstones and contain beautifully preserved radiolarian tests, replaced in many cases by green glauconite minerals. Additionally, the material is cross-bedded in a style indicative of very shallow marine conditions, at or above wave base, suggesting a shallowing-upward sequence prior to subsidence and deposition of the pelagic chert-rich facies.

Material recovered from the second Tamu Massif site (U1348) on the northern flank sharply contrasts with that recovered from Site U1347 and represents sedimentation in a large range of depositional environments. Basaltic basement was not reached at this site despite drilling to >320 m CSF-A, although a large proportion of the material at this site is volcanic in origin and probably represents redeposited hyaloclastic (volcanic glass) material from submarine eruptions (Fig. F8). The sedimentary structures in this succession are suggestive of hydraulic sorting and include laminations and graded bedding (both reverse and normal), as well as erosional contacts, making deposition by the action of turbidites or debris flow probable. Shallow-water fauna such as well-preserved crinoids and gastropods are present within some of these volcanoclastic units, indicating the environment was relatively shallow and marine. Unfortunately, age constraint for these unique volcanoclastic units proves elusive, although a tentative Early Cretaceous age can be assigned based on radiolarian assemblages and the biostratigraphic ages of overlying sediments. Other highlights from Site U1348 include the recovery in Core 324-U1348A-12R of green zeolitic and celadonite-rich clays thought to represent altered ash beds and sandstones predominantly formed of

tabular coral fragments in Core 324-U1348A-11R. A 25 cm section of early–middle Aptian foraminifer-bearing calcareous ooze was recovered in Core 324-U1348A-10R and may provide an invaluable record of Pacific paleoceanography during this crucial mid-Cretaceous transition. Another remarkably well preserved 1 m long section of nanofossil ooze thought to span the Late Cretaceous Santonian to Campanian transition was also recovered in Core 324-U1348A-2R. A small piece of gray ooze at the top of this core and the contents of the wash core (324-U1348A-1W) above are middle Cenozoic in age, suggesting either contamination from material much higher in the borehole or a genuine hiatus between the Late Cretaceous and middle Cenozoic at this site.

Ori Massif, north of Tamu Massif, is thought to represent either a later phase of volcanism or a rifted segment of the larger edifice. Two sites were drilled on Ori Massif; the first (Site U1349) is centered on the summit and the second (Site U1350), ~40 km away, is on the eastern flank of the massif. The basaltic basement at Site U1349 was heavily altered and covered by a sequence of volcanoclastic conglomerate, breccia, and sandstones (Fig. F8). A weathered, highly oxidized horizon in Core 324-U1349A-6R is interpreted as a paleosol, providing direct evidence for subaerial exposure of material at Shatsky Rise. Evidence for very shallow water emplacement of the uppermost lava flows at Site U1349 comes from interbedded oolitic bioclastic limestones in Cores 324-U1349A-7R and 9R. Only sparse sedimentary material, in the form of black chert, was recovered above basement at Site U1350 (Fig. F8), but an interesting sequence of limestones interbedded with small pillow lavas was recovered in the lowest part of the hole within Cores 324-U1350A-25R and 26R.

Northeast of Ori Massif lies Shirshov Massif, presumed to be the youngest of the volcanic edifices at Shatsky Rise based on magnetic lineation data. Site U1346 was drilled on Shirshov Massif on the northern rim of the summit. The basaltic basement at this site was reached at 139.2 m CSF-A, underlying a largely pelagic sedimentary sequence. Only the lower portion of these sediments was cored, beginning at 100.5 m CSF-A. Although sedimentary recovery averaged only ~10%, the diversity and sequential changes within this material provide a record of the tectonic subsidence of the volcanic platform. Directly overlying the basement, shallow-water biogenic limestones were recovered (Fig. F8), consisting primarily of a fine-grained carbonate matrix with abundant shell fragments, foraminifers, radiolarians, echinoids, and authigenic glauconite. Oxidized fragments of scoriaceous material as well as small (millimeter size) possible wood fragments were identified in these limestones, suggesting that there was an emergent landmass nearby. Upward in the sequence the biogenic component

of the limestones decreases, develops laminated bedding structures, and contains larger amounts of siliciclastic material in the silt and clay size range. A large spike in U content was observed in the physical property NGR data toward the top of the limestone succession, within Core 324-U1346A-5R. A fine-grained volcanoclastic turbidite deposit was recovered above the limestones (Fig. F8), which is similar to the finer hyaloclastic material recovered at Site U1348 on Tamu Massif. Present within this meter of laminated mud and fine sandstones are at least three major fining-upward sequences bounded by erosive contacts. The sediments are mostly composed of clays and altered volcanic glass with varying amounts of iron oxyhydroxide minerals, glauconite, and radiolarians. Another limestone package rests above the turbidite; it is interbedded with altered vesicular basalt. The carbonates in this unit are fine grained, occasionally sparry (indicating recrystallization of the calcite), laminated and contain several dark clay-rich bands, and have been interpreted to represent deeper water sedimentation. The basalt/sediment contacts are convolute, indicating the igneous material was likely emplaced while the sediment was still soft. However, there is no evidence of chilled margins, which suggests the basalt had already cooled and solidified before being mixed with the sedimentary material by the process of slumping or debris flow.

## Biostratigraphy

Shipboard studies of calcareous microfossils (calcareous nannofossils, planktonic foraminifers, and benthic foraminifers) allow new micropaleontological constraints to be placed on the evolutionary history of Shatsky Rise. At Sites U1346 and U1347, Early Cretaceous calcareous nannofossils and benthic foraminifers were successfully retrieved from calcareous and/or siliciclastic sediments immediately above the basaltic basement sections. The youngest basement ages based on calcareous nannofossils are Berriasian–Hauterivian for Site U1346 and Berriasian–Valanginian for Site U1347. These estimates compare well with the ages delineated by magnetic lineations (Fig. F3). Benthic foraminifers comprise a unique monofamily assemblage, which has not been reported from any other Cretaceous Pacific deep-sea sections and gives significantly shallow paleowater depths of <500 m for Site U1346 and <200 m for Site U1347 (Fig. F26). This finding provides an independent line of evidence for shallow-water (possibly subaerial?) eruption of Shirshov, Ori, and Tamu massifs, complementing other sedimentological and physical volcanological observations.

At Site U1348, the ~80 m thick pelagic sediment cover of Tamu Massif (northern flank) yields diverse, abundant planktonic foraminifers ranging in age from the mid-

to Late Cretaceous (Aptian–Campanian). The nearly linear age–depth relationship shows the absence of a major sedimentation gap. Noteworthy is the recovery of 120 Ma ooze (early Aptian), probably the oldest known fresh pelagic sediment, and it certainly ensures stable isotopic study of individual foraminifer species. Future progress in taxonomic, paleoecological, and paleoceanographic studies of foraminifers are highly anticipated.

## Physical volcanology and igneous petrology

One of the key objectives of Expedition 324 was to determine the nature, duration, and rates of LIP volcanism for the Shatsky Rise. This oceanic plateau was previously drilled during Leg 198 at Site 1213 on Tamu Massif and revealed a series of three fine-grained massive volcanic flow units, each ~8–15 m thick. A total of five new sites (U1346–U1350) on Shatsky Rise were chosen to drill igneous basement and to provide geographical spread across its three main massifs.

The volcanology of Shatsky Rise is more complex than initially anticipated with each hole exhibiting different characteristics and combinations of units (Fig. F9). The typical igneous units are, in order of increasing size: (1) pillow lavas (~0.2–1.0 m diameter) displaying typical glassy rinds, chilled zones, internal vesicle distributions, and joint patterns; (2) pillowlike inflation units (~0.8–2.0 m thick) displaying glassy rinds or contacts, chilled zones, vesicular tops, and degassed interiors with pipe vesicles; (3) smaller massive flow units (~2–4 m thick) with vesicular tops, homogeneous, coarser grained interiors with pipe vesicles and segregation features, and narrow basal chilled zones; and finally (4) large massive flow units (~5–23 m thick) with narrow, glassy upper contacts, vesicular tops grading down into a vertically extensive, nonvesicular, degassed interiors with sparse, well-developed pipe vesicles and segregation features, a coarser crystal groundmass, and a narrow basal chilled zone. Overall, the vesicularity of the igneous units was high and most sites are characterized by a high proportion of smaller sized inflation units. However, although the large massive flow units are less common, they can constitute a significant proportion of the core. Often the lava flows and pillow basalts are intercalated or directly overlain by relatively to very shallow marine sediments, indicating that most lavas erupted at shallow depths and low hydrostatic pressures. In one instance, at Site U1349, several reddened flow tops occur, probably indicative of subaerial eruption, or at least a period of emergence.

The five volcanic basement sites may be summarized as follows:

- Site U1346 was drilled on Shirshov Massif and consists of ~53 m of highly vesicular pillow lavas and larger pillowlike inflation units consisting of aphyric micro- to cryptocrystalline basalt. These are interpreted as part of a single pillow lava eruption stack. The nature of the sedimentary intercalations within the succession indicates that the environment deepened progressively from nearshore to offshore marine conditions throughout the eruptive time period.
- Site U1347 was drilled on the southeastern flank of Tamu Massif (~200 km north-east of Hole 1213B). The ~160 m thick basement succession consists of massive basalt flows and pillow inflation units intercalated with volcanoclastic sedimentary successions. These include (1) an upper series of four massive lava flows (~8–19 m thick); (2) a ~75 m lava stack with more massive (~3–6 m thick) basaltic flows passing upward in larger pillowlike inflation units (1–2 m thick) and pillow basalts (<1 m thick), which likely represent successive eruptive pulses during which lava effusion rates diminished; and (3) two massive internally homogeneous basaltic lava flows consisting of a very thick (~23 m) upper tabular flow overlying a second (partially drilled) flow. The frequent recovery of thick (often fresh) glassy rinds within the pillow unit stack indicates that alteration was essentially buffered in these rocks.
- Site U1348 was drilled on a basement high on the north flank of Tamu Massif and is unusual in that it provided ~120 m of volcanoclastic sediments, including ~90 m of hyaloclastite. This initially proved difficult to interpret because of the pervasive alteration, which masks both the original texture and structure of this lithology. However, its chemical composition, measured from a few large basaltic clasts, is consistent with the lavas observed at the other sites, and the predominance of altered glass shards material is indicative of substantial submarine volcanism nearby.
- Site U1349 was drilled near the top of Ori Massif. The upper sedimentary section is the usual chert-chalk sequence, which changes downhole to volcanoclastic materials containing fragments of basalt. Beneath the volcanoclastics is a weathered volcanogenic conglomerate that lies unconformably upon red-brown basaltic flows. These thin altered lavas have extremely vesicular flow tops, many of which are deeply reddened, probably as a result of subaerial weathering, and are intercalated with multiple limestone (oolitic) horizons indicative of periodic marine incursions. Increasingly thicker lava inflation units occur toward the bottom of the lower lava section before passing into an underlying submarine succession of lava flow breccias, hyaloclastite fragments, and more massive lava pods. Accordingly, this volcanic succession appears to have developed in progressively shallower to emergent conditions, followed by submergence after volcanism ceased.

- Site U1350 was drilled 70 km east of Site U1349 on the eastern flank of Ori Massif, where the seafloor is ~800 m deeper. Drilling penetrated ~173 m into volcanic basement and yielded (1) a series of massive basalt flows passing downhole into (2) a transitional zone, (3) aphyric to sparsely plagioclase-phyric pillow lavas, (4) a thin layer of hyaloclastite, and (5) a succession of well-preserved plagioclase-phyric pillow lavas set in a matrix of unconsolidated or fluidized micritic limestone. The inflation units above the hyaloclastite are complex, containing a mixture of massive flow and larger pillowlike units sparsely interspersed with thin sedimentary horizons. Beneath the hyaloclastite, the high core recovery preserved in great detail an intricate stack of small pillow lavas (~0.1–0.5 m) and numerous pillow/sediment baked contacts. Alteration was minimal toward the top of this site and is thus comparable with that observed in Hole U1347A.

From a petrological point of view Shatsky Rise presents a basaltic province in which plagioclase-clinopyroxene intergrowths are well developed, from the early crystallization of mottles with ophitic textures (Hole U1349A) to the formation of sparse phenocrysts and glomerocrysts (Holes 1213B, U1347A, and U1350A) to the quench stage and the stage of coarser grained crystallization in the interiors of flows and pillows (all holes). This petrographic attribute is evident even among the rare and tiny quench crystals in the one glassy sample recovered among the hyaloclastites of Hole U1348A. The basalts of Holes U1346A and especially U1349A are more primitive than others, carrying fairly abundant olivine and Cr spinel, and yet the plagioclase-clinopyroxene intergrowths even occur in the altered glass margins of these rocks. The above observations indicate that, at all stages of crystallization, the temperature interval between onset of plagioclase crystallization and that of clinopyroxene is negligible. Experimentally, this is not a usual feature of MORB at low pressure, with the exception of the melt containing significant dissolved water. A range of temperatures may have existed, and that will be determined by onshore mineral studies, but in all cases plagioclase and clinopyroxene crystallized cotectically.

Although some of the basalt at Hole U1349A can be termed picritic, these rocks from the Shatsky Rise differ from the only well-documented picrite found on modern spreading ridges. More evolved olivine tholeiite from drill sites on the Mid-Atlantic Ridge still has an obvious gap in crystallization temperature at all cooling rates between plagioclase and later clinopyroxene. As MORB-like as Shatsky Rise basalt may be in its geochemistry, in this one respect, it is different.

## Alteration

Basaltic rocks forming the Shatsky Rise oceanic plateau have all undergone pervasive fluid-rock interaction, with lateral and vertical variations in degree and conditions of alteration (i.e., temperature, redox, and fluid composition). Overall alteration at Shatsky Rise occurred under relatively low temperature and relatively oxidizing conditions, resulting in a slight to complete replacement of primary phases (glassy mesostasis, olivine, plagioclase, and pyroxene) by clay minerals (i.e., smectites). Calcite and pyrite are also common secondary minerals at Shatsky Rise, replacing primary phases and filling vesicles, veins, and voids. Other alteration minerals at Shatsky Rise commonly include zeolites, rare hematite, and chlorite.

Predominant alteration of Shatsky Rise basalts is a gray alteration, resulting from interaction of basalts with seawater-derived fluids under anoxic-suboxic conditions at low-temperature and low water-rock ratios. This alteration type was encountered at Sites U1346, U1347, and U1350 and affected the basalts to various degrees (from slight to high). Primary phases (olivine and glassy mesostasis) are commonly replaced by clay minerals (i.e., montmorillonite, nontronite, and saponite), whereas pyroxene and plagioclase are generally well preserved. Fresh titanomagnetite is also present in lava flow interiors at these sites when alteration degree is <50%. Significant fresh glass was commonly observed on flow and pillow margins of Holes U1347A and U1350A and more rarely in Hole U1346A. Predominance of calcite and pyrite at these sites also suggests interaction of the basalts with CO<sub>2</sub>- and S-rich fluids.

Basalts recovered at Sites U1348 and U1349 differ in alteration degrees and types. Hole U1348A recovered hyaloclastites in which glassy clasts were altered to palagonite and cemented by calcite and/or zeolite (i.e., phillipsite). Basalts recovered in Hole U1349A have been affected by extensive water-rock interactions with variations in temperature and redox conditions with depth. Secondary low-temperature and oxidizing mineral assemblages, dominated by iddingsite, hematite, and calcite in the upper 205 m CSF-A (Unit IV), change to relatively higher temperature secondary mineral assemblages composed of clay minerals, zeolite, minor chlorite, and rare serpentine below 205 m CSF-A. Unit IV in Hole U1349A shows evidence of subaerial weathering and lavas being in very shallow water (e.g., hematite, nine horizons of intense red alteration interpreted as subaerially exposed flow tops, and thin oolitic limestone). This suggests that prior to typical low-temperature oxidizing seawater-rock interaction, basalts in Hole U1349A were first altered under subaerial oxidative tropical conditions.

## Geochemistry

Alteration has modified the major and trace element compositions of virtually all igneous rocks analyzed during Expedition 324. Compositions of samples from Sites U1347 and U1350 have been affected the least overall (e.g., Fig. F11A). Interelement relationships indicate that the Site U1347 and U1350 rocks are variably evolved tholeiitic basalts. Similar to basalts from Site 1213 on the southern Tamu Massif, the compositions of the Site U1347 and U1350 lavas show some overlap with data for the Ontong Java Plateau but are more similar in many elements to ocean-ridge basalts. More specifically, the Site U1347 lavas and many of the Site U1350 basalts resemble enriched-type ocean-ridge basalts. Some Site U1350 samples, particularly from the deeper part of the basement section, have relatively low Zr/Ti ratios similar to those of normal ocean-ridge basalts. A broad generalization is that results for these sites on the whole suggest a source slightly richer in the more incompatible elements than normal ocean-ridge mantle and/or that the majority of magmas formed by slightly smaller amounts of partial melting than normal ridge basalts and possibly in the presence of residual garnet. Compared to the Site 1213 basalts, some of the Site U1347 and U1350 lavas show slightly greater enrichment in the more incompatible elements.

Seeing through the effects of alteration is a much greater challenge with samples from Sites U1346, U1348, and U1349. However, alteration-resistant elements, particularly Zr and Ti, provide the following insights. All of these rocks are (or were originally) tholeiitic basalts. Those from Shirshov Massif Site U1346 are similar to the Site 1213 basalts, whereas the Site U1348 volcanoclastic rocks from the northern Tamu Massif are broadly similar to the lavas of Site U1347 (Fig. F11B). In addition to severe alteration, the compositions of basalts from Site U1349 atop the Ori Massif have been modified by variable accumulation of olivine and possibly clinopyroxene. Allowing for these effects, the Site U1349 samples appear to represent significantly less differentiated magmas than rocks from the other sites; they show compositional similarities with primitive ocean-ridge and Ontong Java basalts.

## Structure

Primary structural elements observed in Expedition 324 cores include sediment bedding, conjugate joints, veins, breccias, and microfaults. In addition, synmagmatic structures, such as amygdules, vesicles, pipe vesicles, sheet flow structures, and inter-pillow and intrapillow structures, were also examined. Most veins are postmagmatic

and were filled postcooling. Most horizontal veins show syntaxial growth, cutting veins with other orientations, suggesting that horizontal contraction produced the syntaxial veins at a late stage of formation. Syntaxial veins in Holes U1349A and U1350A are more common than those in other holes, possibly implying that Ori Massif experienced more contractional stress than Tamu and Shirshov massifs. The spatial distribution of joints and veins is complex in Shatsky Rise lavas. In general, dip angles of both veins and joints in the holes become steeper gradually downhole except for Hole U1350A. The population of joints and/or veins possibly depends on physical properties of the rocks. Regular veins are commonly well developed in basalts with fine-grained groundmass and low vesicularity in all the holes. Two primary synmagmatic structures, pillow and sheet flow structures, are common in all holes except for U1348A. At the other four sites, sequences of stacked pillow lavas whose sizes range from ~20–200 cm or stacked sheet flows with sizes of up to 23 m were observed. Only the upper part of Hole U1349A implies subaerial eruption; rocks in all other cored sections are those of submarine eruptions.

## Paleomagnetism

The goal of paleomagnetic studies during Expedition 324 was to characterize magnetic remanence of recovered igneous rocks from all the drilled holes on Shatsky Rise. The majority of basalt rock samples showed low coercivity and blocking temperatures characteristic of titanomagnetite (-magnetite) with a range of Ti content. Overall, it was found that stable characteristic magnetization inclinations are shallow and mostly negative. However, several atypical behaviors were encountered and need to be addressed during postcruise research before interpreting the results. For example, in some stratigraphic units, many samples displayed irregular behavior during demagnetization experiments. Additionally, samples from Hole U1349A may show evidence of a chemical remanent magnetization (from hematite) instead of a thermoremanent magnetization (from titanomagnetite). In some samples, partial self-reversal of the magnetization may have occurred during the thermal demagnetization procedure. However, the overall results show shallow average inclinations at all sites, supporting the hypothesis that Shatsky Rise was formed near the paleomagnetic equator. Furthermore, the low scatter in stratigraphic-average inclination groups implies that at most sites, especially Sites U1347 (Tamu Massif) and U1346 (Shirshov Massif), little time passed during the eruption of igneous units (Fig. F27).

Data from the volcaniclastic sediments at Site U1348 were the only sedimentary measurements made during Expedition 324. Samples from this site show higher coerciv-

ity, consistent with single-domain titanomagnetite. The average stable magnetization inclinations from these samples are also low, implying low paleolatitude. Because these rocks are volcanoclastic sediments, the inclinations are from a depositional remanent magnetization, rather than a thermal remanent magnetization as at other sites, that requires further measurements and interpretation.

## Physical properties

Expedition 324 recovered igneous material that had experienced minimal to near-complete alteration, which naturally affected physical properties. Site U1346, atop the Shirshov Massif, and Site U1349, at the summit of the Ori Massif, exhibit the most extreme and variable alteration, which is reflected in their physical properties. Natural gamma radiation counts from the  $^{40}\text{K}$  decay chain are three to four times higher in the altered material recovered at these sites versus fresh material (Sites U1347 and U1350 in Fig. F28). Magnetic susceptibility displays distinct drops associated with oxidative alteration at both Sites U1346 and U1349. Cores from Hole U1349A are remarkable for the extent of oxidative alteration, suggested by the presence of hematite in Sections 324-U1349-7R-1 through 10R-5. In this interval, the magnetic susceptibility drops to levels ubiquitously  $<1000 \times 10^{-5}$  SI (Fig. F29). Below the oxidative front, where hematite is no longer present, there is higher magnetic susceptibility. An analogous relationship is seen in Hole U1346A, whereby gray alteration has a higher magnetic susceptibility than oxidative brown alteration. Other notable physical properties in Hole U1346A include a distinct excursion in NGR from the  $^{238}\text{U}$  decay chain to values of almost 200 cps at 129.6–129.9 m CSF-A (Section 324-U1346-5R-1) in sedimentary material (Fig. F28).

In stark contrast to the altered material of Holes U1346A and U1349A, the comparatively fresh igneous material recovered in Holes U1347A and U1350A have low NGR counts ( $<5$  cps) (Fig. F28). Coring in both Holes U1347A and U1350A recovered igneous material consisting of alternating pillow lavas and massive inflation flows with broadly similar physical properties. Discrete measurements yield densities of 2.32–3.23 g/cm<sup>3</sup>, porosities of 0.17%–29.47%, and *P*-wave velocities (with negligible anisotropy) of 3.04–7.08 km/s. Notable intervals include a massive flow unit (Cores 324-U1347A-26R to 29R) at the bottom of Hole U1347A. This unit displayed the highest consistent readings of magnetic susceptibility, as well as cyclic magnetic susceptibility variations that might be used to decipher the chemical stratigraphy of the flow. Site U1350 was the most consistent with respect to downhole physical properties. There was very little variation in density and a slight downhole decrease in magnetic

susceptibility. Sedimentary interbeds were commonly observed in both Hole U1347A and U1350A cores and readily distinguished by their lower GRA bulk densities and magnetic susceptibility. The variations in density, porosity, and *P*-wave velocity measured on discrete samples were dominantly related sampling bias (e.g., vesicularity) rather than lithologic distinction.

Hole U1348A was quite different from the other sites in terms of its physical properties. Magnetic susceptibility values were  $<110 \times 10^{-5}$  SI and GRA densities were lower compared to igneous material from other sites (Figs. F29, F30). GRA density was also notable for its smooth, gradual increase in individual stratigraphic units, plausibly related to compaction of the sedimentary material. The *P*-wave velocities were the lowest seen at any of the sites in the expedition, with values ranging from 2.09 to 3.32 km/s with an average of  $2.78 \pm 0.79$  km/s ( $2\sigma$ ;  $n = 13$ ). The material was also notable for its high porosity (all between 20% and 40%).

## Downhole logging

Downhole logging data obtained during Expedition 324 included natural and spectral gamma ray, density, neutron porosity, PEF, electrical resistivity, and sonic measurements as well as borehole formation oriented images from the FMS. Interpretation of gamma ray and electrical resistivity downhole logs was used to identify logging units at four sites on Shatsky Rise. Data were recorded in sections covered by the BHA, in the sedimentary sequences in the open hole interval, and in the basaltic basement. The sedimentary sequences throughout the Shatsky Rise sites show prominent gamma ray anomalies associated with U and K enrichments. Some of the most prominent anomalies are found at the sediment/basement interface and in the most altered sites. They may be indicative of focused hydrothermal fluid flow, whereas shallower anomalies recorded through the BHA may correlate to oceanic anoxic events previously interpreted in this area. High K content in the basement section also indicates a high degree of alteration in several of the holes drilled during Expedition 324 when compared to upper crustal sections previously drilled in other oceanic localities (Fig. F31). Electrical resistivity measurements in the basaltic basement show distinctive high-resistivity zones that likely represent massive flows and pillow flow units, interspersed with low-resistivity zones that mark sediment interbeds and highly altered zones. FMS images show zones of distinctive pillow lavas; zones with high fracture and vein densities; vesicular, brecciated, and volcanoclastic intervals; and intervals that represent massive lava flows, flow contacts, and variable dipping beds throughout the Shatsky Rise sites.

## Preliminary scientific assessment

### Plume versus plate

Many of the Expedition 324 objectives relate to the ongoing debate about the source of volcanism and whether the plume head hypothesis explains oceanic plateau formation. To inform this debate, it is critical to know how quickly Shatsky Rise formed and what is the source of the magmas. Three primary objectives addressing these issues are: (1) *to determine the basement age to constrain the temporal evolution of Shastky Rise*, (2) *to determine chemical and isotopic compositions of igneous rocks cored from the plateau*, and (3) *to determine the source temperature and degree of partial melting that produced the plateau lavas*. Achieving these three primary objectives would directly address the aim of the cruise: “Testing plume versus plate tectonic models of ocean plateau formation.” In order to address the primary objectives, we planned to core as many basement lava flows as possible in the allocated time at five sites on the Shatsky Rise (Figs. F2, F3). During this expedition, basement was penetrated at four of the five sites: U1346 (52.6 m basement penetration), U1347 (159.9 m basement penetration), U1349 (85.3 m basement penetration), and U1350 (172.7 m basement penetration). Although basement lavas were not encountered at Site U1348, a thick volcanoclastic sequence was penetrated (~120 m) that can yield important data about submarine emplacement processes and weathering styles on Shatsky Rise.

To obtain reliable  $^{40}\text{Ar}/^{39}\text{Ar}$  radiometric age data, the recovery of lavas of suitable freshness was crucial because submarine alteration can strongly modify the composition of rocks and seriously impact the K-Ar decay system. Shipboard petrographic studies and geochemical data from core samples obtained from Sites U1347 and U1350 show that in general alteration has only slightly affected rocks from these sites, making them especially suitable for high-quality postcruise  $^{40}\text{Ar}/^{39}\text{Ar}$  age determinations. The effects of alteration are more significant for most basement lavas from Sites U1346 and U1349, but some individual samples might be fresh enough to produce reliable age data given special treatment. Because basement lavas have been sampled from all three main massifs (Tamu, Ori, and Shirshov massifs), the age data will constrain the timing and duration of volcanism of the whole Shatsky Rise and reveal if the volcanism shows the expected age progression. Furthermore, with two sites each on Tamu and Ori massifs, it should be possible to determine whether each edifice was formed quickly, as expected for a plume head eruption, or over a longer time span, which would support less effusive, plate tectonic-related models.

Freshness of the recovered rock samples is also important for most chemical and isotopic studies, whose goals are to establish the original elemental compositions of the rocks and their isotopic characteristics. Such data are crucial for determining the mantle source composition. Although the geochemical signature of any lower-mantle source is debated, in general it is expected that mantle plumes give rise to igneous rocks with OIB-type isotopic characteristics and incompatible element ratios that indicate enrichment of highly incompatible elements in the magma source relative to the source of most MORB. The well-preserved lavas from Site U1347 and U1350 are particularly suitable for the determination of isotopic ratios and chemical compositions in postcruise studies. Such data will be important for inferring mantle source compositions. Although the effects of alteration are more severe for lavas from Sites U1346 and U1349, many individual samples from these sites appear suitable for most geochemical studies, particularly for investigations involving ratios of immobile incompatible elements and alteration-resistant isotope systems (e.g., Sm-Nd and Lu-Hf) and several other isotope systems provided special treatment of the samples (e.g., analyses of mineral separates or microanalyses by laser ablation techniques). Most important, large amounts of fresh volcanic glasses were recovered at several intervals from Sites U1346, U1347, and U1350. Fresh glass is also found in a continuous interval within the volcanoclastic succession of Site U1348 (intervals 324-U1348A-23R-1, 110–126 cm, to 23R-2, 1–8 cm). The recovery of fresh glass samples gives us the opportunity to determine volatiles and noble gases and to conduct a number of high-quality isotopic and geochemical studies. If OIB chemistry is found in the fresh glass and/or high ratios of  $^3\text{He}/^4\text{He}$  in mineral separates (generally assumed to indicate lower mantle origin) the plume model will be supported or, conversely, if no evidence of lower-mantle involvement is found, the plate model will be strengthened.

In order to estimate source temperatures and the degree of partial melting, it was important to core primitive rocks with olivine phenocrysts. Such primitive rocks, which are called picritic basalts, were recovered at Site U1349, providing an opportunity to estimate source temperatures by detailed postcruise studies. Although the picritic basalts have suffered from severe alteration as well as accumulation of olivine and clinopyroxene in primary melts, they show compositional similarities with picritic basalts from the Ontong Java Plateau (i.e., Kroenke-type basalts). If the estimated potential temperature and degree of melting indicate an abnormally hot mantle, plume models will be strengthened. On the other hand, if the estimated values are consistent with those of ambient mantle (i.e., MORB-source mantle), plate models will be supported. Another important result of this drilling expedition is the recovery of spinel crystals in Site U1346 and U1349 basalts. Because spinel is crystallized from relatively

primitive magmas, onshore studies of its composition may provide important information on the degree of melting of the mantle source.

## Oceanic plateau evolution

Whereas the primary objectives are directly related to each other, secondary objectives show a wider variety. Thus, preliminary scientific assessments for the secondary objectives are described separately as follows.

### *1. Determine the physical volcanology of Shatsky Rise eruptions.*

Expedition 324 recovered basement lavas from two summit sites (Sites U1346 and U1349) and two flank sites (Sites U1347 and U1350). Lava flows at both summit sites are characterized by high (>40 vol%) vesicularity, implying that the eruptive environment was shallow marine or even subaerial. A subaerial eruption is likely for Site U1349 lavas because of the style of weathering and the recovery of a highly oxidized horizon, which is interpreted as a possible paleosol, found directly above the highly vesiculated lavas. In contrast, lava flows encountered at the two flank sites are mainly composed of pillow basalts and massive inflation units, frequently interbedded with volcanoclastic or marine sediment. One massive basalt unit at Site U1347 is a very thick (~23 m) homogeneous lava flow, which shows similar characteristics to continental flood basalt flows. The presence of both pillow and massive basalts was also found during Ontong Java Plateau drilling (Mahoney et al., 2001). The exceptionally high basement recovery (for RCB drilling) at many sites (averaging 39%–67%, with many individual cores reaching >90%) will allow a detailed examination of flow unit distribution and emplacement. Together with the planned postcruise structural geological investigations and age determinations from calcite veins, an integrated model for the volcanological evolution of the rise can be reconstructed.

### *2. Determine the magmatic polarity of Tamu Massif and paleolatitude of Shatsky Rise.*

Sager and Han (1993) suggested that the magnetic anomaly of Tamu Massif was constructed in a short period of time during a period of reversed magnetic polarity. Shipboard paleomagnetic study for a thick (159.9 m) lava pile at Site U1347 implies that the entire succession has the same magnetic polarity, which supports the model of Sager and Han (1993). Paleolatitude measurements of oriented samples from all sites conclude that Shatsky Rise was located on or near the paleoequator during eruption. Although these preliminary results need to be refined by further, more detailed post-

cruise studies, the general model of a very short term formation of the entire Shatsky Rise in a near-Equator position seem to hold.

### *3. Determine paleodepths of Shatsky Rise.*

Seismic profiles of two massifs (Ori and Shirshov) show flat basement summits beneath the sediment cover, indicating wave erosion; although these massifs are all in >2000 m water depth today. This fact may be explained by significant lithospheric uplift before/during Shatsky Rise formation and later subsidence below sea level as the massifs moved away from the magma source, consistent with the plume model (e.g., Ito and Clift, 1998). If we assume that all four basement sites of Expedition 324 (Sites U1346, U1347, U1349, and U1350) subsided at rates similar to normal oceanic lithosphere, their calculated original eruption depths would have been shallow marine or above sea level (Fig. F26). Furthermore, Expedition 324 coring provided a number of other observations that imply shallow submarine and/or subaerial eruption of Shatsky Rise. Benthic foraminifers in sediments immediately overlying the igneous basements imply shallow paleowater depths of <500 m for Site U1346 and <200 m for Site U1347. At Sites U1346, U1347, and U1349, sediments just above the basements are interpreted as shallow-water bioclastic sandstones with volcanic clasts. The high vesicularity (>40 vol%) of recovered basalts at two summit sites (U1346 and U1349) also indicate shallow submarine or subaerial eruption because erupted magma must have been oversaturated with water. Assuming that the primary water content of the magma was similar to MORB and Ontong Java Plateau magmas (<0.5 wt%), we estimate that the volatilization depth must have been <300 m (Newman and Lowenstern, 2002). Assuming original eruption depths in shallow water (or in air) and taking into account the contribution of the sediment load (Crough, 1983), the estimated subsidence for the basement sites, except for Site U1350 is 3200–3400 m (Fig. F26). This value is in excellent agreement with the prediction (3000–3600 m subsidence) for 140–150 Ma normal oceanic lithosphere. Figure F26 also shows that Sites U1346, U1347, and U1349 were significantly shallower (2000–2500 m) during eruption time compared to normal mid-oceanic ridges. Although an eruption depth for Site U1350 is undetermined so far, postcruise studies will determine dissolved CO<sub>2</sub> in the few preserved fresh glass rims. Because of the strong pressure dependence of CO<sub>2</sub> solubility in basaltic melts and because fresh glasses were recovered at almost all sites (U1346–U1348 and U1350), we can expect further constraints of the uplift and subsidence history of Shatsky Rise.

4. *Determine magma evolution and magma chamber process of Shatsky Rise.*

In order to determine crustal magma chamber and evolution processes, obtaining lava samples from several evolutionary stages is desired (from less evolved, Mg-rich compositions to more differentiated, Mg-poor compositions). Expedition 324 recovered samples ranging from picritic basalts with high MgO content (as much as 15.6 wt%) to more differentiated tholeiitic basalts with low MgO content (as little as 4.9 wt%). The picritic basalts were cored at Site U1349, and tholeiitic basalts were sampled from the other three basement sites (U1346, U1347, and U1350). Phenocryst assemblages of the basement rocks correlate well with rock compositions; picritic basalts have only olivine phenocrysts with spinel inclusions and the tholeiitic basalts are olivine-bearing plagioclase-clinopyroxene-phyric basalts. This correlation will be further examined by more detailed postcruise studies, but it is expected that the recovered material is suitable to address magmatic evolutionary processes. For example, plagioclase phenocrysts with reverse zoning and oscillatory zoning are observed in several rocks from Sites U1347 and U1350. The zoning profiles will be investigated by postcruise studies and will help to constrain magma evolution processes.

## Operations

Expedition 324 began in Yokohama, Japan, and drilled five holes at five sites at Shatsky Rise (Sites U1346–U1350) before transiting to Townsville, Australia. Times in this operations section are given in local ship time. During the transit to the first site (U1346), shipboard clocks were advanced 1 h, resetting local ship time to Sydney Standard Time (Universal Time Coordinated + 10). No further adjustments to the clock were made during the expedition.

## Yokohama port call

Expedition 324 started on 4 September 2009 at the port of Yokohama with the changing and crossover of Overseas Drilling Limited and Integrated Ocean Drilling Program personnel. Expedition 324 scientists boarded the ship on 5 September. In addition to the routine resupply of expendables and the offloading of Expedition 323 cores and returning freight, some items of note were the loading of 1800 MT of marine gas oil, overhaul of the passive heave compensator, and service visits by Novenco (air conditioning), RigNet (Very Small Aperture Terminal [VSAT]), and Hose-McCann (ship phone/intercom/alarm system) field engineers. This port call was also noteworthy for

the extensive number of visitors that were treated to a tour of the vessel including visitors of the Museum of Nature and Sciences in Tokyo, members of the Japanese scientific community, and U.S. embassy personnel. A press conference for Japanese and international media was held on 5 September.

During this ~5 day port call, we were not able to send or receive e-mail or use the ship's phone system because of local electromagnetic interference, which prevented VSAT operation. Although some maintenance was possible on the aft antenna, the RigNet engineer was unable to perform a systems check and calibration to the VSAT system because of the interference.

Once the last line was released at 0950 h on 9 September, the vessel was under way to the pilot station. The RigNet engineer stayed aboard and attempted last-minute adjustments while working with rig-based technicians. The pilot and RigNet representative disembarked at the pilot station at ~1130 h. A short time after this, VSAT operation was restored and remained until the first course change. At this time, the signal was lost and in spite of the best efforts of onboard technicians communicating with the RigNet engineer in the hotel using the Inmarsat GMDSS satellite phone, the VSAT system could not be restored to normal working order. A decision was made to reverse course, return to a convenient rendezvous point close to the head of Sagami Bay, and bring the RigNet engineer back to work on the system.

The RigNet engineer was welcomed aboard shortly before 0600 h on 10 September and remained for nearly 2 h restoring the VSAT to operation. Once he departed at 0740 h, the vessel began its voyage to Site U1346.

## **Transit to Shatsky Rise and Site U1346 (Shirshov Massif)**

After a transit of 4 days, the *JOIDES Resolution* set position on Site U1346 (proposed Site SRNH-2) at 0930 h on 14 September 2009. The RCB drilling assembly was prepared, the pipe lengths were measured, and the drillers proceeded to run pipe through the moonpool. At 0140 h on 15 September, the seafloor was tagged at 3630.0 m drilling depth below rig floor (DRF) and Hole U1346A was advanced without coring to 100.5 m drilling depth below seafloor (DSF). Rotary coring was initiated at 100.5 m DSF and deepened the hole to a total depth of 191.8 m DSF by 0915 h on 18 September (Table T1). Basaltic basement was contacted at 139.2 m CSF-A (total basement penetration = 52.6 m). The average penetration rate for basement coring was 1.3 m/h with an average recovery of 38.7%. Because of the slow penetration rate combined

with the successful recovery of material suitable to address most of the objectives for this site, it was decided to end coring at this depth and prepare the hole for logging operations. An additional factor in the decision to cease coring operations at this site was the approach of Typhoon Choi-Wan. The hole was logged with triple combo on 18 September. Poor hole conditions, however, did not warrant deployment of the FMS tool string. The vessel departed for Site U1347 at 1800 h on 19 September. Because of the proximity of Sites U1348 and U1349 to the projected track of Typhoon Choi-Wan, it was decided to proceed directly to the more southerly and higher priority site.

### Site U1347 (Tamu Massif)

The *JOIDES Resolution* established position on Site U1347 (proposed Site SRSB-3B) at 1730 h on 21 September 2009, and at 0500 the next morning, the seafloor was tagged at 3461.0 m DRF. Hole U1347A was drilled with a wash barrel in place to 71.0 m DSF, where rotary coring was initiated. Basaltic basement was reached at 157.6 m CSF-A (Table T1). Coring into basement continued until 2145 h on 25 September when operations were suspended in order to change to a fresh bit after the initial rotary bit had accumulated 60 rotating hours. A FFF was deployed and the bit was pulled out of the FFF early on the morning of 26 September. A new C-4 bit was affixed to the rotary drilling assembly and run through the moonpool toward the seafloor.

Hole U1347A was successfully reentered at 2250 h on 26 September. The drill string was advanced to the bottom of the hole where the driller found only 1 m of soft fill. At 0500 h on 27 September coring resumed but had to be suspended for 5.75 h to replace the broken core winch motor. Once the new motor was mounted and tested, coring resumed. From 1530 h on 27 September to 1230 h on 30 September rotary coring deepened the hole from 242.7 m DSF to a final depth of 317.5 m DSF. Operations were concluded when the last core was only able to advance 1 m in 3 h, possibly because of either a worn bit, an extremely hard formation, or a combination of both.

Total penetration into basement in Hole U1347A was 159.9 m cored at an average rate of penetration (ROP) of 1.5 m/h. While coring basement, the ROP for individual cores ranged from a lethargic 0.7 m/h to a more energetic 4.1 m/h. The average recovery for basement coring was 64.2%.

In preparation for logging, the bit was released at the bottom of the hole and the bore was displaced with 83.5 bbl of 10.5 ppg mud. The drill string was pulled back in the

hole and set at a depth of 131.5 m DSF. The first logging run was made with the triple combo and succeeded in reaching within 2 m of the bottom of the hole. A preliminary analysis of the results of the first logging run indicated that the hole was in good condition and suitable for the additional measurement runs planned for this site. The second tool deployed was the FMS-sonic which was also successfully run (two complete passes). The third logging tool suite, which included the UBI, had to be cancelled because of hardware problems with the logging tools.

After the logging equipment was secured, the drill string and the beacon were retrieved in routine fashion. Once the drilling equipment was secured, the vessel departed for the next site at 0400 h on 2 October. The total time devoted to Site U1347 was 10.4 days.

### **Site U1348 (Tamu Massif)**

The *JOIDES Resolution* established position on Site U1348 (proposed Site SRS-6) at 1515 h on 2 October 2009. After a delay of 4 h to fix a problem with the drawworks clutch, the driller tagged seafloor at 1130 h on 3 October at 3275.0 m DRF. Hole U1348A was drilled with a wash barrel in place to 84.2 m DSF where rotary coring was initiated. Coring proceeded from 84.2 to 189.9 m DSF (105.7 m) with a poor average recovery of 3.5% caused mostly by the prevalence of soft sediment and chert. Once past this depth and starting with Core 324-U1348A-13R, the recovery improved markedly as the sediments transitioned to sandstone and then to volcanoclastics. After discussion, the science party elected to terminate the hole at a depth of 324.1 m DSF (Table T1). The bottom 134.2 m of the hole was cored at an average ROP of 8.9 m/h with an average recovery of 57.5%. The average recovery for the cored interval of 239.9 m was 33.7%.

The hole was prepared for logging operations with a wiper trip and displacement with 86 bbl of heavy mud. Following the release of the bit at the bottom of the hole, the drill string was pulled back and the end of pipe placed at 97.6 m DSF. At 2030 h on 5 October, the Schlumberger equipment was rigged up and the first tool string (triple combo) was successfully deployed to ~322 m DSF, only 2 m above the bottom of the hole. Once the triple combo was recovered, the second logging suite (FMS-sonic) was made up and deployed at 0700 h on 6 October. This tool was also able to reach within 2 m of the bottom of the hole. As the tool was being drawn back into the drill string, it became firmly stuck in the BHA with the electrical pad arms at the level of the top

connector of the mechanical bit release. For 1.5 h the logging winch operator attempted to advance the tool with no success.

The only option remaining was to use the Kinley crimper and cutter system to recover the recalcitrant instrument. The Kinley crimper was deployed and severed the logging line just above the cable head of the tool suite. The severed end of the logging line was recovered and the drill string retrieved. When the BHA was at the surface, the FMS-sonic tool was still firmly pinned by the springs of the broken FMS pad arms inside the top connector of the mechanical bit release.

After the logging equipment was disassembled, the vessel departed for the next site at 0848 h on 7 October. The total time on site was 4.7 days.

### Site U1349 (Ori Massif)

The *JOIDES Resolution* arrived at Site U1349 (proposed Site SRCH-5) at the summit of Ori Massif at 2145 h on 7 October 2009 after a transit of 12.9 h. The drill string was routinely deployed and after the driller tagged seafloor at 3138.0 m DRF, or ~5 m shallower than the corrected precision depth recorder depth, Hole U1349A was spudded with the rotary system at 0600 h on 8 October. The hole was drilled with a wash barrel to 116 m DSF, where coring was initiated. The sediment portion of the hole was cored with the usual low average recovery (23%) because of the prevalence of chert within the soft pelagic ooze. At 165.1 m CSF-A, basement was encountered. Coring in the hole continued into basement without incident to 250.4 m DSF (85.3 m into basement) (Table T1) by 1430 h on 11 October, when coring in the hole was terminated. The decision to stop coring at this site was made during a science meeting held earlier in the day. Hole U1349A was cored with an overall average recovery of 49.0%. The basement portion of the hole was cored at an average ROP of 1.8 m/h and with an average recovery of 67.4%.

The hole was prepared for logging with a 50 bbl mud flush followed by a round trip of the drill string from 250 to 86 m DSF. After one more 50 bbl mud treatment, the bit was released at the bottom of the hole with the rotary shifting tool on the coring line. Prior to tripping the drill string to the logging depth of 119.3 m DSF, the hole was displaced with 56 bbl of 10.5 ppg heavy mud. The first logging run of Hole U1349A was made with the triple combo, which was deployed at 2140 h on 11 October and retrieved at 0240 h the next morning. The second logging run was conducted with the FMS, which was deployed at 0355 h and recovered at 0930 h. The hole was

found in good condition (except for one tight spot just below the end of the pipe) and both the triple combo and FMS runs retrieved excellent data.

After the logging equipment was secured and the drill string and beacon were recovered, the vessel departed for Site U1350 at 1930 h on 12 October. The time expended on Site U1349 was 126.8 h, or 5.3 days.

## Site U1350

The vessel positioned on Site U1350 (proposed Site SRNH-2) at 0115 h on 13 October 2009 after a 53 nmi voyage from Site U1349. The driller tagged the seafloor at 4067.0 m DRF at 1030 h. Hole U1350A was spudded with a wash barrel in place and drilled to 104.6 m DSF, where rotary coring was initiated. The sediment portion (48.0 m) of the hole was cored with the usual poor recovery (1.6%) resulting from chert stringers intermixed with the host sediments, which likely consisted of soft ooze and chalk. Igneous basement was reached with Core 324-U1350A-6R at 143.1 m DSF, which was slightly higher than expected (~157 m below seafloor, calculated from the site survey seismic data).

Rotary coring deepened the hole to a final depth of 315.8 m DSF (Table T1) by 2015 h on 18 October when operating time expired. The final depth corresponds to a total penetration of 172.7 m in basement, which was cored with an average recovery of 43.2% and an average ROP of 2.0 m/h. The total interval of 315.8 m was cored with an average recovery of 35.6% at an average ROP of 3.5 m/h. When coring was halted, the bit had accumulated 91.2 rotating hours and was still viable.

In preparation for logging, the hole was flushed with a 50 bbl mud sweep followed by a wiper trip up to 84 m DSF and back to 316 m DSF. Following another 50 bbl sweep, the bit was released with the rotary shifting tool and the hole was displaced with 90 bbl of 10.5 ppg heavy mud. The pipe was then pulled back in the hole with the end of pipe placed at the logging depth of 117 m DSF.

The first of potentially two logging runs was attempted with the triple combo, which was deployed at 0640 h on 19 October and lowered at a speed of 2200 m/h to a depth of 3600 m DRF. At this depth, the head tension decreased dramatically and the cable speed was reduced to ~90–120 m/h to avoid potential damage to the wireline. The slow progress required pumping pressure down the drill pipe to aid the descent. After making very slow progress to a depth of 4000 m DRF it was decided to pull out of the

hole to check the tool string and cable for damage. With the tool string on the rig floor, high volumes of water were pumped through the pipe to remove any potential obstruction. The tool string was deployed a second time with similar results, reaching 4122 m DRF. As time was running out and the weather was progressively deteriorating (initial ship heave conditions of ~2 m changed to ~4 m with wind gusts of up to 56 kt) and without knowing the cause of the low-tension problem, it was decided to terminate the logging operations. The tool was recovered at 2330 h and after the logging equipment was rigged down the drill string was pulled out of the hole, clearing the seafloor at 0125 h on 20 October. Following the securing of the drilling equipment and hydrophones and recovery of the beacon, the vessel departed for its long voyage to Townsville at 1245 h on 20 October. The total time at Site U1350 was 7.5 days.

Magnetic field data were collected during the transit to Townsville using the borrowed Geometrics magnetometer. On the way south, the ship was steered first across Helios Basin, south of Ori Massif, and along a gap between magnetic track lines on Tamu Massif. The ship continued to collect magnetic data after departing Shatsky Rise, including a north–south profile across western Ontong Java Plateau. The transit ended at 0800 h on 2 November, when the ship finally reached the sea buoy outside of Townsville.

## References

- Allègre, C.J., and Turcotte, D.L., 1985. Geodynamic mixing in the mesosphere boundary layer and the origin of oceanic islands. *Geophys. Res. Lett.*, 12(4):207–210. doi:10.1029/GL012i004p00207
- Anderson, D.L., 1995. Lithosphere, asthenosphere, and perisphere. *Rev. Geophys.*, 33(1):125–149. doi:10.1029/94RG02785
- Anderson, D.L., 2001. Top-down tectonics? *Science*, 293(5537):2016–2018. doi:10.1126/science.1065448
- Anderson, D.L., 2005. Scoring hotspots; the plume and plate paradigms. In Foulger, G.R., Natland, J.H., Presnall, D.C., and Anderson, D.L. (Eds.), *Plates, Plumes, and Paradigms*. Spec. Pap.—Geol. Soc. Am., 388:31–54.
- Anderson, D.L., and Natland, J.H., 2005. A brief history of the plume hypothesis and its competitors: concept and controversy. In Foulger, G.R., Natland, J.H., Presnall, D.C., and Anderson, D.L. (Eds.), *Plates, Plumes, and Paradigms*. Spec. Pap.—Geol. Soc. Am., 388:119–146.
- Anderson, D.L., Tanimoto, T., and Zhang, Y.-S., 1992. Plate tectonics and hotspots: the third dimension. *Science*, 256(5064):1645–1651. doi:10.1126/science.256.5064.1645
- Bach, W., Hegner, E., Erzinger, J., and Satir, M., 1994. Chemical and isotopic variations along the superfast spreading East Pacific Rise from 6°S to 30°S. *Contrib. Mineral. Petrol.*, 116:365–380.
- Bercovici, D., and Mahoney, J., 1994. Double flood basalts and plume head separation at the 660-kilometer discontinuity. *Science*, 266(5189):1367–1369. doi:10.1126/science.266.5189.1367
- Brandon, A.D., Graham, D.W., Waight, T., and Gautason, B., 2007. <sup>186</sup>Os and <sup>187</sup>Os enrichments and high-<sup>3</sup>He/<sup>4</sup>He sources in the Earth's mantle: evidence from Icelandic picrites. *Geochim. Cosmochim. Acta*, 71(18):4570–4591. doi:10.1016/j.gca.2007.07.015
- Campbell, I.H., 1998. The mantle's chemical structure: insights from the melting products of mantle plumes. In Jackson, I. (Ed.), *The Earth's Mantle: Composition, Structure, and Evolution*: Cambridge (Cambridge Univ. Press), 259–310.
- Coffin, M.F., and Eldholm, O., 1994. Large igneous provinces: crustal structure, dimensions, and external consequences. *Rev. Geophys.*, 32(1):1–36. doi:10.1029/93RG02508
- Coffin, M.F., Pringle, M.S., Duncan, R.A., Gladchenko, T.P., Storey, M., Müller, R.D., and Gahagan, L.A., 2002. Kerguelen hotspot magma output since 130 Ma. *J. Petrol.*, 4(7)3:1121–1140. doi:10.1093/petrology/43.7.1121
- Courtillot, V., Davaille, A., Besse, J., and Stock, J., 2003. Three distinct types of hotspots in Earth's mantle. *Earth Planet. Sci. Lett.*, 205(3–4):295–308. doi:10.1016/S0012-821X(02)01048-8
- Crough, S.T., 1983. The correction for sediment loading on the seafloor. *J. Geophys. Res.*, [Solid Earth], 88:6449–6454. doi:10.1029/JB088iB08p06449
- Davaille, A., Le Bars, M. and Carbonne, C., 2003. Thermal convection in a heterogeneous mantle. *C. R. Geosci.*, 335(1):141–156. doi:10.1016/S1631-0713(03)00003-8
- Davaille, A., Stutzmann, E., Silveira, G., Besse, J., and Courtillot, V., 2005. Convective patterns under the Indo-Atlantic “box.” *Earth Planet. Sci. Lett.*, 239(3–4):233–252. doi:10.1016/j.epsl.2005.07.024

- Davies, G.F., 1992. Plates and plumes: dynamics of the earth's mantle. *Science*, 256(5069):493–494. doi:10.1126/science.257.5069.493
- Den, N., Ludwig, W.J., Murauchi, S., Ewing, J.I., Hotta, H., Edgar, N.T., Yoshii, T., Asanuma, T., Hagiwara, K., Sato, T., and Ando, S., 1969. Seismic-refraction measurements in the north-west Pacific Basin. *J. Geophys. Res.*, 74(6):1421–1434. doi:10.1029/JB074i006p01421
- DePaolo, D.J., and Manga, M., 2003. Deep origin of hotspots—the mantle plume model. *Science*, 300(5621):920–921. doi:10.1126/science.1083623
- Duncan, R.A., 2002. A time frame for construction of the Kerguelen Plateau and Broken Ridge. *J. Petrol.*, 43(7):1109–1119. doi:10.1093/petrology/43.7.1109
- Duncan, R.A., and Richards, M.A., 1991. Hotspots, mantle plumes, flood basalts, and true polar wander. *Rev. Geophys.*, 29(1):31–50. doi:10.1029/90RG02372
- Eldholm, O., and Coffin, M.F., 2000. Large igneous provinces and plate tectonics. In Richards, M.A., Gordon, R.G., and van der Hilst, R.D. (Eds.), *The History and Dynamics of Global Plate Motions*. Geophys. Monogr., 121:309–326.
- Ewing, M., Saito, T., Ewing, J.I., and Burckle, L.H., 1966. Lower Cretaceous sediments from the Northwest Pacific. *Science*, 152(3723):751–755. doi:10.1126/science.152.3723.751
- Farnetani, C.G., and Samuel, H., 2005. Beyond the thermal plume paradigm. *Geophys. Res. Lett.*, 32(7):L07311. doi:10.1029/2005GL022360
- Fischer, A.G., Heezen, B.C., et al., 1971. *Init. Repts. DSDP*, 6: Washington, DC (U.S. Govt. Printing Office). doi:10.2973/dsdp.proc.6.1971
- Fitton, J.G., and Godard, M., 2004. Origin and evolution of magmas on the Ontong Java Plateau. In Fitton, J.G., Mahoney, J.J., Wallace, P.J., and Saunders, A.D. (Eds.), *Origin and Evolution of the Ontong Java Plateau*. Geol. Soc. Spec. Publ., 229:151–178.
- Fitton, J.G., Mahoney, J.J., Wallace, P.J., and Saunders, A.D., 2004. Leg 192 synthesis: origin and evolution of the Ontong Java Plateau. In Fitton, J.G., Mahoney, J.J., Wallace, P.J., and Saunders, A.D. (Eds.), *Proc. ODP, Sci. Results*, 192: College Station, TX (Ocean Drilling Program), 1–8. doi:10.2973/odp.proc.sr.192.101.2004
- Foulger, G.R., 2002. Plumes, or plate tectonic processes? *Astron. Geophys.*, 43(6):19–23.
- Foulger, G.R., 2007. The “plate” model for the genesis of melting anomalies. In Foulger, G.R., and Jurdy, D.M. (Eds.), *Plates, Plumes, and Planetary Processes*. Spec. Pap.—Geol. Soc. Am., 430:1–28.
- Foulger, G.R., and Anderson, D.L., 2005. A cool model for the Iceland hotspot. *J. Volcanol. Geotherm. Res.*, 141(1–2):1–22. doi:10.1016/j.jvolgeores.2004.10.007
- Foulger, G.R., and Natland, J.H., 2003. Is “hotspot” volcanism a consequence of plate tectonics? *Science*, 300(5621):921–922. doi:10.1126/science.1083376
- Georgen, J.E., and Lin, J., 2002. Three-dimensional passive flow and temperature structure beneath oceanic ridge–ridge–ridge triple junctions. *Earth Planet. Sci. Lett.*, 204(1–2):115–132. doi:10.1016/S0012-821X(02)00953-6
- Gettrust, J.F., Furukawa, K., and Kroenke, L.W., 1980. Crustal structure of the Shatsky Rise from seismic refraction measurements. *J. Geophys. Res.*, [Solid Earth], 85:5411–5415. doi:10.1029/JB085iB10p05411
- Glen, W., 2005. The origins and early trajectory of the mantle plume quasi-paradigm. In Foulger, G.R., Natland, J.H., Presnall, D.C., and Anderson, D.L. (Eds.), *Plates, Plumes, and Paradigms*. Spec. Pap.—Geol. Soc. Am., 388:91–117.
- Gradstein, F.M., Ogg, J.G., and Smith, A. (Eds.), 2004. *A Geologic Time Scale 2004*: Cambridge (Cambridge Univ. Press). <http://www.stratigraphy.org/>

- Griffiths, R.W., and Campbell, I.H., 1990. Stirring and structure in mantle starting plumes. *Earth Planet. Sci. Lett.*, 99(1–2):66–78. doi:10.1016/0012-821X(90)90071-5
- Griffiths, R.W., and Campbell, I.H., 1991. Interaction of mantle plume heads with the earth's surface and onset of small-scale convection. *J. Geophys. Res., [Solid Earth]*, 96(B11):18295–18310. doi:10.1029/91JB01897
- Herzberg, C., Asimov, P.D., Arndt, N., Niu, Y., Lesher, C.M., Fitton, J.G., Cheadle, M.J., and Saunders, A.D., 2007. Temperatures in ambient mantle and plumes: constraints from basalts, picrites, and komatiites. *Geochem., Geophys., Geosyst.*, 8(2):Q02006. doi:10.1029/2006GC001390
- Hilde, T.W.C., Isezaki, N., and Wageman, J.M., 1976. Mesozoic sea-floor spreading in the North Pacific. In Woolard, G.P., Sutton, G.H., Manghnani, M.H., and Moberly, R. (Eds.), *The Geophysics of the Pacific Ocean Basin and its Margins*. Geophys. Monogr., 19:205–226.
- Hildebrand, A.R., and Boynton, W.V., 1990. Proximal Cretaceous–Tertiary boundary impact deposits in the Caribbean. *Science*, 248(4957):843–847. doi:10.1126/science.248.4957.843
- Hoernle, K., Hauff, F., and van den Bogaard, P., 2004. 70 m.y. history (139–69 Ma) for the Caribbean large igneous province. *Geology*, 32(8):697–700. doi:10.1130/G20574.1
- Ingle, S., and Coffin, M., 2004. Impact origin of the greater Ontong Java Plateau? *Earth Planet. Sci. Lett.*, 218(1–2):123–134. doi:10.1016/S0012-821X(03)00629-0
- Ito, G., and Clift, P.D., 1998. Subsidence and growth of Pacific Cretaceous plateaus. *Earth Planet. Sci. Lett.*, 161(1–4):85–100. doi:10.1016/S0012-821X(98)00139-3
- Ishikawa, A., Nakamura, E., and Mahoney, J.J., 2005. Jurassic oceanic lithosphere beneath the southern Ontong Java Plateau: evidence from xenoliths in alnöite, Malaita, Solomon Islands. *Geology*, 33(5):393–396. doi:10.1130/G21205.1
- Janney, P.E., and Castillo, P.R., 1999. Isotope geochemistry of the Darwin Rise seamounts and the nature of long-term mantle dynamics beneath the south central Pacific. *J. Geophys. Res., [Solid Earth]*, 104(B5):10,571–10,589. doi:10.1029/1998JB900061
- Johnson, S.T., and Thorkelson, D.J., 2000. Continental flood basalts: episodic magmatism above long-lived hotspots. *Earth Planet. Sci. Lett.*, 175(3–4):247–256. doi:10.1016/S0012-821X(99)00293-9
- Kellogg, L.H., Hager, B.H., and van der Hilst, R.D., 1999. Compositional stratification in the deep mantle. *Science*, 283(5409):1881–1884. doi:10.1126/science.283.5409.1881
- Klaus, A., and Sager, W.W., 2002. Data report: high-resolution site survey seismic reflection data for ODP Leg 198 drilling on Shatsky Rise, northwest Pacific. In Bralower, T.J., Premoli Silva, I., Malone, M.J., et al., *Proc. ODP, Init. Repts.*, 198: College Station, TX (Ocean Drilling Program), 1–21. doi:10.2973/odp.proc.ir.198.111.2002
- Kleinrock, M.C., and Phipps Morgan, J., 1988. Triple junction reorganization. *J. Geophys. Res.*, 93(B4):2981–2996. doi:10.1029/JB093iB04p02981
- Koppers, A.A.P., Staudigel, H., Pringle, M.S., and Wijbrans, J.R., 2003. Short-lived and discontinuous intraplate volcanism in the South Pacific: hot spots or extensional volcanism? *Geochem., Geophys., Geosyst.*, 4(10):1089. doi:10.1029/2003GC000533
- Larson, R.L., 1991. Latest pulse of Earth: evidence for a mid-Cretaceous super plume. *Geology*, 19(6):547–550. doi:10.1130/0091-7613(1991)019<0547:LPOEEF>2.3.CO;2
- Larson, R.L., and Chase, C.G., 1972. Late Mesozoic evolution of the western Pacific Ocean. *Geol. Soc. Am. Bull.*, 83(12):3627–3644. doi:10.1130/0016-7606(1972)83[3627:LMEOTW]2.0.CO;2

- Larson, R.L., Pockalny, R.A., Viso, R.F., Erba, E., Abrams, L.J., Luyendyk, B.P., Stock, J.M., and Clayton, R.W., 2002. Mid-Cretaceous tectonic evolution of the Tongareva triple junction in the southwestern Pacific Basin. *Geology*, 30(1):67–70. doi:10.1130/0091-7613(2002)030<0067:MCTEOT>2.0.CO;2
- Lassiter, J.C., Blichert-Toft, J., Hauri, E.H., and Barszczus, H.G., 2003. Isotope and trace element variations in lavas from Raivavae and Rapa, Cook–Austral islands: constraints on the nature of HIMU- and EM-mantle and the origin of mid-plate volcanism in French Polynesia. *Chem. Geol.*, 202(1–2):115–138. doi:10.1016/j.chemgeo.2003.08.002
- Le Maitre, R.W., Bateman, P., Dudek, A., Keller, J., Lameyre, J., Le Bas, M.J., Sabine, P.A., Schmid, R., Sorensen, H., Streckeisen, A., Woolley, A.R., and Zanettin, B., 1989. *A Classification of Igneous Rocks and Glossary of Terms*: Oxford (Blackwell).
- Lin, S.-C., and van Keken, P.E., 2006a. Dynamics of thermochemical plumes: 1. Plume formation and entrainment of a dense layer. *Geochem., Geophys., Geosyst.*, 7(2):Q02006. doi:10.1029/2005GC001071
- Lin S.-C., and van Keken, P.E., 2006b. Dynamics of thermochemical plumes: 2. Complexity of plume structures and its implications for mapping mantle plumes. *Geochem., Geophys., Geosyst.*, 7(3):Q03003. doi:10.1029/2005GC001072
- Ludwig, W.J., and Houtz, R.E., 1979. Isopach Map of Sediments in the Pacific Ocean Basin and Marginal Sea Basins. *AAPG Map Ser.*, 647.
- Lithgow-Bertelloni, C., and Richards, M.A., 1998. The dynamics of Cenozoic and Mesozoic plate motions. *Rev. Geophys.*, 36(1):27–78. doi:10.1029/97RG02282
- Macdonald, G.A., 1968. Composition and origin of Hawaiian lavas. In Coats, R.R., Hay, R.L., and Anderson, C.A. (Eds.), *Studies in Volcanology: A Memoir in Honor of Howel Williams*. Mem.—Geol. Soc. Am., 116:477–522.
- Macdonald, G.A., and Katsura, T., 1964. Chemical composition of Hawaiian lavas. *J. Petrol.*, 5:82–133.
- Machel, P., and Humler, E., 2003. High mantle temperature during Cretaceous avalanche. *Earth Planet. Sci. Lett.*, 208(3–4):125–133. doi:10.1016/S0012-821X(03)00041-4
- Mahoney, J.J., Duncan, R.A., Tejada, M.L.G., Sager, W.W., and Bralower, T.J., 2005. Jurassic–Cretaceous boundary age and mid-ocean-ridge–type mantle source for Shatsky Rise. *Geology*, 33(3):185–188. doi:10.1130/G21378.1
- Mahoney, J.J., Fitton, J.G., Wallace, P.J., et al., 2001. *Proc. ODP, Init. Repts.*, 192: College Station, TX (Ocean Drilling Program). doi:10.2973/odp.proc.ir.192.2001
- Mahoney, J.J., Sinton, J.M., Kurz, M.D., Macdougall, J.D., Spencer, K.J., and Lugmair, G.W., 1994. Isotope and trace element characteristics of a super-fast spreading ridge: East Pacific Rise 13–23°S. *Earth Planet. Sci. Lett.*, 121(1–2):173–193. doi:10.1016/0012-821X(94)90039-6
- Mahoney, J.J., and Spencer, K.J., 1991. Isotopic evidence for the origin of the Manihiki and Ontong Java oceanic plateaus. *Earth Planet. Sci. Lett.*, 104(2–4):196–210. doi:10.1016/0012-821X(91)90204-U
- Mahoney, J.J., Storey, M., Duncan, R.A., Spencer, K.J., and Pringle, M.S., 1993. Geochemistry and age of the Ontong Java Plateau. In Pringle, M.S., Sager, W.W., Sliter, W.V., and Stein, S. (Eds.), *The Mesozoic Pacific: Geology, Tectonics, and Volcanism*. Geophys. Monogr., 77:233–262.
- McNutt, M.K., and Fischer, K.M., 1987. The South Pacific superswell. In Keating, B.H., Fryer, P., Batiza, R., and Boehlert, G.W. (Eds.), *Seamounts, Islands, and Atolls*. Geophys. Monogr., 43:25–34.

- Morgan, W.J., 1971. Convection plumes in the lower mantle. *Nature (London, U. K.)*, 230(5288):42–43. doi:10.1038/230042a0
- Morgan, W.J., 1972. Deep mantle convection plumes and plate motions. *AAPG Bull.*, 56:203–213.
- Morgan, W.J., 1981. Hotspot tracks and the opening of the Atlantic and Indian Oceans. In Emiliani, C. (Ed.), *The Sea* (Vol. 7): New York (Wiley), 443–487.
- Nakanishi, M., Sager, W.W., and Klaus, A., 1999. Magnetic lineations within Shatsky Rise, northwest Pacific Ocean: implications for hot spot–triple junction interaction and oceanic plateau formation. *J. Geophys. Res.*, 104(B4):7539–7556. doi:10.1029/1999JB900002
- Nakanishi, M., Tamaki, K., and Kobayashi, K., 1989. Mesozoic magnetic anomaly lineations and seafloor spreading history of the northwestern Pacific. *J. Geophys. Res.*, 94(B11):15437–15462. doi:10.1029/JB094iB11p15437
- Natland, J.H., and Winterer, E.L., 2005. Lithospheric stresses, great fissures, and volcanism at seamounts and plateaus in the Pacific since the Jurassic. In Foulger, G.R., Natland, J.H., Presnall, D.C., and Anderson, D.L. (Eds.), *Plates, Plumes, and Paradigms*. Spec. Pap.—Geol. Soc. Am., 388:687–710.
- Neprochnov, Y.P., Merklin, L.R., and Khankishiyeva, L.M., 1984. Distribution map of the sedimentary cover on the Shatsky Rise. *Dokl. Akad. Nauk SSSR*, 277(5):1204–1207.
- Newman, S., and Lowenstern, J.B., 2002. VolatileCalc: a silicate melt-H<sub>2</sub>O-CO<sub>2</sub> solution model written in Visual Basic for Excel. *Comput. Geosci.*, 28(5):597–604. doi:10.1016/S0098-3004(01)00081-4
- Olson, P., and Nam, I.S., 1986. Formation of seafloor swells by mantle plumes. *J. Geophys. Res.*, [Solid Earth], 91:7181–7191. doi:10.1029/JB091iB07p07181
- Parsons, B., and Sclater, J.G., 1977. An analysis of the variation of ocean floor bathymetry and heat flow with age. *J. Geophys. Res.*, [Solid Earth], 82:803–827. doi:10.1029/JB082i005p00803
- Putirka, K., 2008. Excess temperatures at ocean islands: implications for mantle layering and convection. *Geology*, 36(4):283–286. doi:10.1130/G24615A.1
- Ray, J.R., Mahoney, J.J., Duncan, R.A., Ray, J.S., Wessel, P., and Naar, D., submitted. Chronology and geochemistry of the Nazca Ridge and Easter Seamount Chain: a 30 Myr hotspot record. *J. Petrol.*
- Ray, J.S., Mahoney, J.J., Johnson, K.T.M., Pyle, D.G., Naar, D., and Wessel, P., 2003. Geochemistry of volcanism along the Nazca Ridge and Easter Seamount Chain [EGS-AGU-EUG Joint Assembly, Nice, 06–11 April 2003].
- Richards, M.A., Duncan, R.A., and Courtillot, V.E., 1989. Flood basalts and hot-spot tracks: plume heads and tails. *Science*, 246(4926):103–107. doi:10.1126/science.246.4926.103
- Roddy, D.J., Schuster, S.H., Rosenblatt, M., Grant, L.B., Hassig, P.J., and Kreyenhagen, K.N., 1987. Computer simulations of large asteroid impacts into oceanic and continental sites—preliminary results on atmospheric, cratering and ejecta dynamics. *Int. J. Impact Eng.*, 5(1–4):525–541. doi:10.1016/0734-743X(87)90068-6
- Rogers, G.C., 1982. Oceanic plateaus as meteorite impact signatures. *Nature (London, U. K.)*, 299(5881):341–342. doi:10.1038/299341a0
- Roberge, J., Wallace, P.J., White, R.V., and Coffin, M.F., 2005. Anomalous uplift and subsidence of the Ontong Java Plateau inferred from CO<sub>2</sub> contents of submarine basaltic glasses. *Geology*, 33(6):501–504. doi:10.1130/G21142.1

- Sager, W.W., 2005. What built Shatsky Rise, a mantle plume or ridge processes? *In* Foulger, G.R., Natland, J.H., Presnall, D.C., and Anderson, D.L. (Eds.), *Plates, Plumes, and Paradigms*. Spec. Pap.—Geol. Soc. Am., 388:721–733.
- Sager, W.W., and Han, H.-C., 1993. Rapid formation of the Shatsky Rise oceanic plateau inferred from its magnetic anomaly. *Nature (London, U. K.)*, 364(6438):610–613. [doi:10.1038/364610a0](https://doi.org/10.1038/364610a0)
- Sager, W.W., Handschumacher, D.W., Hilde, T.W.C., and Bracey, D.R., 1988. Tectonic evolution of the northern Pacific plate and Pacific-Farallon Izanagi triple junction in the Late Jurassic and Early Cretaceous (M21–M10). *Tectonophysics*, 155(1–4):345–364. [doi:10.1016/0040-1951\(88\)90274-0](https://doi.org/10.1016/0040-1951(88)90274-0)
- Sager, W.W., Kim, J., Klaus, A., Nakanishi, M., and Khankishieva, L.M., 1999. Bathymetry of Shatsky Rise, northwest Pacific Ocean: implications for ocean plateau development at a triple junction. *J. Geophys. Res., [Solid Earth]*, 104(4):7557–7576. [doi:10.1029/1998JB900009](https://doi.org/10.1029/1998JB900009)
- Sandwell, D.T., and MacKenzie, K.R., 1989. Geoid height versus topography for oceanic plateaus and swells. *J. Geophys. Res., [Solid Earth]*, 94:7403–7418. [doi:10.1029/JB094iB06p07403](https://doi.org/10.1029/JB094iB06p07403)
- Shipboard Scientific Party, 2002a. Leg 198 summary. *In* Bralower, T.J., Premoli Silva, I., Malone, M.J., et al., *Proc. ODP, Init. Repts.*, 198: College Station, TX (Ocean Drilling Program), 1–148. [doi:10.2973/odp.proc.ir.198.101.2002](https://doi.org/10.2973/odp.proc.ir.198.101.2002)
- Shipboard Scientific Party, 2002b. Site 1213. *In* Bralower, T.J., Premoli Silva, I., Malone, M.J., et al., *Proc. ODP, Init. Repts.*, 198: College Station, TX (Ocean Drilling Program), 1–110. [doi:10.2973/odp.proc.ir.198.109.2002](https://doi.org/10.2973/odp.proc.ir.198.109.2002)
- Sinton, J.M., Smaglik, S.M., Mahoney, J.J., and Macdonald, K.C., 1991. Magmatic processes at superfast spreading mid-ocean ridges: glass compositional variations along the East Pacific Rise 13°–23°S. *J. Geophys. Res., [Solid Earth]*, 96:6133–6155. [doi:10.1029/90JB02454](https://doi.org/10.1029/90JB02454)
- Sleep, N.H., 2003. Mantle plumes. *Astron. Geophys.*, 44(1):1.11–1.13. [doi:10.1046/j.1468-4004.2003.44111.x](https://doi.org/10.1046/j.1468-4004.2003.44111.x)
- Sleep, N.H., 2007. Plate tectonics through time. *Treatise Geophys.*, 9:145–169. [doi:10.1016/B978-044452748-6/00143-7](https://doi.org/10.1016/B978-044452748-6/00143-7)
- Sliter, W.V., and Brown, G.R., 1993. Shatsky Rise: seismic stratigraphy and sedimentary record of Pacific paleoceanography since the Early Cretaceous. *In* Natland, J.H., Storms, M.A., et al., *Proc. ODP, Sci. Results*, 132: College Station, TX (Ocean Drilling Program), 3–13. [doi:10.2973/odp.proc.sr.132.302.1993](https://doi.org/10.2973/odp.proc.sr.132.302.1993)
- Smith, A.D., 2003. The regular distribution of intraplate volcanism in the Pacific Basin [Penrose Conference, Plume IV: Beyond the Plume Hypothesis, Hveragerdi, Iceland, 25–29 August 2003].
- Smith, A.D., 2007. A plate model for Jurassic to recent intraplate volcanism in the Pacific Ocean Basin. *In* Foulger, G.R., and Jurdy, D.M. (Eds.), *Plates, Plumes and Planetary Processes*. Spec. Pap.—Geol. Soc. Am., 430:471–495.
- Smith, A.D., and Lewis, C., 1999. The planet beyond the plume hypothesis. *Earth Sci. Rev.*, 48(3):135–182. [doi:10.1016/S0012-8252\(99\)00049-5](https://doi.org/10.1016/S0012-8252(99)00049-5)
- Smith, W.H.F., and Sandwell, D.T., 1997. Global seafloor topography from satellite altimetry and ship depth soundings. *Science*, 277:1956–1962. [doi:10.1126/science.277.5334.1956](https://doi.org/10.1126/science.277.5334.1956)

- Staudigel, H., Park, K.-H., Pringle, M., Rubenstone, J.L., Smith, W.H.F., and Zindler, A., 1991. The longevity of the South Pacific isotopic and thermal anomaly. *Earth Planet. Sci. Lett.*, 102(1):24–44. doi:10.1016/0012-821X(91)90015-A
- Stein, M., and Hofmann, A.W., 1994. Mantle plumes and episodic crustal growth. *Nature (London, U. K.)*, 372(6501):63–68. doi:10.1038/372063a0
- Stein, C.A., and Stein, S., 1992. A model for the global variation in oceanic depth and heat flow with lithospheric age. *Nature (London, U. K.)*, 359(6391):123–129. doi:10.1038/359123a0
- Sun, S.-S., and McDonough, W.F., 1989. Chemical and isotopic systematics of oceanic basalts: implications for mantle composition and processes. In Saunders, A.D., and Norry, M.J. (Eds.), *Magmatism in the Ocean Basins*. Geol. Soc. Spec. Publ., 42(1):313–345. doi:10.1144/GSL.SP.1989.042.01.19
- Tackley, P.J., Stevenson, D.J., Glatzmaier, G.A., and Schubert, G., 1993. Effects of an endothermic phase transition at 670 km depth in a spherical model of convection in the earth's mantle. *Nature (London, U. K.)*, 361(6414):699–704. doi:10.1038/361699a0
- Tarduno, J.A., Sliter, W.V., Kroenke, L., Leckie, M., Mayer, H., Mahoney, J.J., Musgrave, R., Storey, M., and Winterer, E.L., 1991. Rapid formation of Ontong Java Plateau by Aptian mantle plume volcanism. *Science*, 254(5030):399–403. doi:10.1126/science.254.5030.399
- Tatsumi, Y., Shinjoe, H., Ishizuka, H., Sager, W.W., and Klaus, A., 1998. Geochemical evidence for a mid-Cretaceous superplume. *Geology*, 26(2):151–154. doi:10.1130/0091-7613(1998)026<0151:GEFAMC>2.3.CO;2
- Tejada, M.L.G., 1998. Geochemical studies of Pacific oceanic plateaus: the Ontong Java Plateau and Shatsky Rise [Ph.D. dissert.]. Univ. Hawaii, Honolulu.
- Tejada, M.L.G., Mahoney, J.J., Castillo, P.R., Ingle, S.P., Sheth, H.C., and Weis, D., 2004. Pinpricking the elephant: evidence on the origin of the Ontong Java Plateau from Pb-Sr-Hf-Nd isotopic characteristics of ODP Leg 192 basalts. In Fitton, J.G., Mahoney, J.J., Wallace, P.J., and Saunders, A.D. (Eds.), *Origin and Evolution of the Ontong Java Plateau*. Geol. Soc. Spec. Publ., 229:133–150.
- Tejada, M.L.G., Mahoney, J.J., Duncan, R.A., and Hawkins, M.P., 1996. Age and geochemistry of basaltic and alkalic rocks of Malaita and Santa Isabel, Solomon Islands, southern margin of Ontong Java Plateau. *J. Petrol.* 37(2):361–394. doi:10.1093/petrology/37.2.361
- Tejada, M.L.G., Mahoney, J.J., Neal, C.R., Duncan, R.A., and Petterson, M.G., 2002. Basement geochemistry and geochronology of Central Malaita, Solomon Islands, with implications for the origin and evolution of the Ontong Java Plateau. *J. Petrol.*, 43(3):449–484. doi:10.1093/petrology/43.3.449
- Tominaga, M., Sager, W.W., and Channell, J.E.T., 2005. Paleomagnetism of the igneous section, Hole 1213B, Shatsky Rise. In Bralower, T.J., Premoli Silva, I., and Malone, M.J. (Eds.), *Proc. ODP, Sci. Results*, 198: College Station, TX (Ocean Drilling Program), 1–15. doi:10.2973/odp.proc.sr.198.113.2005
- Wallace, P.J., 2002. Volatiles in submarine basaltic glasses from the Northern Kerguelen Plateau (ODP Site 1140): implications for source region compositions, magmatic processes, and plateau subsidence. *J. Petrol.*, 43(7):1311–1326. doi:10.1093/petrology/43.7.1311
- White, R., and McKenzie, D., 1989. Magmatism at rift zones: the generation of volcanic continental margins and flood basalts. *J. Geophys. Res., [Solid Earth]*, 94(B6):7685–7729. doi:10.1029/JB094iB06p07685

- Whitehead, J.A., and Luther, D.S., 1975. Dynamics of laboratory diapir and plume models. *J. Geophys. Res., [Solid Earth]*, 80(5):705–717. doi:10.1029/JB080i005p00705
- Wilson, J.T., 1963. A possible origin of the Hawaiian Islands. *Can. J. Phys.*, 41:863–870.
- Winterer, E.L., 1976. Anomalies in the tectonic evolution of the Pacific. In Sutton, G.H., Manghani, M.H., and Moberly, R. (Eds.), *The Geophysics of the Pacific Ocean Basin and its Margin*. Geophys. Monogr., 19:269–278.

**Table T1. Operations and hole statistics, Expedition 324.**

Hole	Latitude	Longitude	Water depth (m)	Total depth (m DSF)	Time in hole (h)	Cores (N)	Onset of coring (m DSF)	Cored (m)	Recovered (m)	Average recovery (%)	Igneous basement depth (m CSF-A)	Igneous basement cored (m)	Average basement recovery (%)
U1346A	38°00.401'N	162°38.710'E	3619	191.80	128.5	16	100.50	91.3	25.52	28.00	139.20	52.6	38.70
U1347A	32°30.475'N	159°14.078'E	3450	317.50	250.5	29	71.00	246.5	116.10	47.10	157.60	159.9	64.20
U1348A	34°24.940'N	159°22.907'E	3264	324.10	113.5	26	84.20	239.9	80.91	33.70		0	
U1349A	36°06.945'N	158°27.527'E	3127	250.40	126.8	16	116.00	134.4	65.87	49.00	165.10	85.3	67.40
U1350A	36°04.491'N	159°17.065'E	4056	315.80	179.5	26	104.60	211.2	75.19	35.60	143.10	172.7	43.19

**Figure F1.** Location of Shatsky Rise and other features in the northwest Pacific Ocean. Red circles = Expedition 324 drill sites, yellow line = track of the *JOIDES Resolution*.

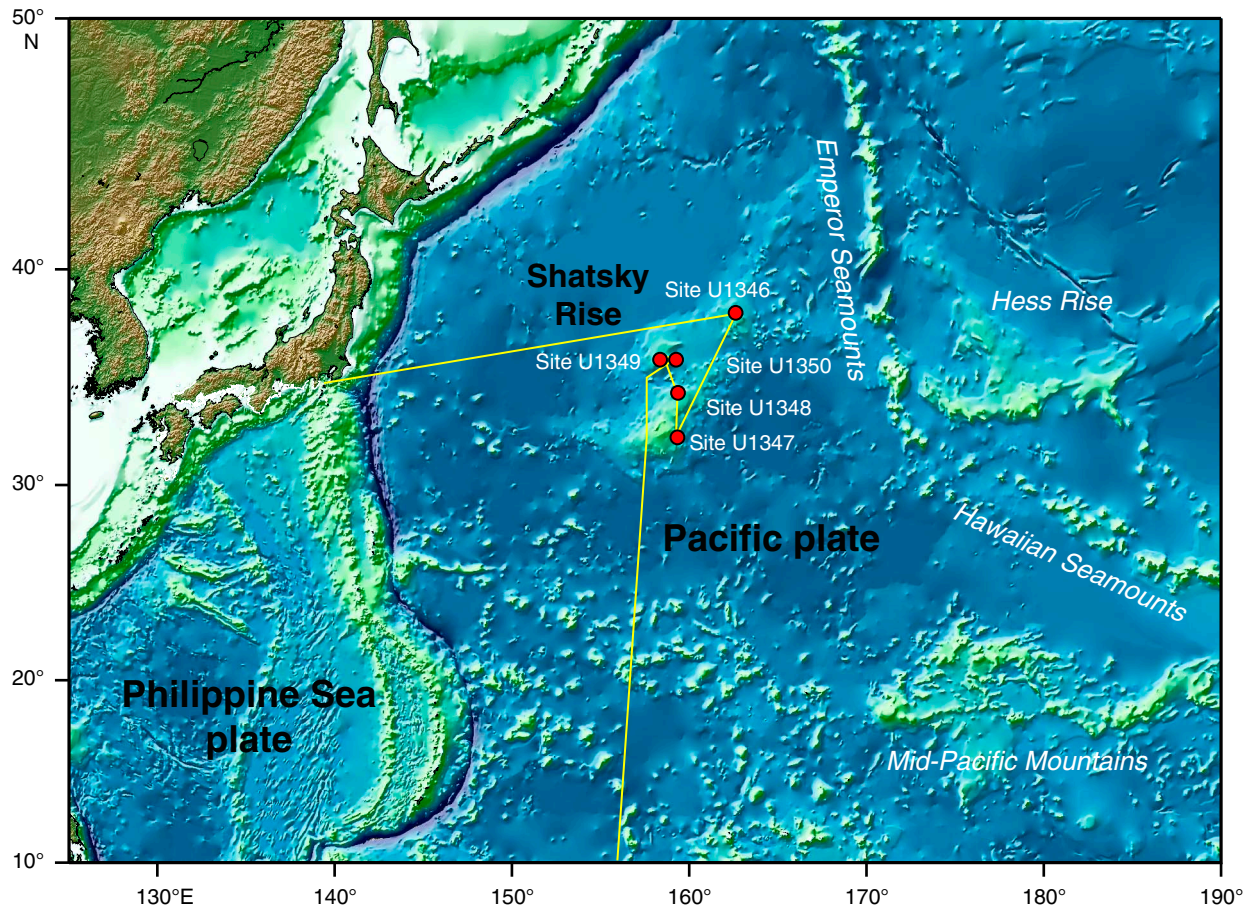


**Figure F2.** Location chart of major feature names (blue), the Cruise TN037 site survey seismic tracks, Cruise TN037 dredges, DSDP and ODP drill sites, proposed alternate Expedition 324 sites, and sites drilled during Expedition 324. Light blue shading = elevations shallower 5 km on Shatsky Rise. Site 1213 is the location where igneous rocks were drilled during ODP Leg 198 (Shipboard Scientific Party, 2002a). Inset illustrates the location of Shatsky Rise in relation to western Pacific magnetic lineations (thin lines), trenches (toothed line), and Japan.

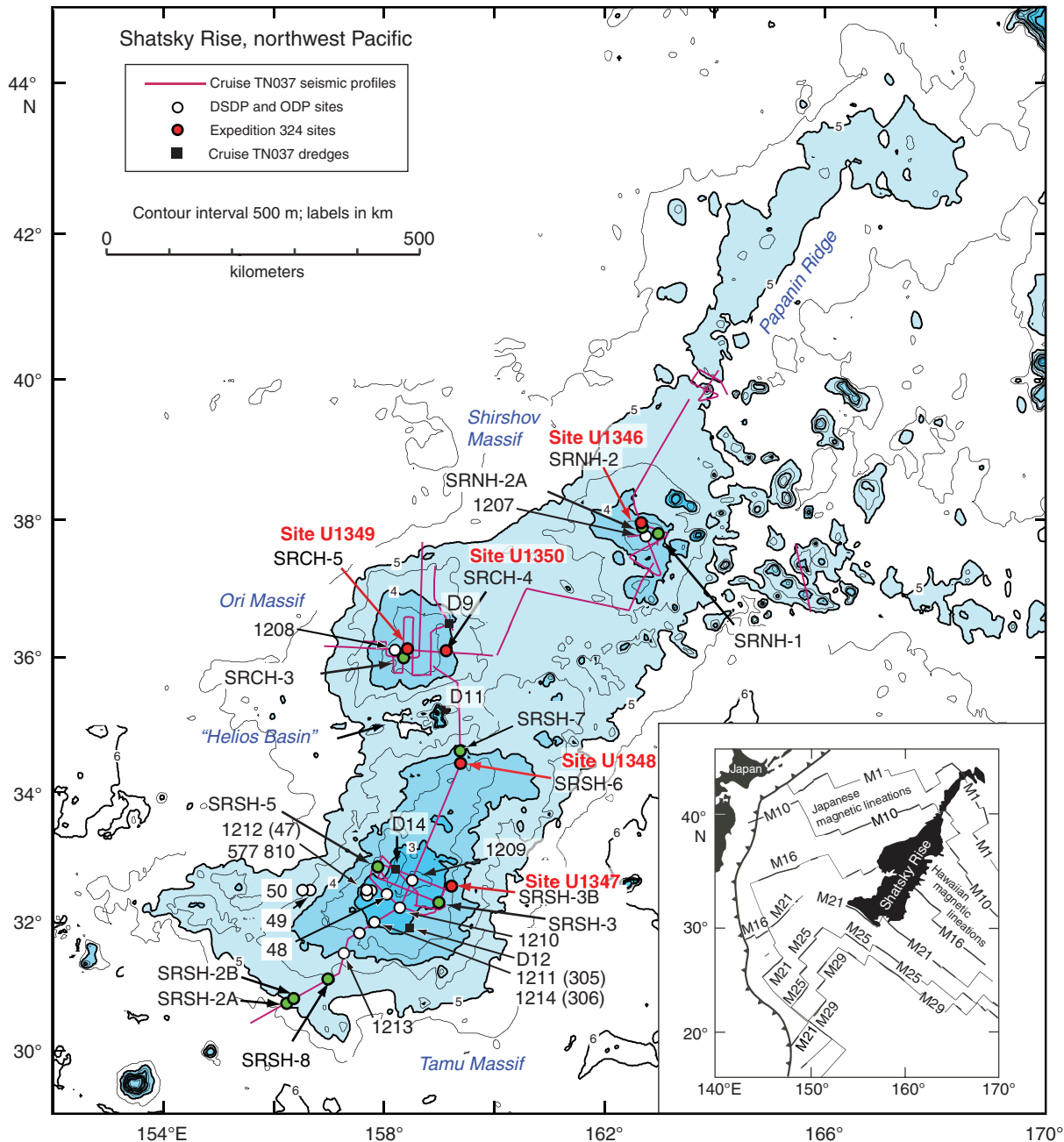


**Figure F3.** Magnetic lineations within and around Shatsky Rise and Expedition 324 sites (red circles). Heavy red lines = magnetic lineations and fracture zones, open circles = prior drill sites, blue circle = location of Site 1213. Satellite-predicted bathymetry (Smith and Sandwell, 1997) contours shown at 500 m intervals. Modified from Nakanishi et al. (1999).

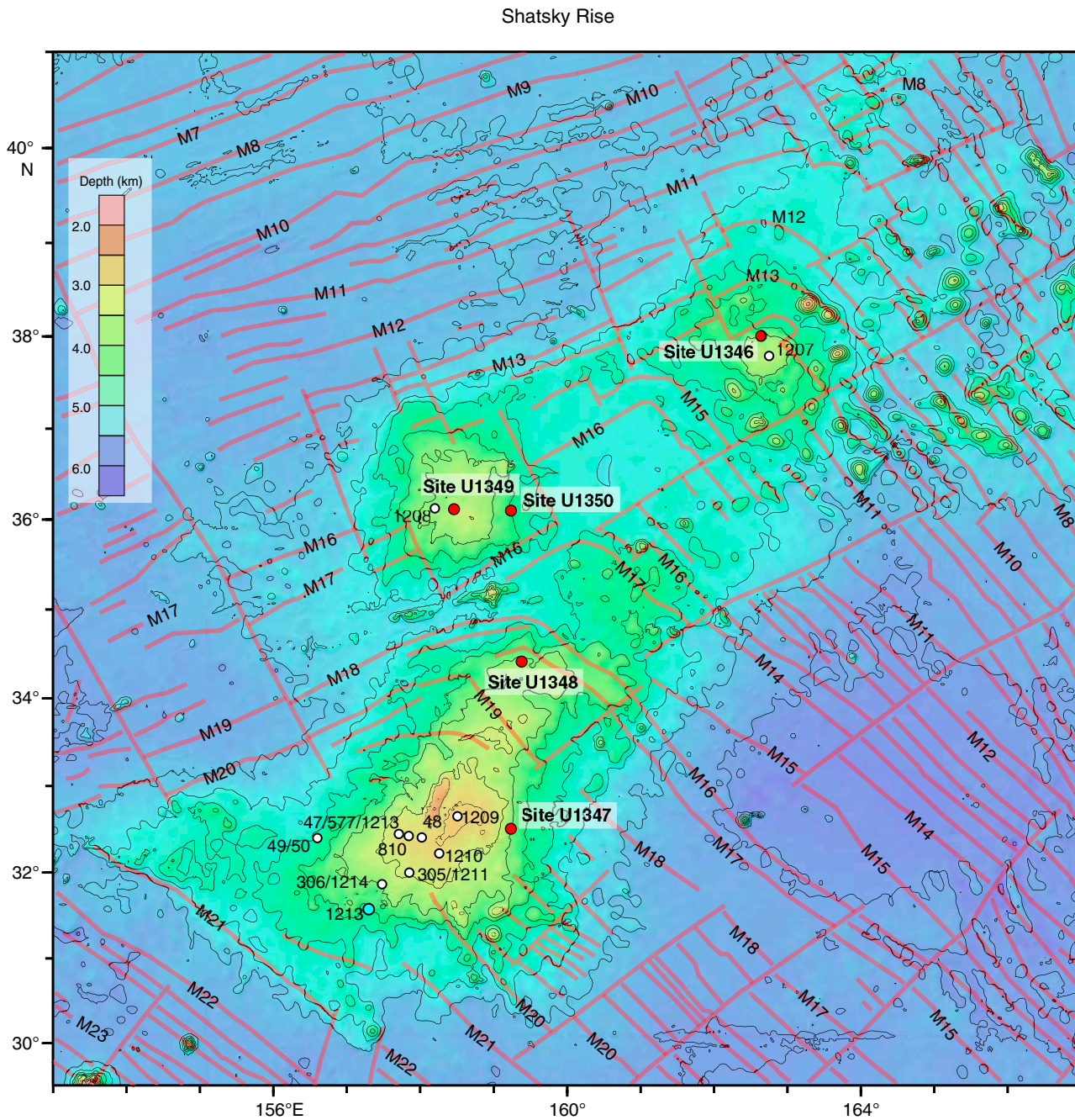


**Figure F4.** Tectonic history of Shatsky Rise, illustrating the migration of ridges and triple junctions (TJ) during formation of the rise. Dark magnetic lineations existed on the Pacific plate at the time given for each panel. Red lines = ridges, light purple lines = future isochrons, blue arrows = path of triple junction, yellow arrows = jumps and changes in direction (modified from Nakanishi et al., 1999).

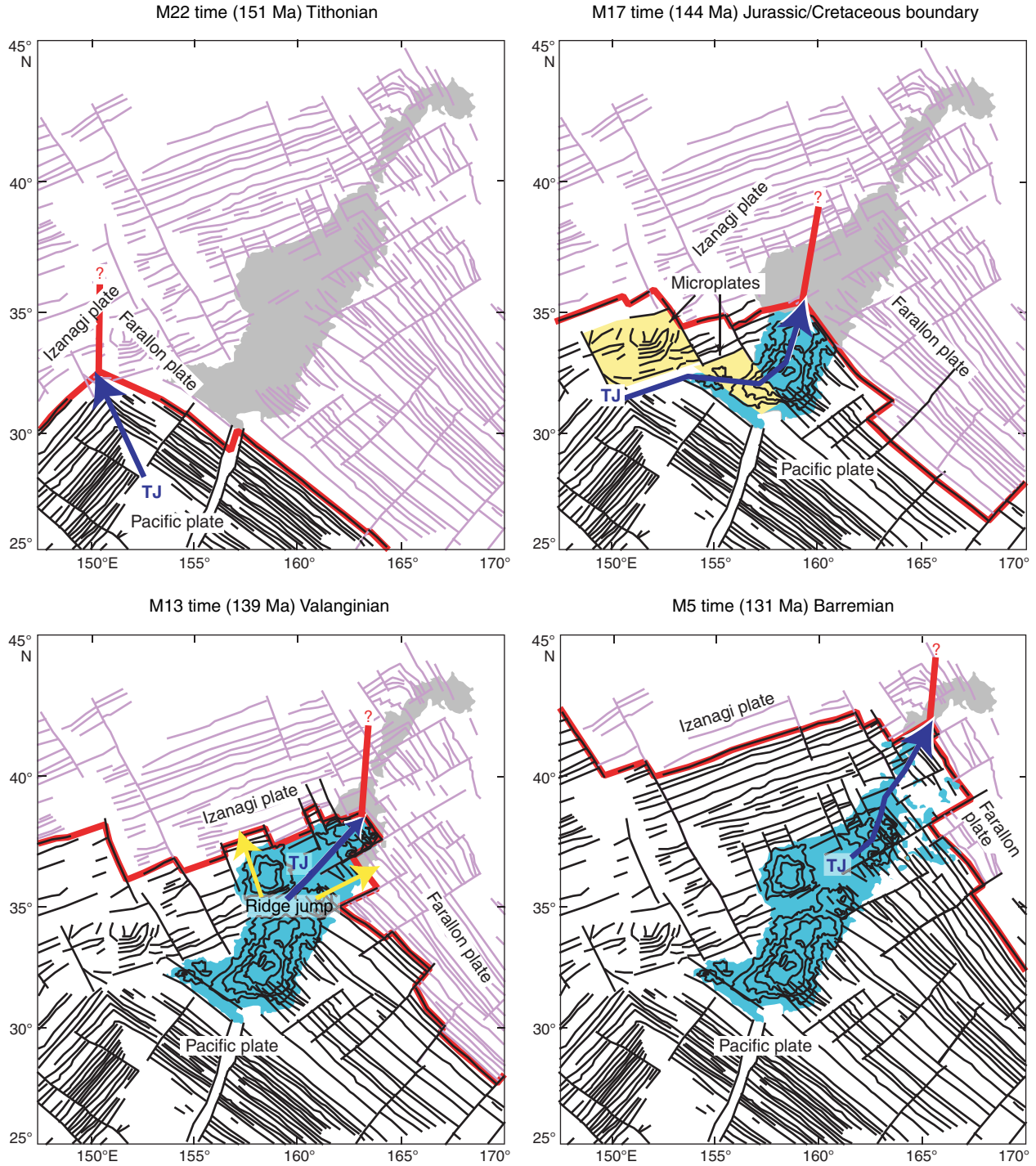


**Figure F5. A.** Age-corrected isotope data. Fields for Pacific mid-ocean-ridge basalt (MORB) and the Easter-Nazca Ridge hotspot chain are adjusted for radiogenic ingrowth to the estimated 144 Ma positions of the mantle sources (see Tejada et al., 2004). Pb isotope data for Holes 1213B and 1179D (and Easter-Nazca Ridge) were acquired using a double spike. Fields are from Mahoney and Spencer (1991), Tejada et al. (2004), Ray et al. (2003), and references therein (after Mahoney et al., 2005). SOTW = Southtow Expedition. **B.** Incompatible element diagram for Site 1213 samples compared with Ontong Java and mid-ocean-ridge basalt (MORB). Ontong Java pattern is from Fitton and Godard (2004); average normalized-MORB (N-MORB) pattern and normalizing values are from Sun and McDonough (1989) (after Mahoney et al., 2005).

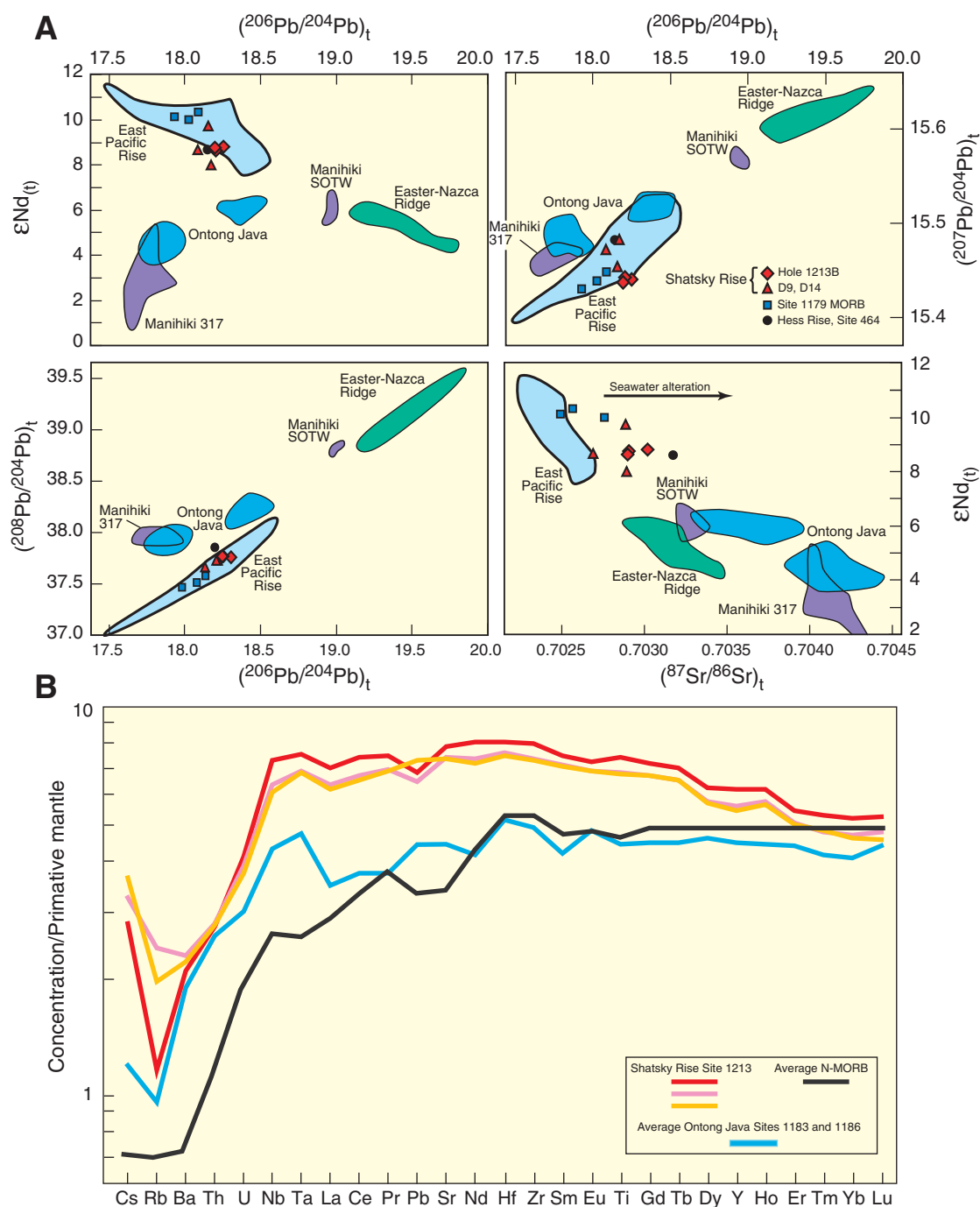


**Figure F6.** Bathymetry of Shirshov Massif and location of Site U1346. Contours and colors indicate bathymetric depths predicted by satellite altimetry (Smith and Sandwell, 1997). Site 1207 cored during ODP Leg 198 (Shipboard Scientific Party, 2002a). Contours shown at 200 m intervals; dark contours shown for kilometer multiples. Red line = track of Cruise TN037 site survey (Klaus and Sager, 2002).

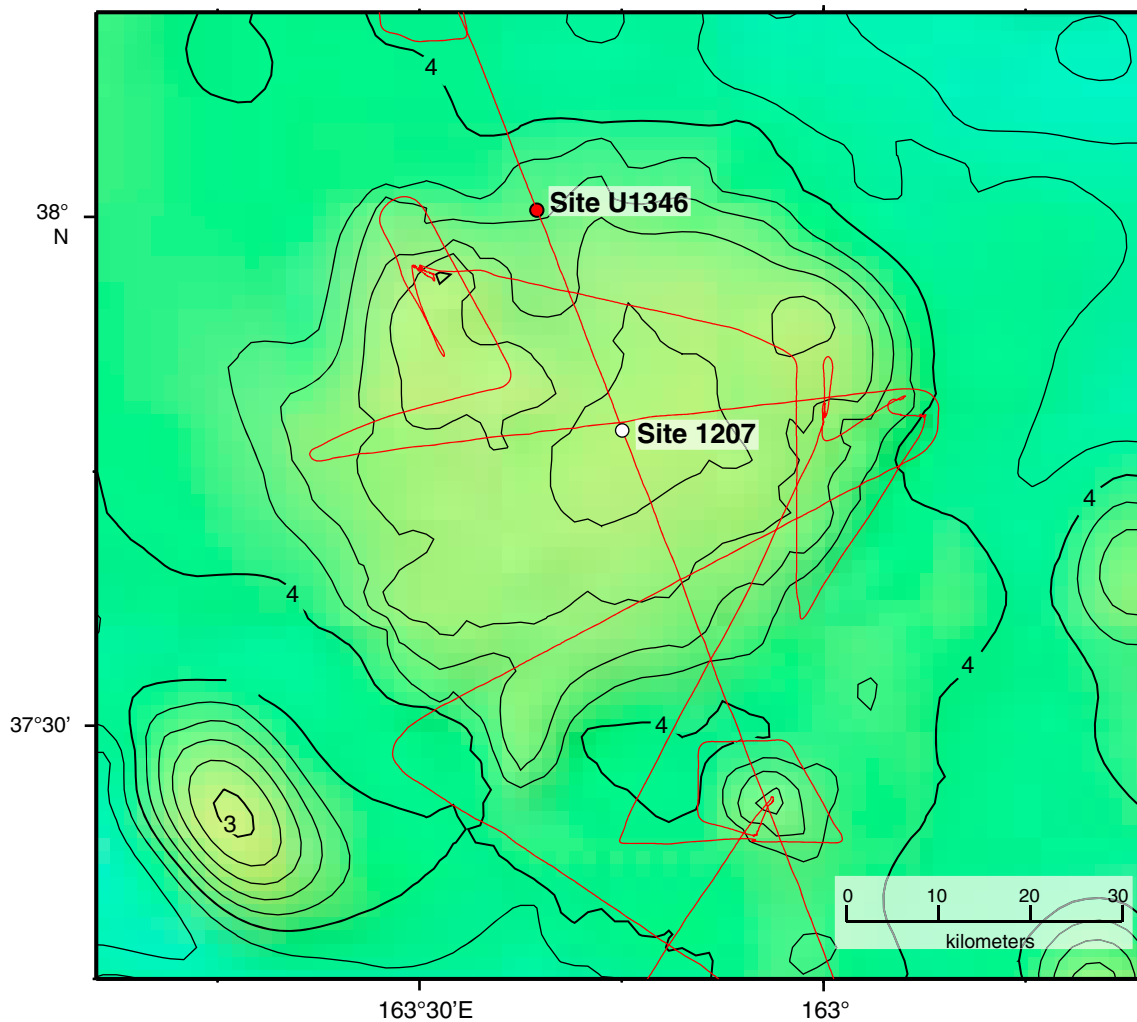


**Figure F7.** Seismic section and interpretation, Site U1346. See Klaus and Sager (2002). UTC = Universal Time Coordinated.

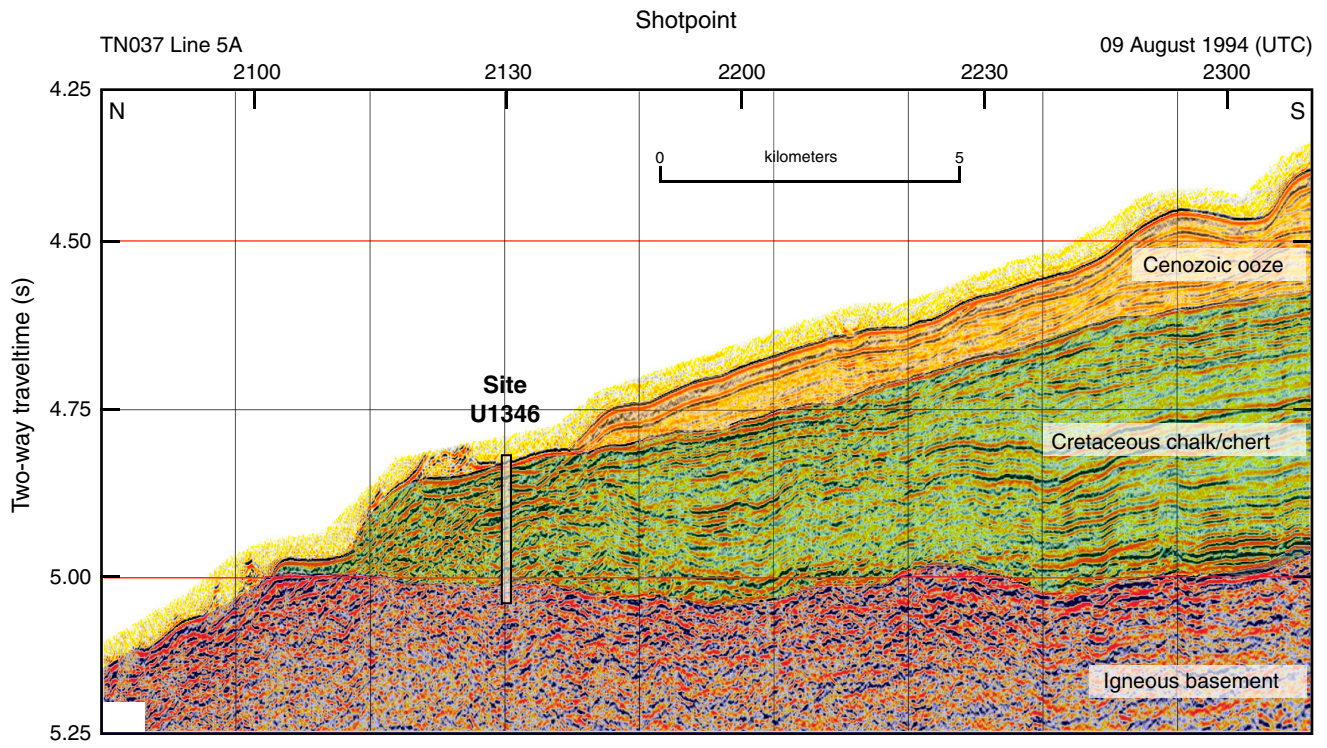


**Figure F8.** Overview of lithostratigraphy above igneous basement, Expedition 324. Sites arranged from left to right in geographical order. Age deduced from biostratigraphy indicated to the right of each column. Sites are arranged vertically to suggest general relative distribution of ages at all sites. Early Cretaceous = Berriasian to Albian, Late Cretaceous = Cenomanian to Campanian, Cen = middle Cenozoic. Note hiatus or lack of recovery between Campanian and middle Cenozoic at Site U1348. Gray shaded area = gap between last datable sediment and top of igneous basement (or top of the volcanoclastic sequence, Unit III, at Site U1348).

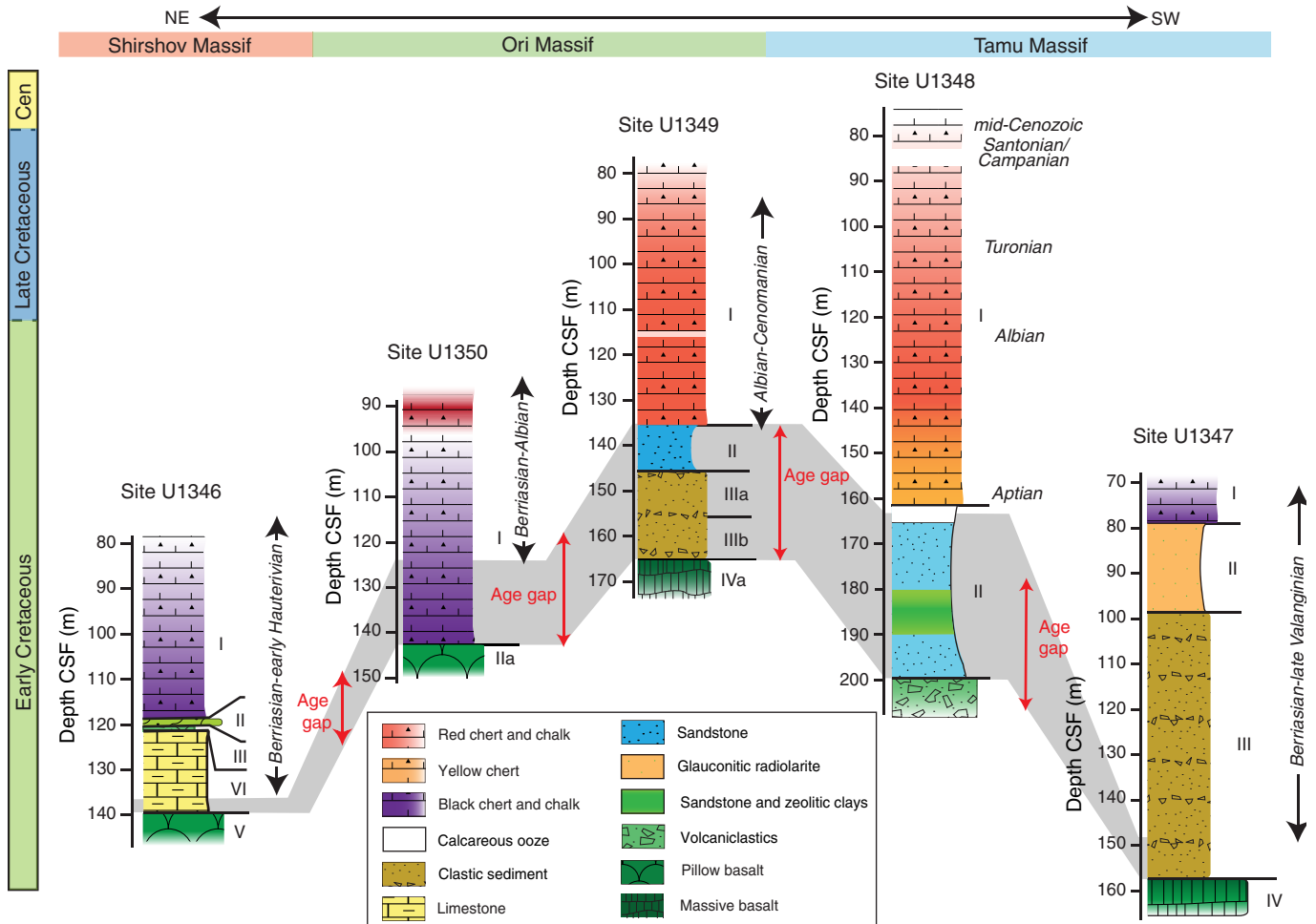
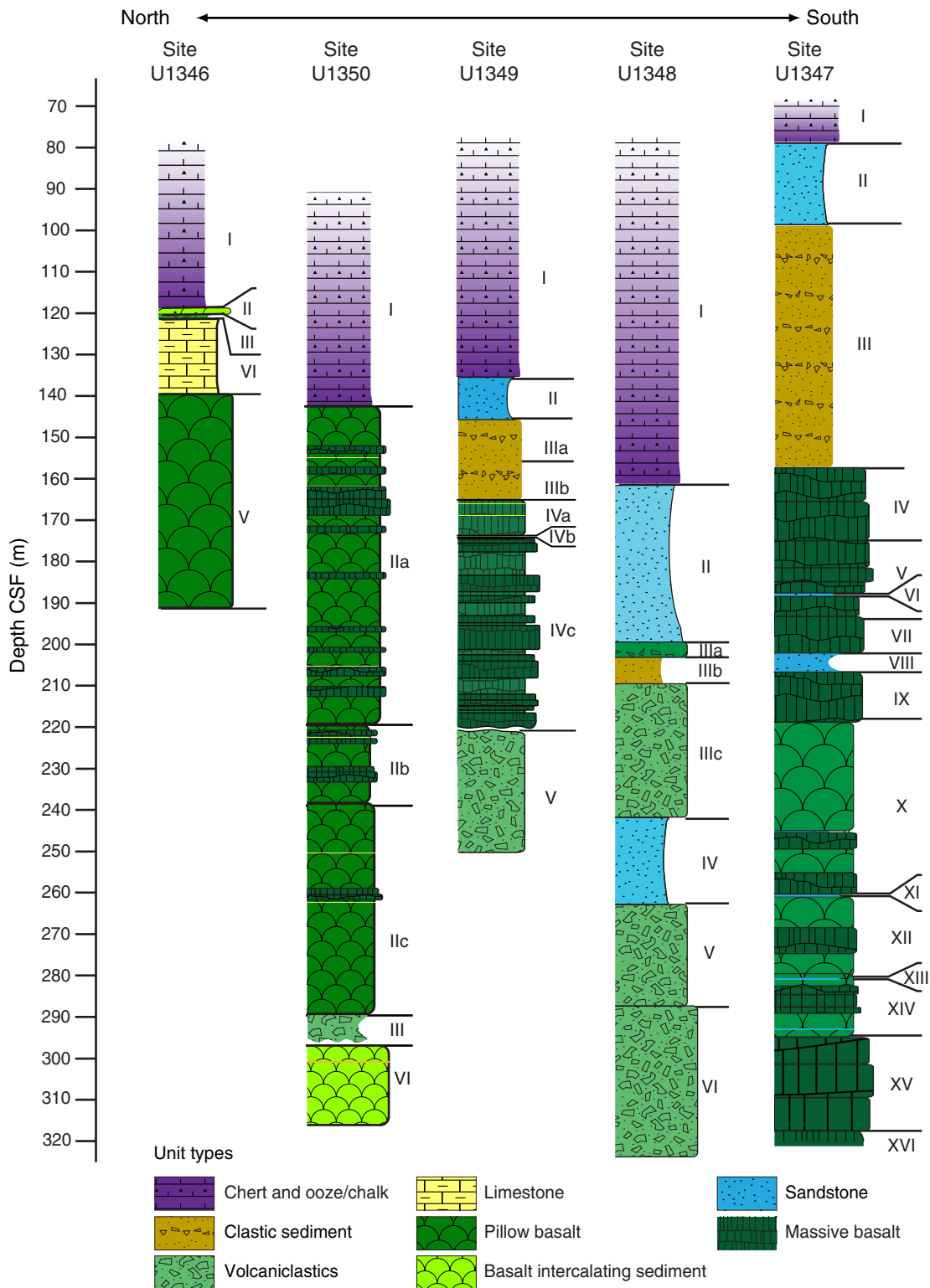
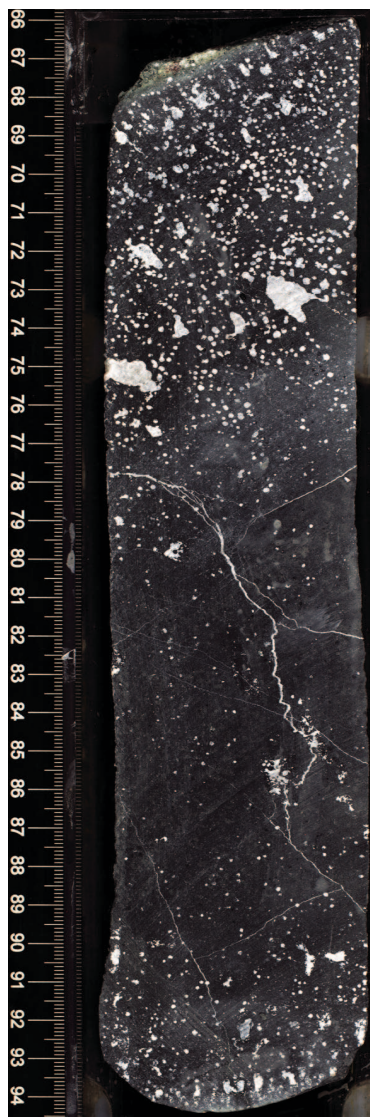


Figure F9. Lithologic summary, Expedition 324.



**Figure F10.** Cross-section of an idealized flow unit of amygdaloidal basalt observed at Site U1346 (interval 324-U1346A-14R-1 [Piece 7, 66–94 cm]).

Section 324-U1346A-14R-1, Piece 7



Cross section of complete pillow basaltic unit

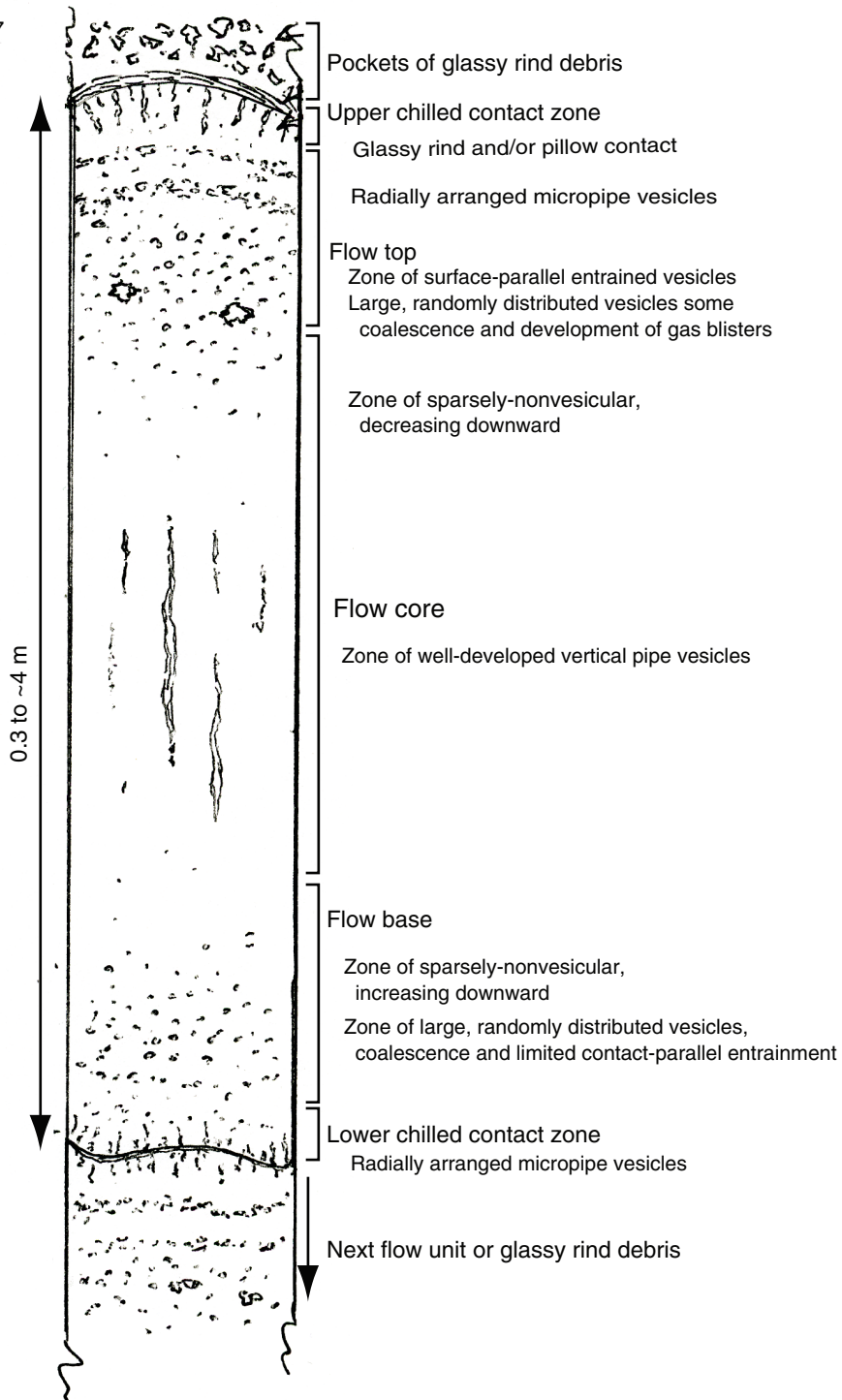


**Figure F11. A.** Total alkalis vs. silica, with Le Maitre et al.'s (1989) classification of volcanic rock types. Dashed line = Hawaiian tholeiitic and alkalic lava data division (Macdonald and Katsura, 1964; Macdonald, 1968), black arrow = compositional change caused by seawater alteration. All data are normalized to 100 wt% totals. **B.** TiO<sub>2</sub> vs. Zr. ODP Leg 191 Site 1179 and Leg 198 Site 1213 data from Mahoney et al. (2005). OJP = Ontong Java Plateau (data of Tejada et al., 1996, 2002; Fitton and Godard, 2004), EPR = East Pacific Rise (data of Sinton et al., 1991; Bach et al., 1994; Mahoney et al., 1994), ESC = Easter Seamount Chain (data of Ray et al., submitted). Nazca Ridge and Easter Seamount Chain together form the hotspot trail of the Easter–Salas hotspot.

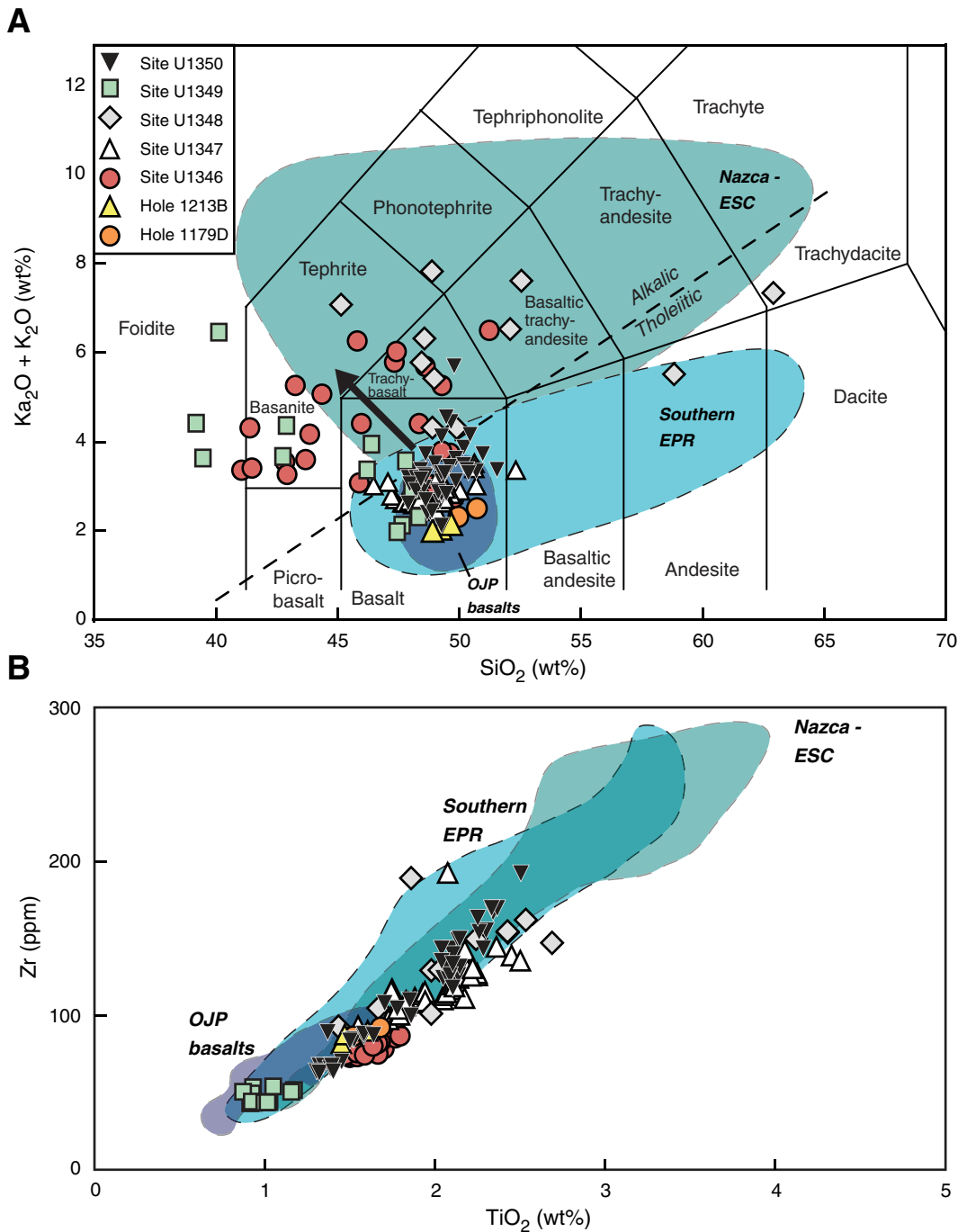


**Figure F12.** Bathymetry of Tamu Massif and location of Sites U1347 and U1348. Contours and colors indicate bathymetric depths predicted by satellite altimetry (Smith and Sandwell, 1997). Contours shown at 200 m intervals; dark contours shown for kilometer multiples. Red line = track of Cruise TN037 site survey (Klaus and Sager, 2002), open circles = prior drill sites, blue circle = location of Site 1213.

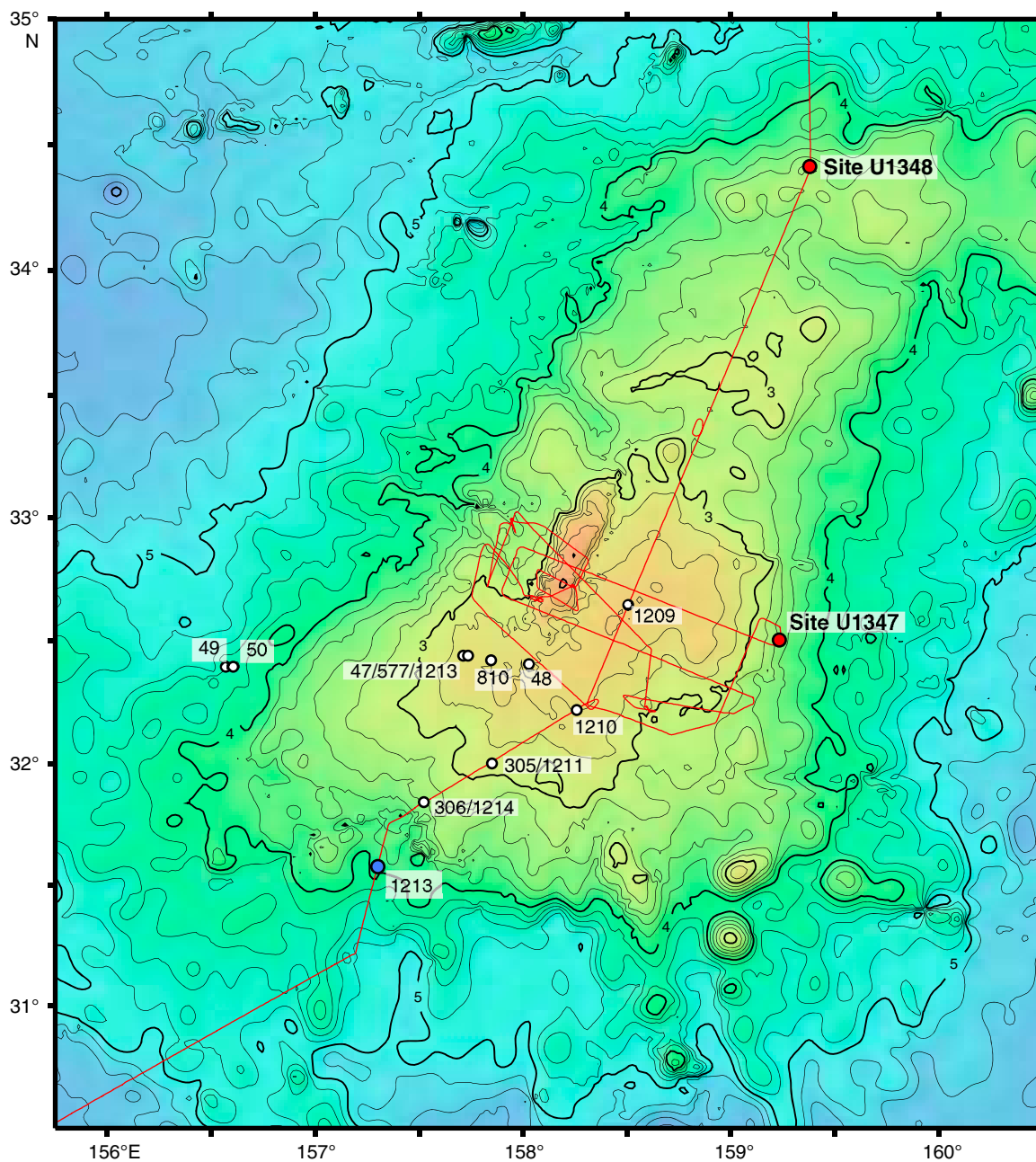


**Figure F13.** Seismic section and interpretation, Site U1347. See Klaus and Sager (2002). Dashed yellow lines = coherent reflections within igneous basement. UTC = Universal Time Coordinated, c/c = course change.

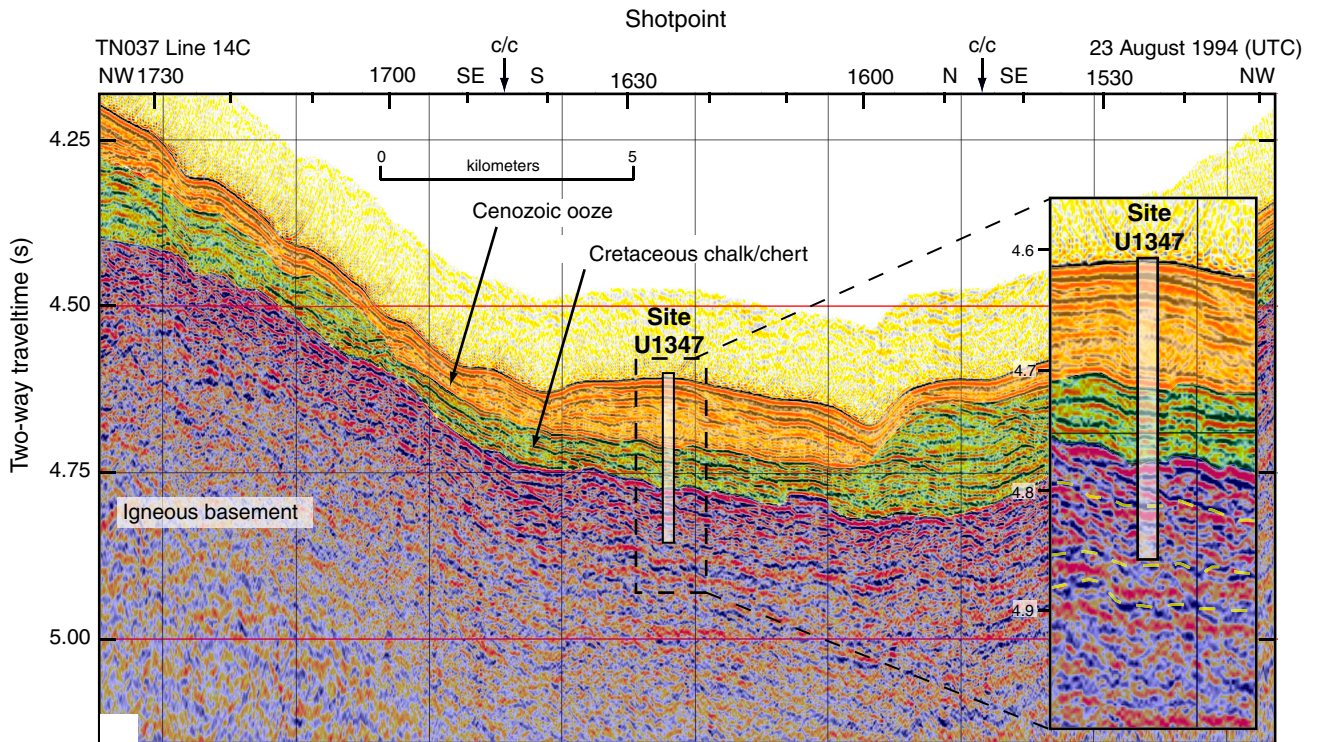


**Figure F14.** Core section images annotated with volcanological features for a massive submarine basalt flow (Unit V) from Sections 324-U1347A-13R-7 to 15R-1. The lithologic column on the left shows the upper and lower bounds of the sections (red dashed lines). These core sections exhibit primary magmatic features including folded glassy crusts and vesicular zones. Interflow sediment occurs between the massive flows in Section 324-U1347A-15R-1 and appears to be ~5 m thick in downhole logging measurements.

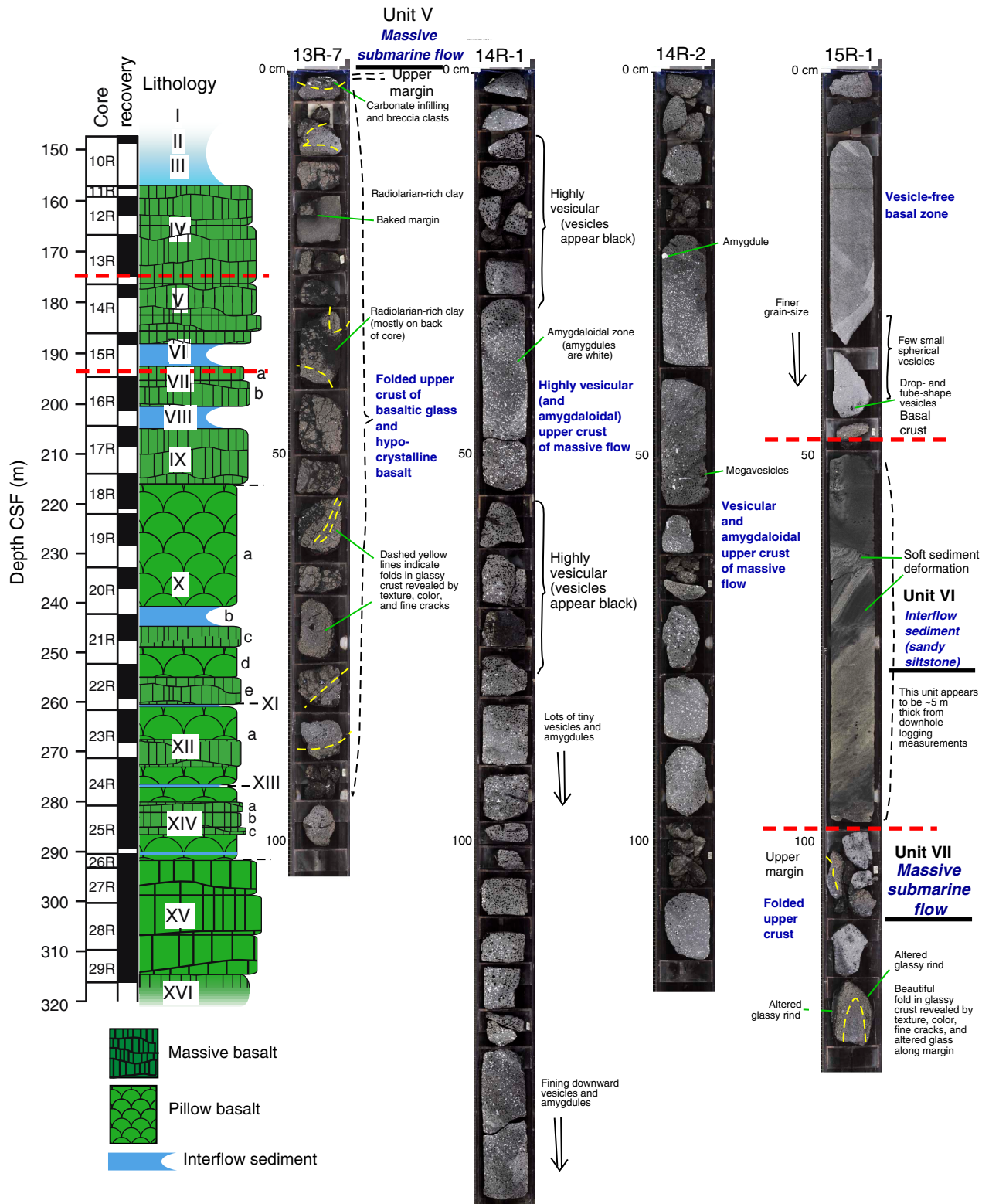




**Figure F16.** Seismic section and interpretation, Site U1348. See Klaus and Sager (2002). UTC = Universal Time Coordinated.

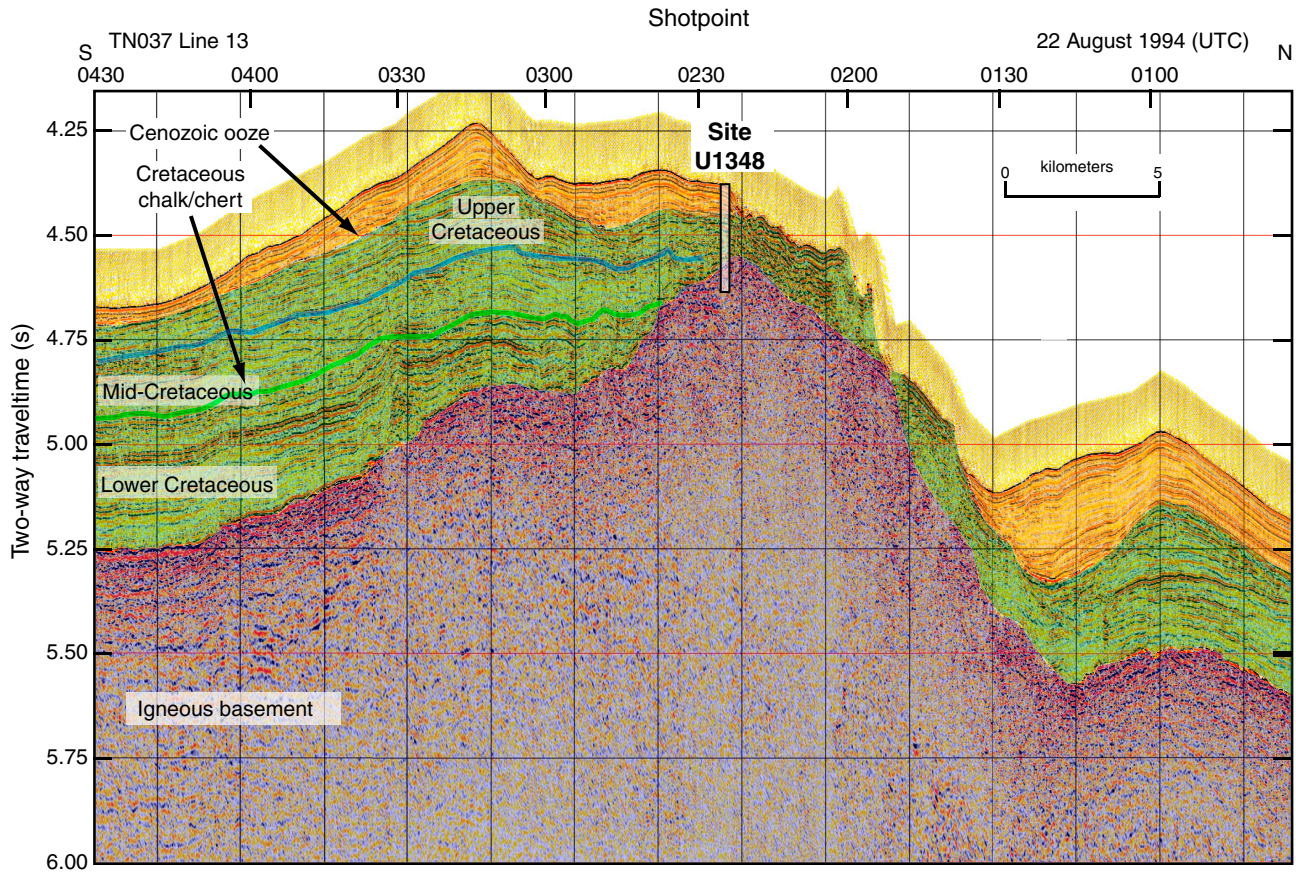


**Figure F17.** (A) Core section image, (B) thin section scan, and photomicrographs (plane-polarized transmitted light) of sparsely vesicular vitric tuff in Section 324-U1348A-18R-1, top of Unit III, with (C) glass shards and bubble wall fragments with elongate vesicular shard at bottom, (D) subrounded vesicular basalt clasts, and (E) fine hyaloclastite matrix. Thin section scan location of B is indicated by the red box in A. Width of field of view of photomicrographs is ~15 mm (1.25 $\times$ ) in panels C, D, and E. Yellow arrows = orientation in core.

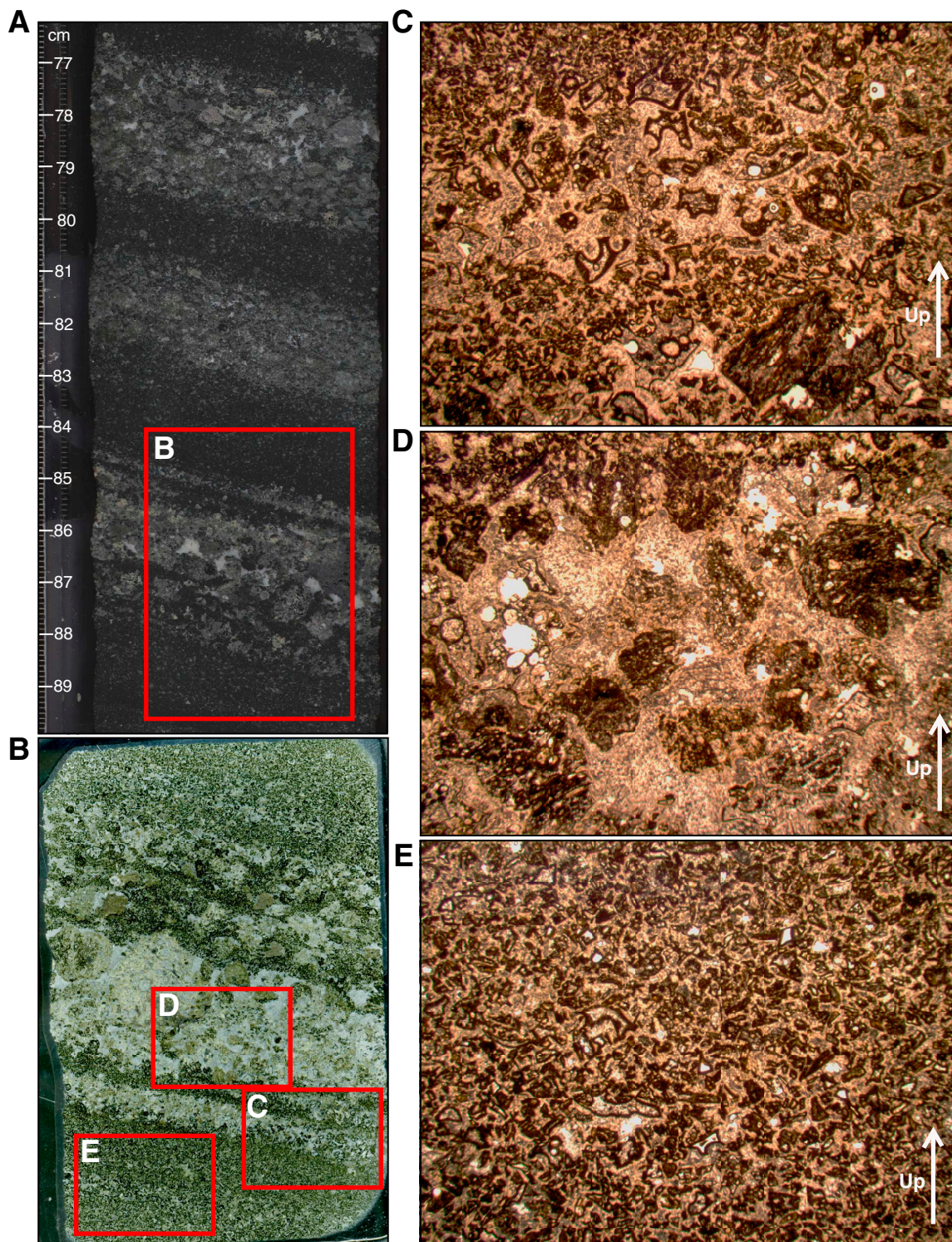


**Figure F18.** Bathymetry of Ori Massif and location of Sites U1349 and U1350. Contours and colors indicate bathymetric depths predicted by satellite altimetry (Smith and Sandwell, 1997). Contours shown at 200 m intervals; dark contours shown for kilometer multiples. Red line = track of Cruise TN037 site survey (Klaus and Sager, 2002), open circle = location of ODP Leg 198 Site 1208.

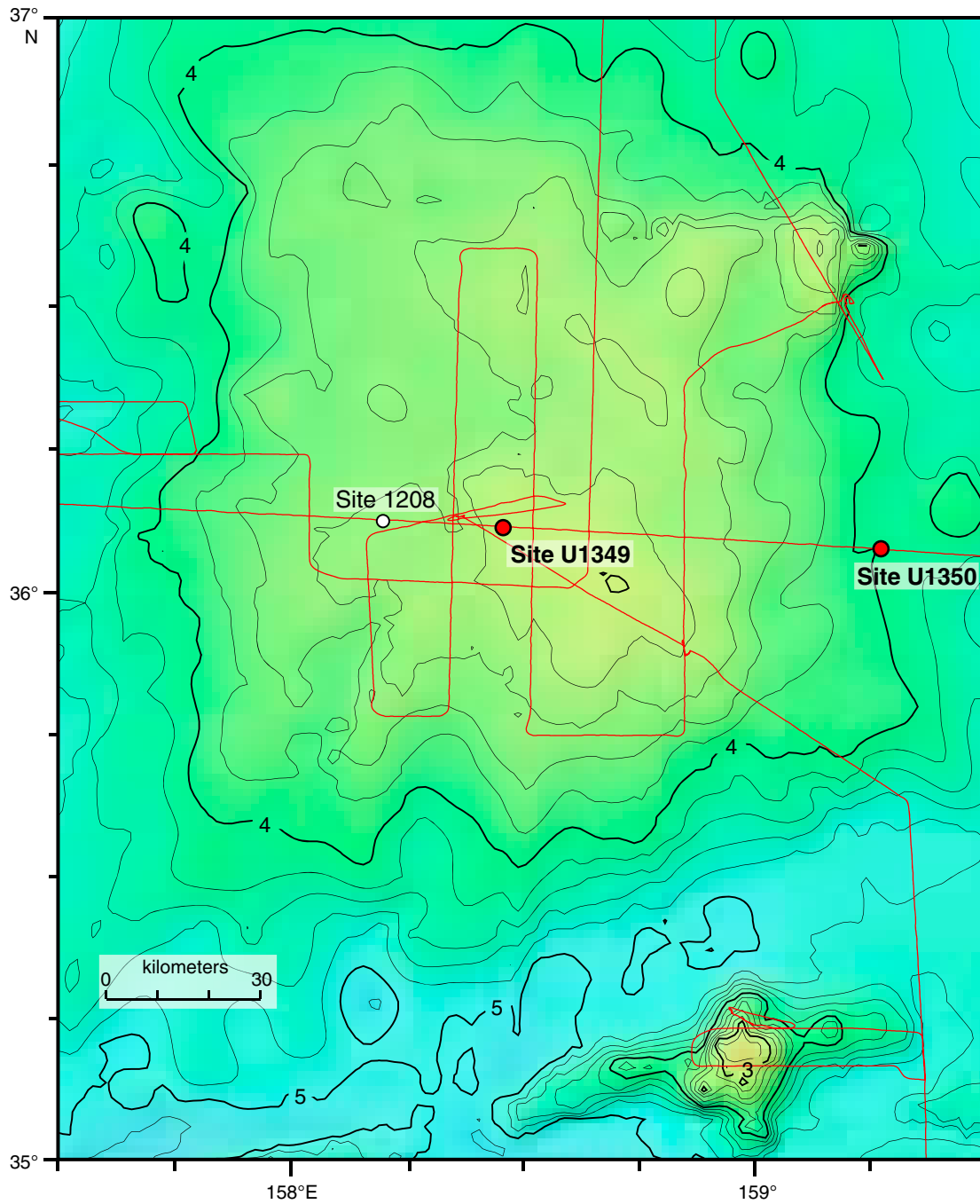
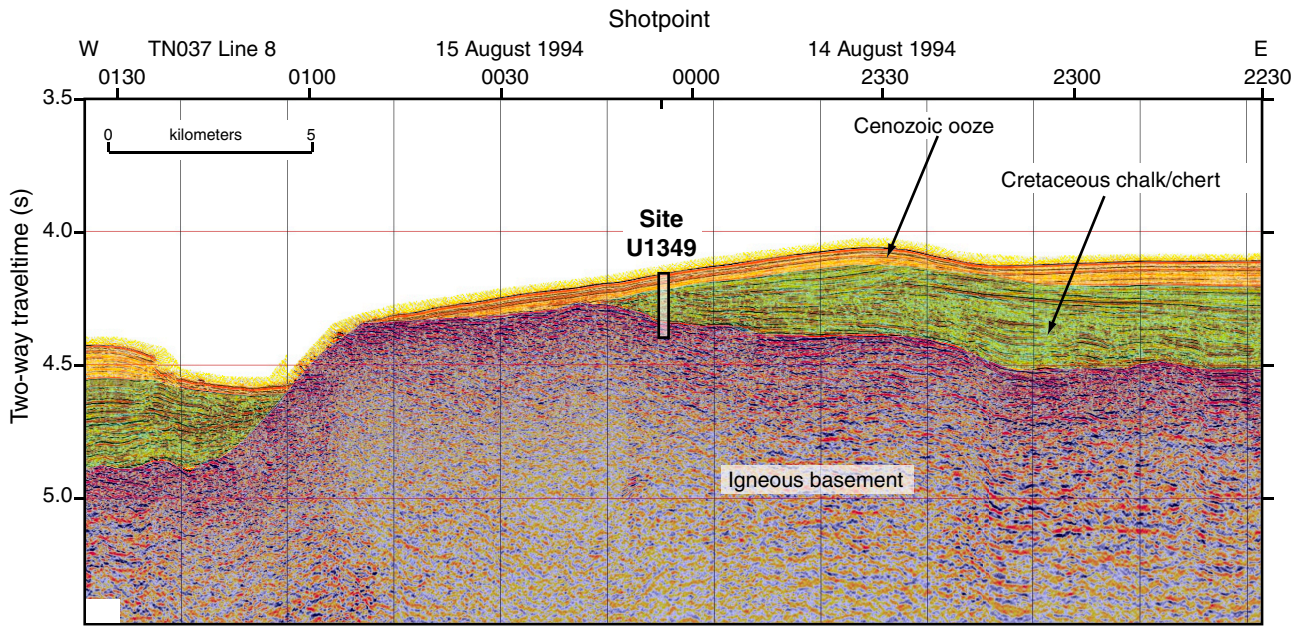


Figure F19. Seismic section and interpretation, Site U1349. See Klaus and Sager (2002).



**Figure F20.** Core section images of Sections (A) 324-U1349-11R-3 and (B) 11R-5, (C) thin section scan, and (D–G) photomicrographs (plane-polarized transmitted light) of lava mixing features in Core 324-U1349A-11R, top of Unit IV. Thin section scan location of D is indicated by the red box in B. Red box in D indicates photomicrograph location. Field of view for D is 36 cm × 54 cm. Width of field of view of F and G is ~6 mm (2.5×) and E is 15 mm (1.25×).

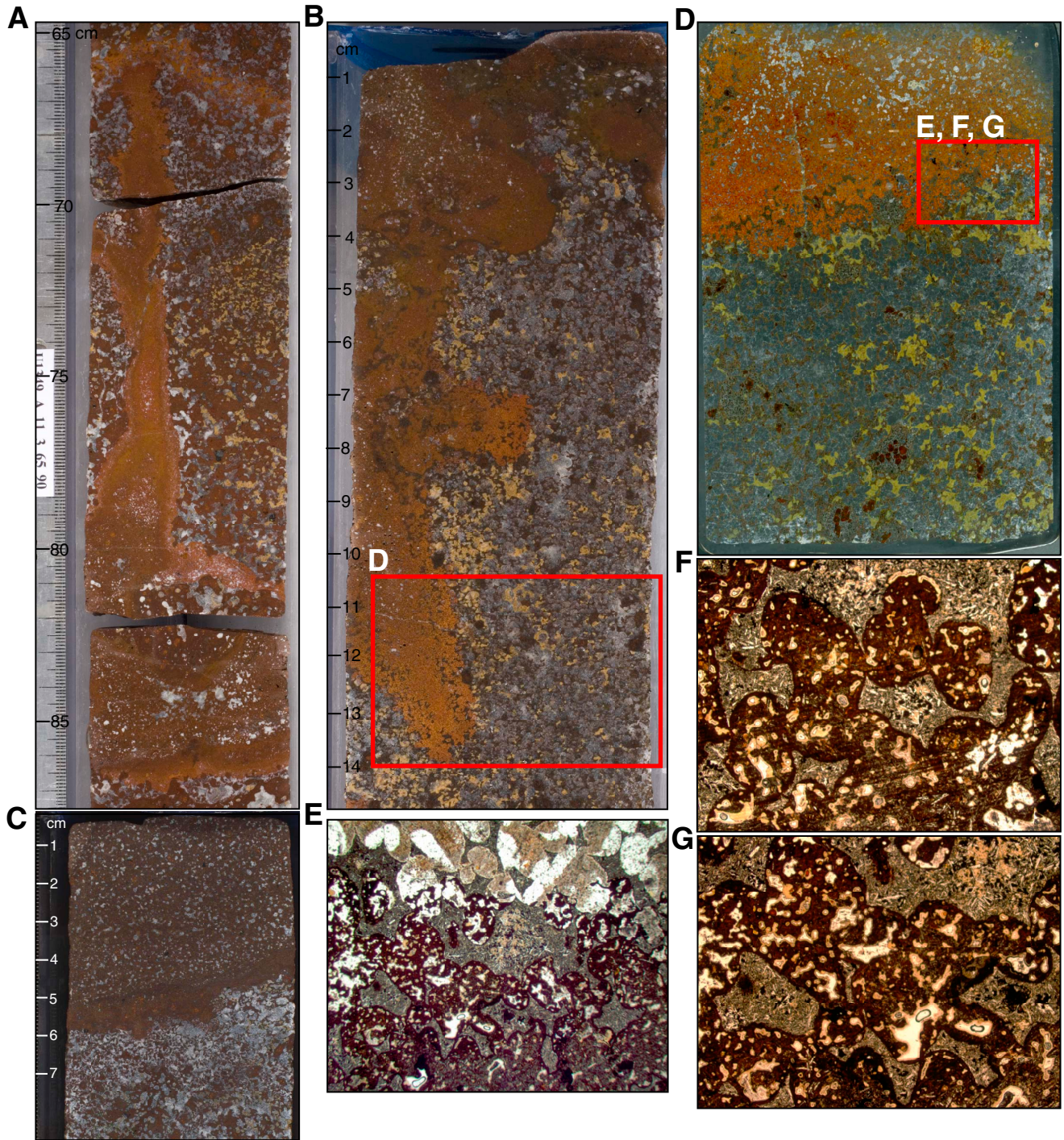
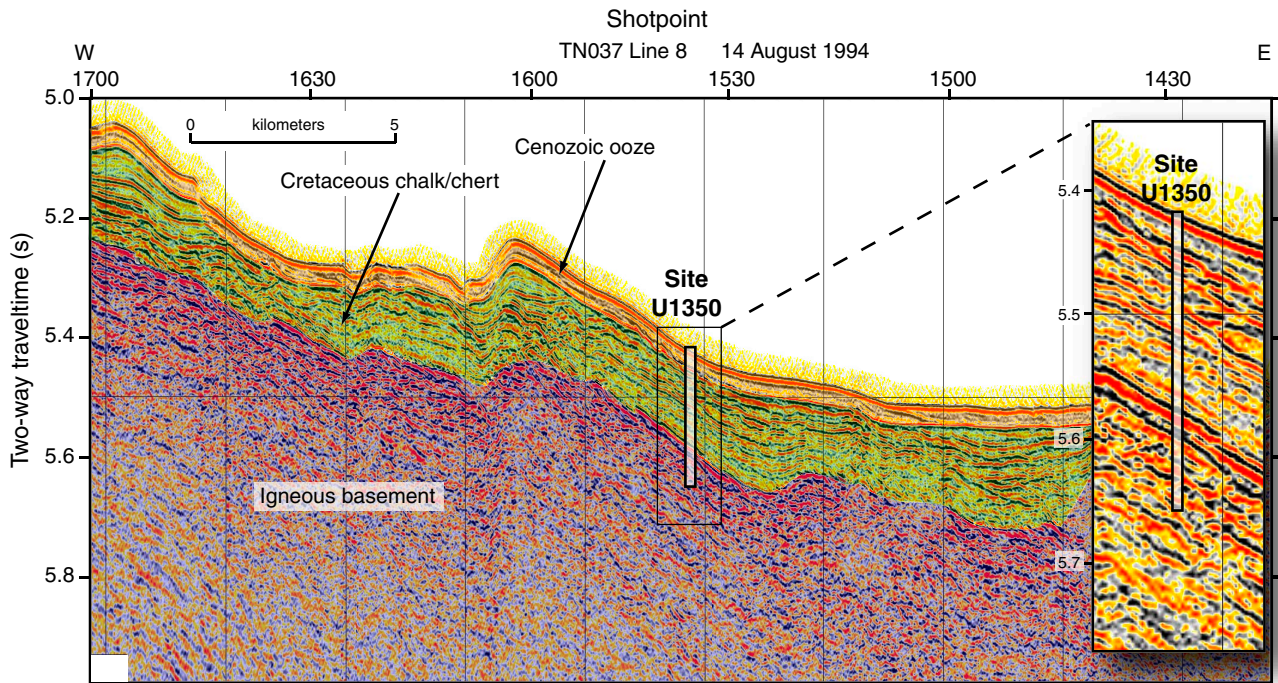
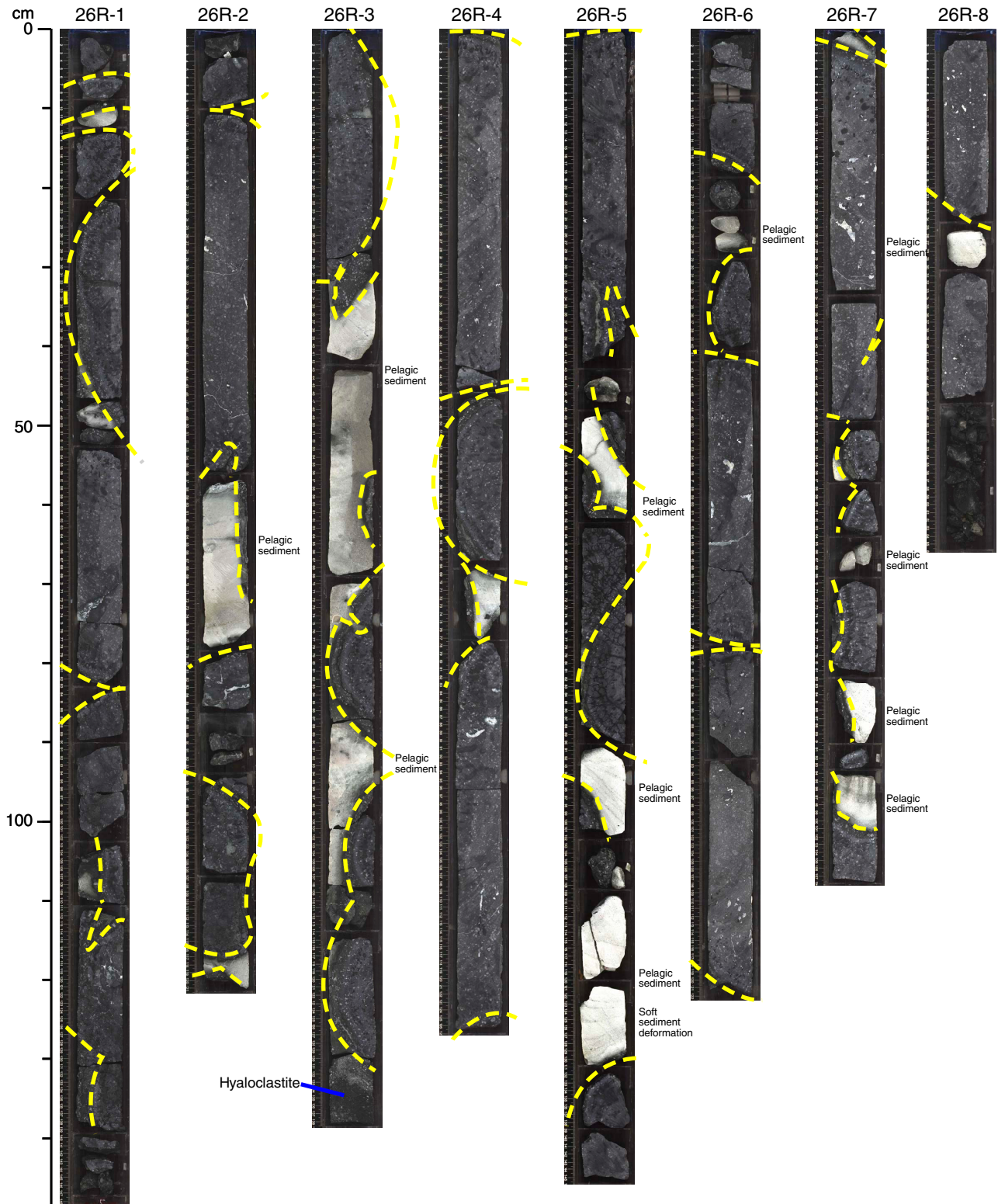


Figure F21. Seismic section and interpretation, Site U1350. See Klaus and Sager (2002).



**Figure F22.** Core section images annotated with volcanological features for pillow basalts from Unit IV (Sections 324-U1350-26R-1 through 26R-8). Yellow dashed lines = pillow margins or interpillow crusts. These core sections exhibit interior pillow cracks, concentric vesicles in pillow margins, and sediment incorporated into pillow interiors.



**Figure F23.** Examples of massive flows, Hole U1350A. **A.** Lithologic column. **B.** Images of Sections 324-U1350A-9R-5, 9R6, 10R-1, and 11R-2 (location shown as red dashed lines in A). **C–E.** Thin section photomicrographs (plane-polarized transmitted light); (C, D) Sample 324-U1350A-10R-2, 33–35 cm (TS 274). Height of view is 12 mm for C and 6 mm for D; (E) Sample 324-U1350A-11R-2, 80–83 cm (TS 277). Yellow box = location of sample. Height of view is 6 mm.

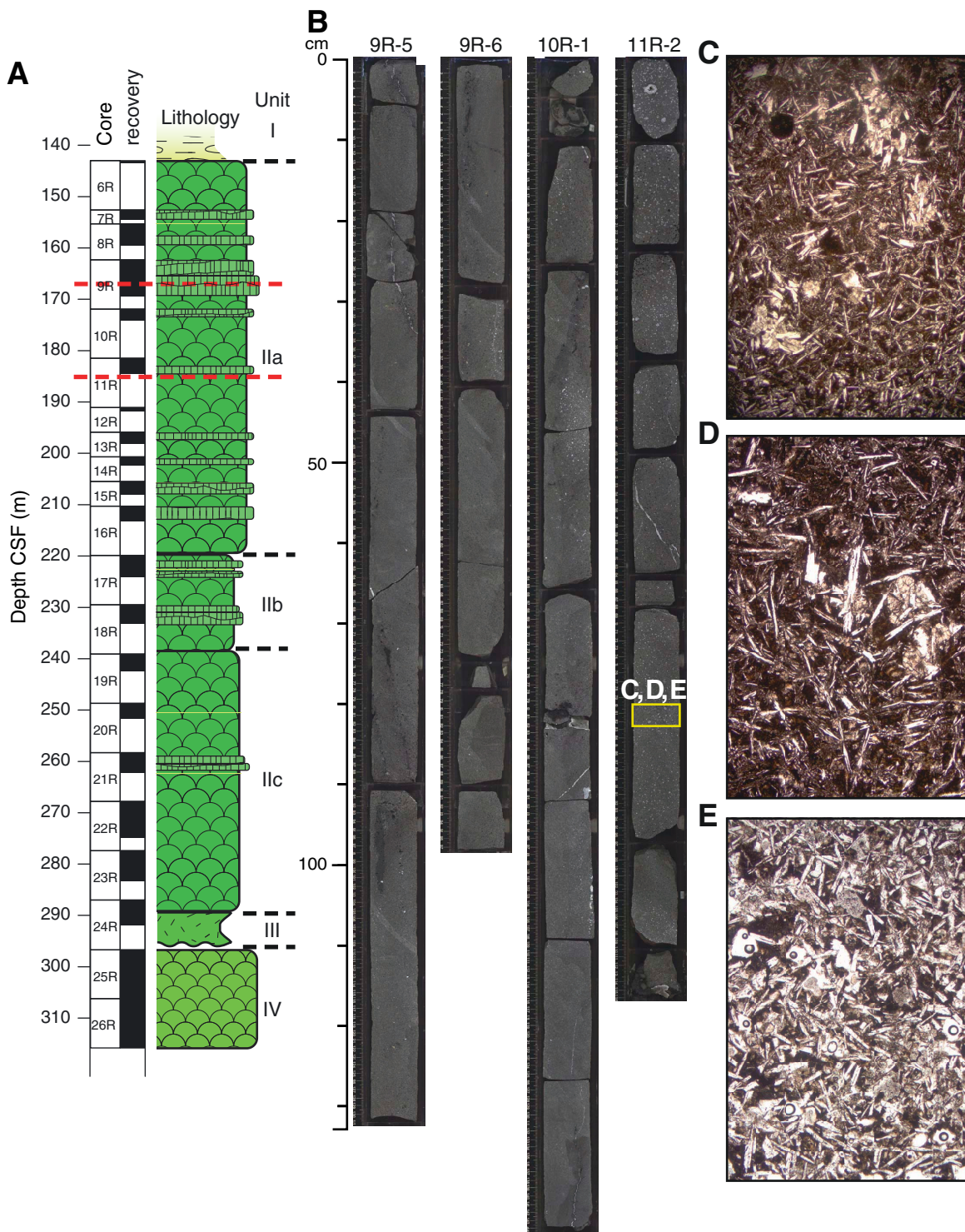


**Figure F24.** Examples of pillow lavas, Hole U1350A. **A.** Lithologic column. **B.** Images of Sections 324-U1350A-22R-2 through 22R-5 (location shown as red dashed lines in A). Yellow boxes on core images show locations of thin sections. **C–E.** Thin section photomicrographs of aphyric pillow basalt from Subunit IIc showing small spherical vesicles in the upper parts of pillows, characteristic jointing patterns, tube- and drop-shape vesicles inside chilled margins, and thin subhorizontal glassy rinds (plane-polarized transmitted light); (C) Sample 324-U1350A-22R-5, 81–87 cm (TS 307); (D) close-up of area in yellow box in C (length of view = 12 mm); (E) Sample 324-U1350A-22R-3, 117–119 cm (TS 306; length of view = 6 mm).

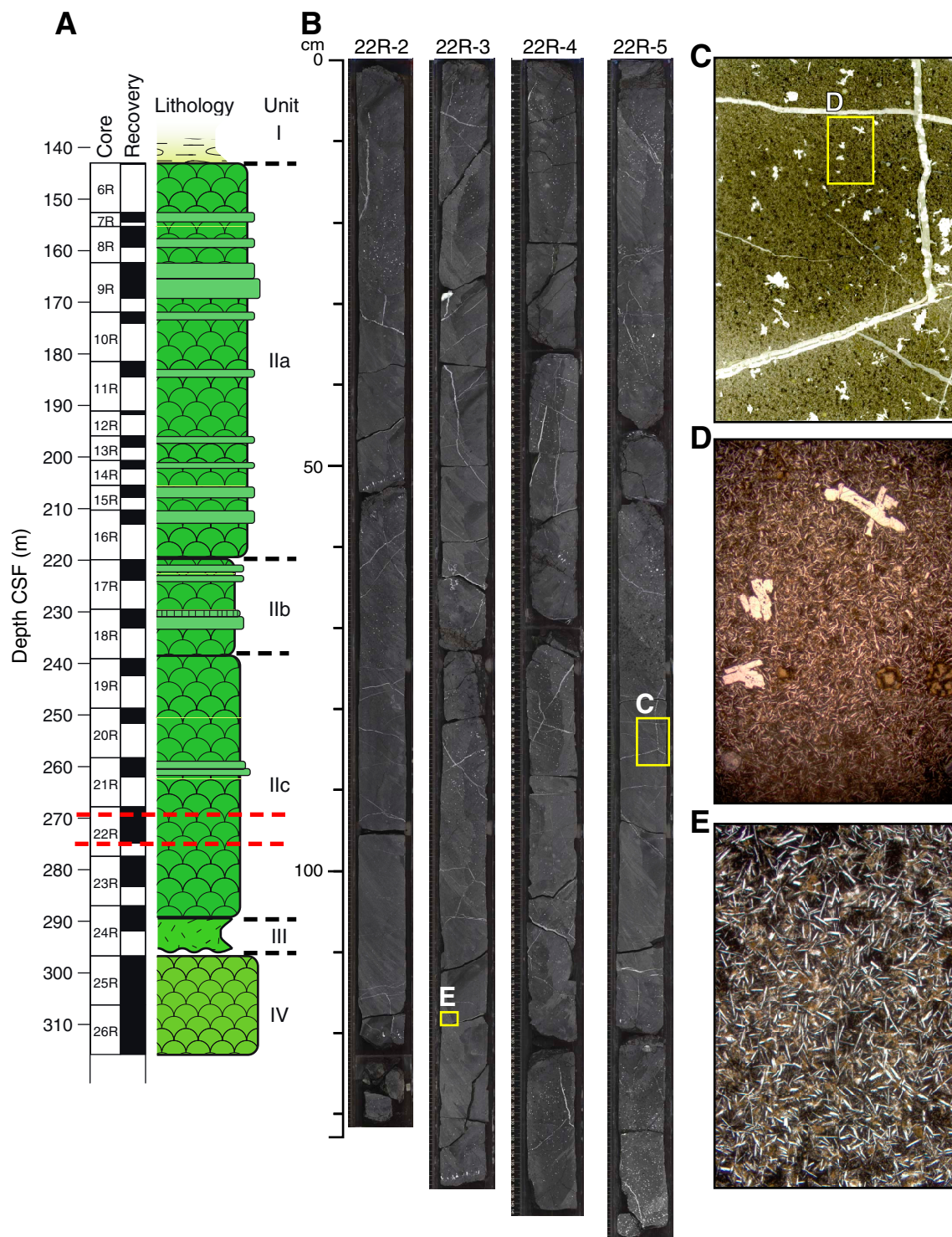


**Figure F25.** Examples of pillow breccia/hyaloclastite, Hole U1350A. **A.** Lithologic column. **B.** Image of Section 324-U1350A-24R-3 showing pillow breccia/hyaloclastite from Unit III (location shown as red dashed lines in A), which exhibits pillow fragments and several globular clasts with chilled margins in a matrix of hyaloclastite. Yellow boxes on core image indicate the locations thin sections. **C.** Sample 324-U1350A-24R-3, 105–120 cm. **D.** Sample 324-U1350A-24R-3, 90–105 cm. **E.** Sample 324-U1350A-24R-3, 49–67 cm.

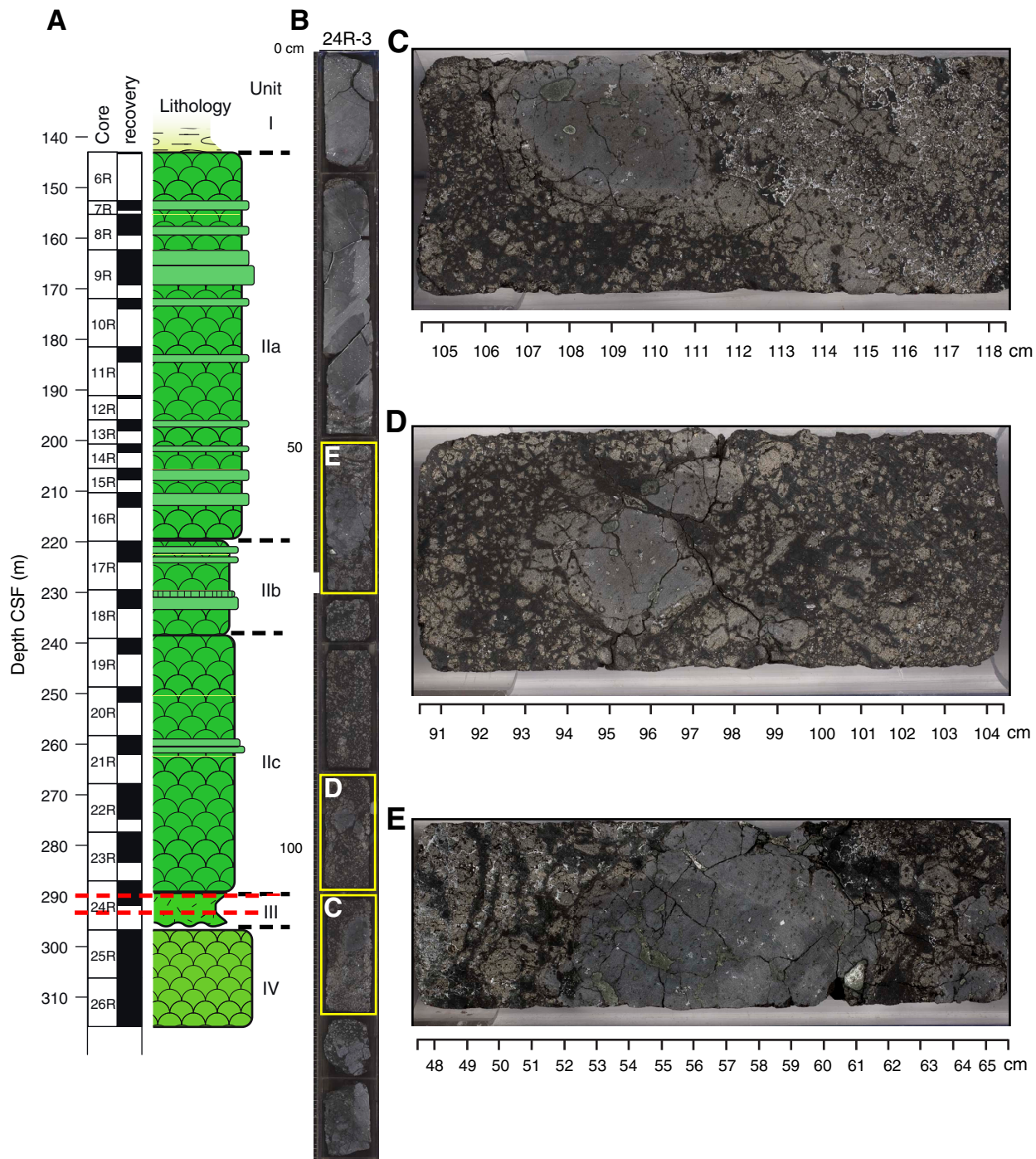


**Figure F26.** Subsidence curves, Expedition 324. **A.** Site U1346 (Shirshov Massif summit). **B.** Site U1349 (Ori Massif summit). **C.** Site U1350 (Ori Massif flank). **D.** Site U1347 (Tamu Massif flank). Colored curves = extrapolated site depth at the time of eruptions, calculated by backtracking from the present depth (corrected for sediment loading; Crough, 1983). PS = Parsons and Sclater (1977) model, SS = Stein and Stein (1994) model. Paleodepth estimates from backtracking are compared with paleodepth indicators from Expedition 324 cores. Black curves = normal mid-ocean ridges, red arrow = difference between normal ridge and observed paleodepth, taken as the amount of uplift caused by volcano construction. Magnetic lineation ages are from Nakanishi et al. (1999) and Gradstein et al. (2004).

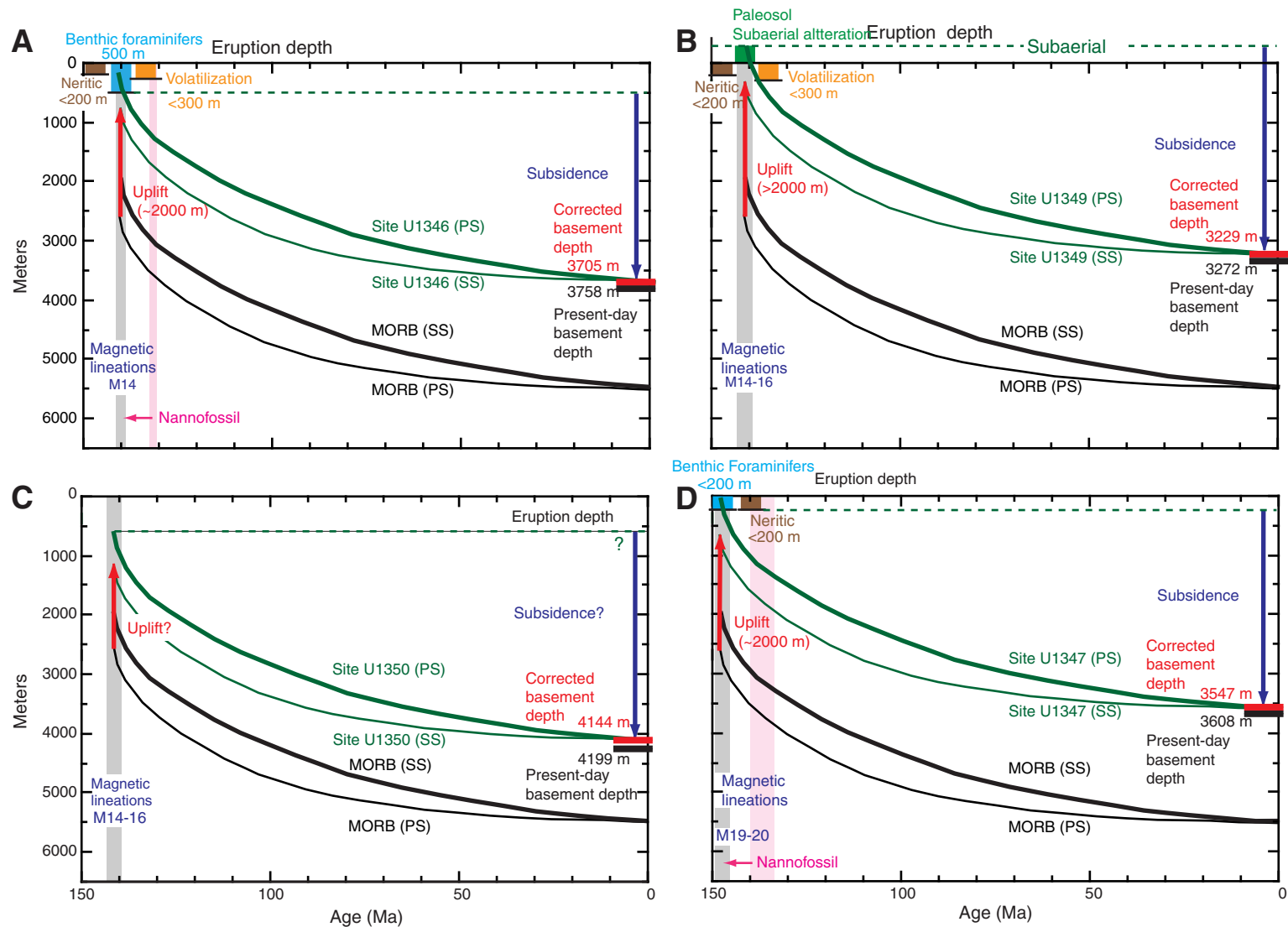


**Figure F27.** Paleomagnetic inclinations measured from discrete basalt samples plotted versus depth, Sites U1346, U1347, U1349, and U1350. AF = alternating-field demagnetization, TH = thermal demagnetization.

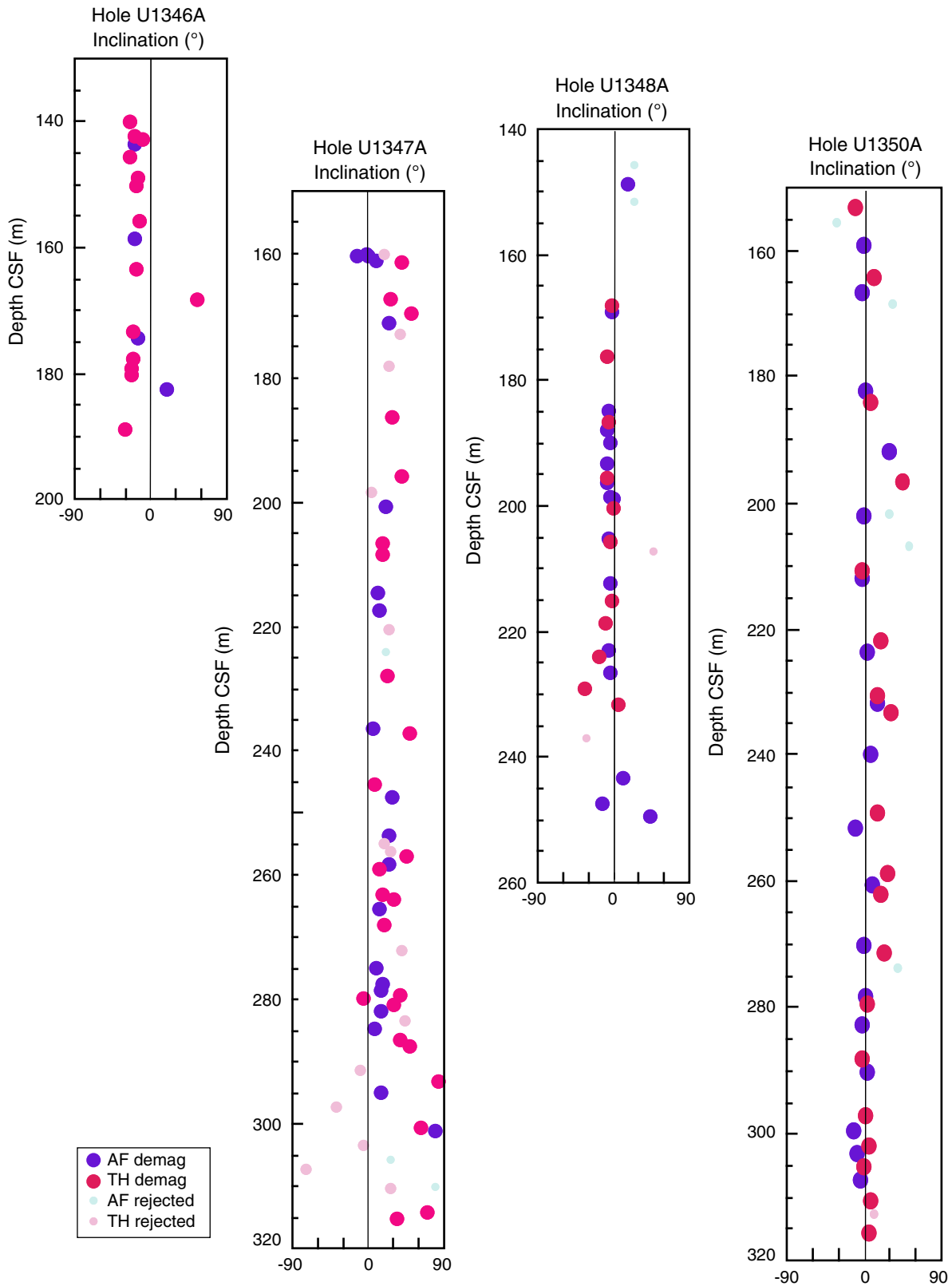


**Figure F28.** Summary of total NGR counts measured from core sections, Expedition 324. Maximum value per section plotted at depth where that maximum occurs. Dashed line = contact between sediments and igneous basement.

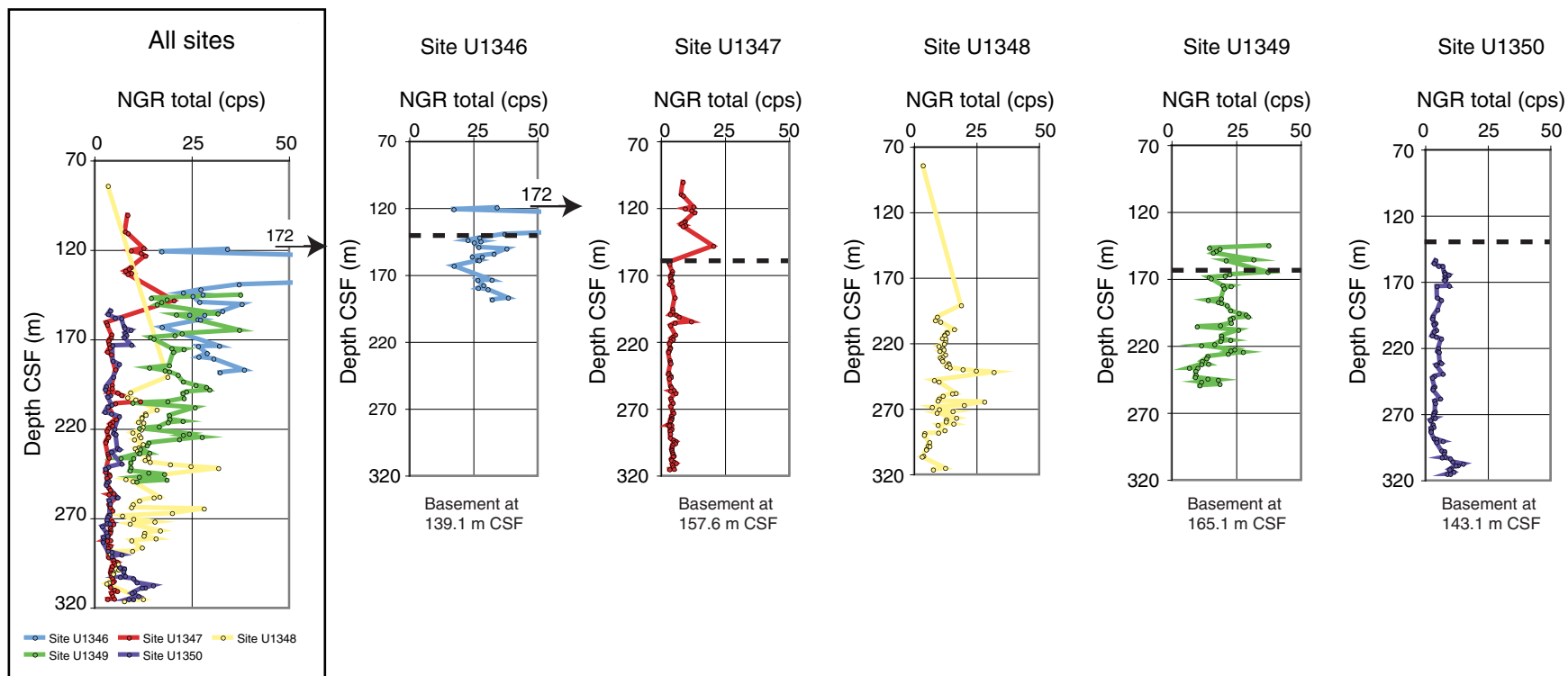


**Figure F29.** Summary of magnetic susceptibility measured from core sections, Expedition 324. Maximum value per section plotted at depth where that maximum occurs, meaning that features such as sediment interbeds with lower magnetic susceptibility are not visible. Dashed line = contact between sediments and igneous basement.

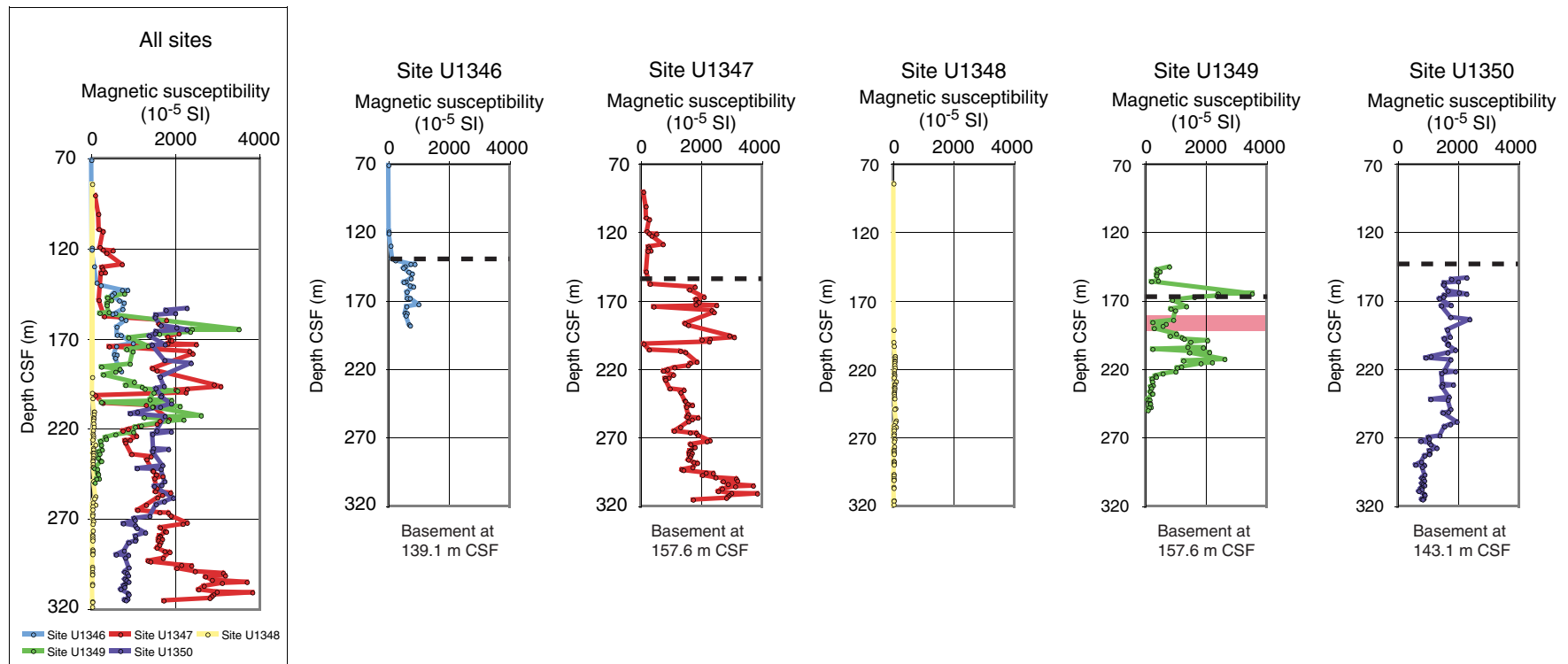


**Figure F30.** Summary of GRA bulk density measured from core sections, Expedition 324. Maximum value per section plotted at depth where that maximum occurs, meaning that features such as sediment interbeds with lower GRA densities than igneous material are not visible in this figure. Dashed line = contact between sediments and igneous basement.

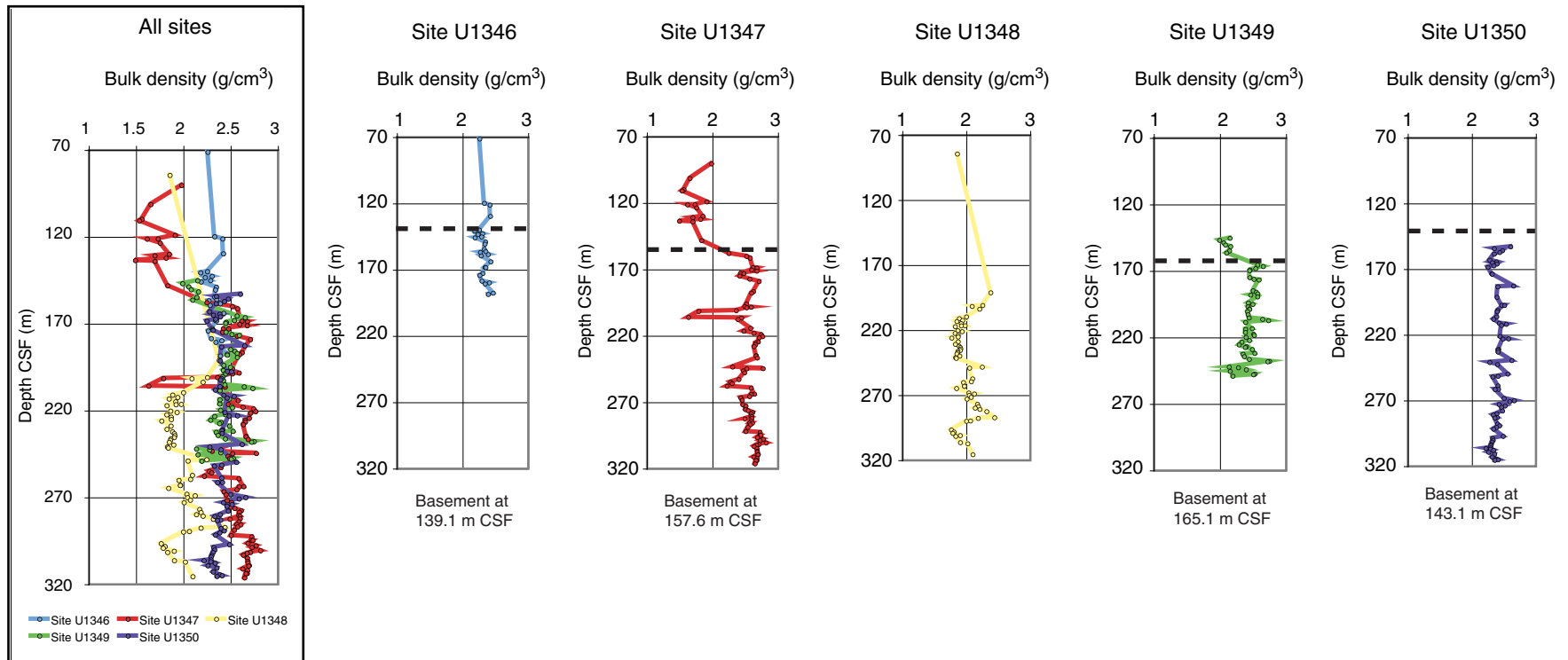


**Figure F31.** Potassium content results from downhole logging measurements in the upper basaltic basement sections of different localities.

